THIN-FILM GaAs PHOTOVOLTAIC SOLAR ENERGY CELLS

by

P. A. CROSSLEY *(Project Scientist)*
R. B. GILL
A. SPIELMAN
M. WOLF *(Project Supervisor)*

Prepared for

NATIONAL AERONAUTICS AND SPACE ADMINISTRATION

CONTRACT NAS 3-8510

ASTRO-ELECTRONICS DIVISION
DEFENSE ELECTRONIC PRODUCTS
RADIO CORPORATION OF AMERICA
PRINCETON, NEW JERSEY 08540

Requests for copies of this report should be referred to

National Aeronautics and Space Administration
Office of Scientific and Technical Information
Attention: AFSS-A
Washington, D.C. 20546

FINAL REPORT

THIN-FILM GaAs PHOTOVOLTAIC SOLAR ENERGY CELLS

by

P. A. Crossley *(Project Scientist)*
R. B. Gill
A. Spielman
M. Wolf *(Project Supervisor)*

Prepared for

NATIONAL AERONAUTICS AND SPACE ADMINISTRATION

August 28, 1967

Contract NAS 3-8510

Technical Management
NASA Lewis Research Center
Cleveland, Ohio

Astro-Electronics Division
Defense Electronic Products
Radio Corporation of America
Princeton, New Jersey 08540

THIN-FILM GaAs PHOTOVOLTAIC SOLAR ENERGY CELLS

by

P. A. Crossley (Project Scientist), R. B. Gill,
A. Spielman, and M. Wolf (Project Supervisor)

ABSTRACT

The results of experimental work aimed at improving device conversion efficiency are reported. Measurements of the optical and electrical properties of cuprous selenide layers, and electrical measurements on the barrier contact characteristics, were made. The operating characteristics of the cells are described, including the results of a stability testing program, and the development of a successful antireflection coat. A review of all previous work under related contracts is also given.

TABLE OF CONTENTS

TABLE OF CONTENTS (Cont'd.)

TABLE OF CONTENTS (Cont'd.)

ILLUSTRATIONS

ILLUSTRATIONS (Cont'd.)

ILLUSTRATIONS (Cont'd.)

SYMBOLS

A	constant in the diode equation
α	optical absorption constant
$\overline{\alpha}$	average optical absorption constant
b	ratio of electron mobility to hole mobility
C	capacitance per unit area
d	lattice spacing
E_G	forbidden bandgap
E_{opt}	optical energy gap
ϵ	dielectric constant
F	fill-factor
I	current density
I_L	light-generated current density
I_m	current density at maximum power point
I_o	reverse saturation current density
I_{sc}	short-circuit current density
k	Boltzmann's constant
λ	wavelength
L_n	diffusion length for electron in p region
L_p	diffusion length for hole in n region
m*	electron effective mass
μ	refractive index
μ_n	electron mobility
μ_p	hole mobility
N	carrier concentration
N_c	density of states in the conduction band
N_d	donor concentration
n_{pn}	equilibrium density of majority carrier
N_v	density of states in the valence band
P	power
q	electronic charge
R	optical reflectivity
R_s	series resistance
R_{sh}	shunt resistance
σ_n	conductivity of n-type semiconductor
σ_p	conductivity of p-type semiconductor
t	film thickness
T	optical transmission or absolute temperature, depending on context
τ	time
V	electrical potential difference
V_b	reverse bias breakdown voltage
V_d	diffusion potential
V_m	voltage at maximum power point
V_{oc}	open-circuit voltage

FOREWORD

During experimental work under this contract, many measurements were made using equipment which provided a continuous plot of a variable. Where this information has been reproduced in the figures of this report, a continuous line has been shown on graphs, with no experimental points marked. In these cases, the reproduced curve follows the original data, or a derived set of data points, within the limits of drawing accuracy. In no case have data points been omitted to improve the appearance of the curve.

The cells under investigation have been made with a barrier layer of non-stoichiometic cuprous selenide. Where the stoichiometry of the layers has been measured, the known stoichiometry has been indicated in the text, e.g., $Cu_{1.83}Se$. In the majority of cases, however, the film stoichiometry is not known with accuracy, since it cannot be assumed that this will be the same as that of the evaporant used in the vacuum deposition process. For brevity in such cases, a nominal stoichiometry of Cu_2Se has been used in the text. There is no ambiguity between the two usages, since material with stoichiometry exactly Cu_2Se is not stable under the experimental conditions of this work.

THIN-FILM GaAs PHOTOVOLTAIC SOLAR ENERGY CELLS

by

P. A. Crossley, R. B. Gill, A. Spielman, and M. Wolf
RCA Astro-Electronics Division

SUMMARY

The objective of the program is to develop an economical solar cell fabrication technique to produce cells with 5% sunlight efficiency, high power-to-weight ratio, and stability under storage and operating conditions.

During the second half of the contract period, the work has been concentrated on improving the efficiency and evaluating the stability of the cells. The optical properties of thin films of the barrier layer material, cuprous selenide, have been examined in detail, and the electrical properties have also been measured. The electrical characteristics of the barrier contact have been examined using I-V and C-V measurements, and the factors governing open-circuit voltage have been investigated using thin-film and single-crystal barrier-contact cells. Possible approaches to the provision of an antireflection coat have been examined, with some positive results being achieved. Spectral response measurements on the thin-film cells have shown some anomalous results, which have been demonstrated to be due to optical interference effects in the barrier layer.

The intrinsic stability of the cells has been evaluated by a two-month life test, and the stability under operation in various degrading atmospheres has been examined during a separate test of similar duration. The results indicate that the methods which have been developed for stabilizing the cells are successful.

A comparison between experimental data on cell performance, and those which may be expected on theoretical grounds, indicates that the present efficiency limitation (4.2%), is governed mainly by the values of reverse saturation current (which affects V_{oc}), and a combination of factors tending to reduce I_{sc}.

SECTION I

GALLIUM ARSENIDE FILMS

A. SUBSTRATES

Two types of substrates were utilized during this report period for the vapor growth of the GaAs films. The primary substrate, which has been fully described elsewhere[1] consists of a 5-μm-thick Al foil base on which are deposited 3 to 4 μm of n-type polycrystalline InAs by vapor transport from polycrystalline InAs wafers. The other type of substrate, on which only a limited number of cells were made (primarily for the initial stability tests), consisted of a 25-μm Mo sheet on which were deposited 7 to 10μm of InAs by the technique described above. The thicker InAs film was required on the Mo sheet to obtain uniform and complete coverage of the substrate.

The modified InAs growth process fully described in an earlier report[1] proved to be completely satisfactory during the current period and, consequently, no changes were made in either the vapor transport system or the experimental procedure employed.

B. GaAs GROWTH PROCESS

The modified GaAs vapor transport process and small-area furnaces described elsewhere[1] were employed, except for a modification in the hydrogen gas flow system described below, throughout this report period. Approximately two-thirds of the way through this period, it became evident that to prepare reproducibly conducting GaAs films suitable for the fabrication of solar cells was extremely difficult. Since there was no significant increase in growth rate for the high-resistance films the difficulty was felt to be not primarily associated with an uncontrolled increase in either water vapor or oxygen within the furnace. Initially, the difficulty was thought to be associated with either contamination of the furnaces or the use of GaAs source crystals containing too low a donor concentration. Subsequent testing elimated the possibility of either of these effects being the primary cause of the nonreproducibility of the GaAs films. Eventually, the source of the problem was traced to the palladium hydrogen purifier which was then removed from the vapor transport system. In place of this hydrogen supply, cylinder hydrogen of ultra-high purity was used, and it was found essential to pass this through a trap at dry ice temperature to remove water vapor. Some grams of water were collected in this trap during the course of the work, and this explains why it was not possible to obtain reproducible GaAs transport when this hydrogen was used direct from the cylinder during earlier contracts. After drying the hydrogen in this way, controlled amounts

of water vapor were then introduced before passing the hydrogen to the furnaces. Having made these changes in the system it was once again possible to control the properties of the GaAs films by systematically varying the amount of water vapor introduced into the hydrogen gas entering the furnace.

C. GaAs FILM PROPERTIES (MECHANICAL)

With the exception noted above, it has been possible to control reproducibly both the electrical properties of the GaAs films (as discussed later), and the growth rate for the films. This has been achieved by controlling the concentration of water vapor in the furnace during growth. The concentration has been controlled by supplying the hydrogen to the furnace as a mixture of dry gas and gas saturated with water vapor by passage through water at $0^{\circ}C$. The flow system and control methods have been fully described previously,[1] and have not been altered during the reporting period. Control of the growth rate by varying the ratio between the dry and the saturated hydrogen is summarized by the data in Table I, obtained from one of the GaAs growth furnaces. The average thickness of the films was determined by differential weighing.

To obtain information on uniformity and surface topography of the GaAs films, two cells were sectioned and several edge micrographs taken on each cell.* Two of the micrographs showing the cross section of one of the cells are shown in Figures 1(a) and (b). In Figure 1(a) one observes the cross section near the center of the cell while in Figure 1(b) a cross section near the edge of the cell is shown. While no large deviation of mean thickness is observed, it is apparent that the crystallite size near the center of the cell is much greater than near the outer edge. (It should be noted that one usually obtains maximum sensitivity to a focussed white light source near the center of the cell.) The average thickness estimated from the micrographs is 14.6 μm while that determined for the entire GaAs film by the differential weight method was 13.1 μm. This indicates that portion of the GaAs film not used for cell fabrication contains a considerable gradient in the GaAs film thickness.

An attempt to obtain more uniform GaAs films by modifying the source-substrate spacer in the growth furnace was inconclusive since it is believed that it was during this series of experiments that the effects of the breakdown of the palladium purifier described earlier began to be observed.

---

* The authors are indebted to the NASA Lewis Research Center, who obtained these photographs.

TABLE I

EFFECT OF ADDITION OF H_2O VAPOR
ON GaAs GROWTH RATE

Film #	Growth Rate $\mu m\ hr^{-1}$	Total H_2 Flow Rate $cm^3\ ^2\ min^{-1}$	Ratio of H_2 Passed Through H_2O Trap:	"Dry" H_2
R103	0.56	10	1	2
R104	0.70	10	1	2
R105	0.63	10	1	2
R107	0.74	10	2	3
R71	0.90	10	1	1
R72	0.86	10	1	1
R76	1.09	10	2	1
R77	0.94	10	2	1

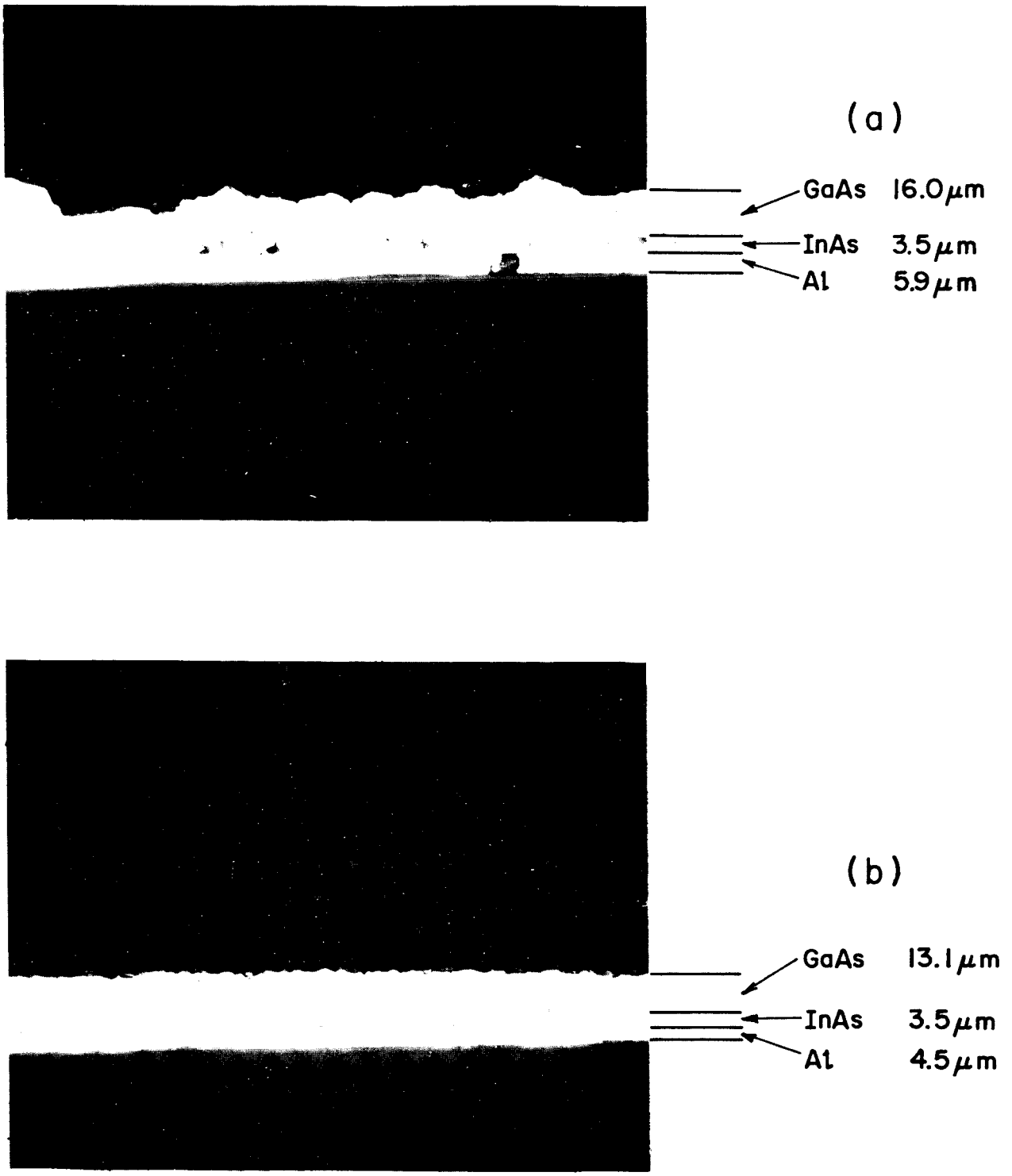

Figure 1. (a) Cross section micrograph of GaAs cell, central region
(b) Cross section micrograph of GaAs cell, edge region

SECTION II

CUPROUS SELENIDE

A. PREPARATION

1. Cuprous Selenide Polycrystalline Ingots

A number of polycrystalline ingots of $Cu_{2-x}Se$, where $0.1 < x < 0.3$, were prepared by reaction of the elements in the liquid state. The desired quantities of high-purity copper and selenium were weighed either into a graphite crucible (previously cleaned by hydrogen firing) which was placed in a clean quartz tube, or directly into the quartz tube. The tube was then evacuated to less than 10^{-4} Torr and sealed off. The reactant mixture was heated in a horizontal furnace to above 1150°C for several hours and was then permitted to cool slowly. The resulting polycrystalline $Cu_{2-x}Se$ ingots were crushed under clean conditions, sieved, and separated into two batches. One consisted of material which would pass a 0.297-mm mesh but be stopped by a 0.25-mm mesh, and the other consisted of material which would pass a 0.25-mm mesh. Both groupings of material were used in the flash evaporation process with no significantly different results.

The crystals prepared using the above-described technique were characterized by both x-ray diffractometry (to determine the phases present) and by chemical analysis (to determine the composition); the results are given in Table II.

The uncertainty with respect to the identification of the tetragonal phase as β- Cu_2Se is largely due to the absence of values of the lattice constant in the literature. This phase has been observed within this laboratory numerous times[2] as well as by other workers.[3] To date this material has been prepared neither as a single crystal nor in a form suitable for chemical analysis.

2. Cuprous Selenide Films

The flash evaporator described in an earlier report[1] was utilized throughout this period for the preparation of thin films of cuprous selenide. In addition to the film transmission monitor also discussed earlier, a quartz crystal oscillator film thickness monitor has been used to determine the cuprous selenide film thickness during evaporation.

Results of a large number of evaporations using this system have indicated that cuprous selenide films suitable for solar cell fabrication can be reproducibly obtained. It has also been possible to obtain information relating to the electrical and optical properties of the cuprous selenide during film formation.

TABLE II

$Cu_{2-x}Se$ PREPARATION

Ingot	Chemical Analysis	X-ray Diffraction Analysis
CS-1	$Cu_{1.80}Se$	f.c.c. $Cu_{2-x}Se$ d = 5.765Å
CS-2	$Cu_{1.80}Se$	f.c.c. $Cu_{2-x}Se$ d = 5.768Å
CS-3	$Cu_{1.88}Se$	f.c.c. $Cu_{2-x}Se$ d = 5.7654Å plus a small proportion of possibly a tetragonal phase, perhaps β-Cu_2Se.
CS-4	$Cu_{1.80}Se$	f.c.c. Cu_{2-x} d = 5.7654Å
CS-5	$Cu_{1.83}Se$	f.c.c. Cu_{2-x} d = 5.754Å
CS-6	$Cu_{1.87}Se$	f.c.c. $Cu_{2-x}Se$ d = 5.770Å plus a small proportion of a tetragonal phase, identified as β-Cu_2Se.
CS-7*	$Cu_{1.86}Se$	f.c.c. $Cu_{2-x}Se$ d = 5.759Å

*The composition and structure of CS-7 is uncertain at this time since the material submitted for analysis may not have been representative of the bulk.

B. CUPROUS SELENIDE FILM PROPERTIES

To obtain a better understanding of the influence of the cuprous selenide films on the solar cell properties a number of experiments were performed on films prepared from single-phase cubic $Cu_{1.8}Se$.

Figure 2 shows the result of an experiment in which the sheet resistance of a cuprous selenide film on glass was continuously monitored as a function of film thickness during the deposition process. Continuity of the cuprous selenide film was observed at a film thickness of 18 Å (as indicated by the film thickness monitor). The sheet resistance of the film, when 25 Å thick, was about 2.5×10^3 ohms per square. For films greater than 100 Å but less than 500 Å in thickness the sheet resistance was found to be proportional to t^{-1}. As observed in the past, the sheet resistance of a

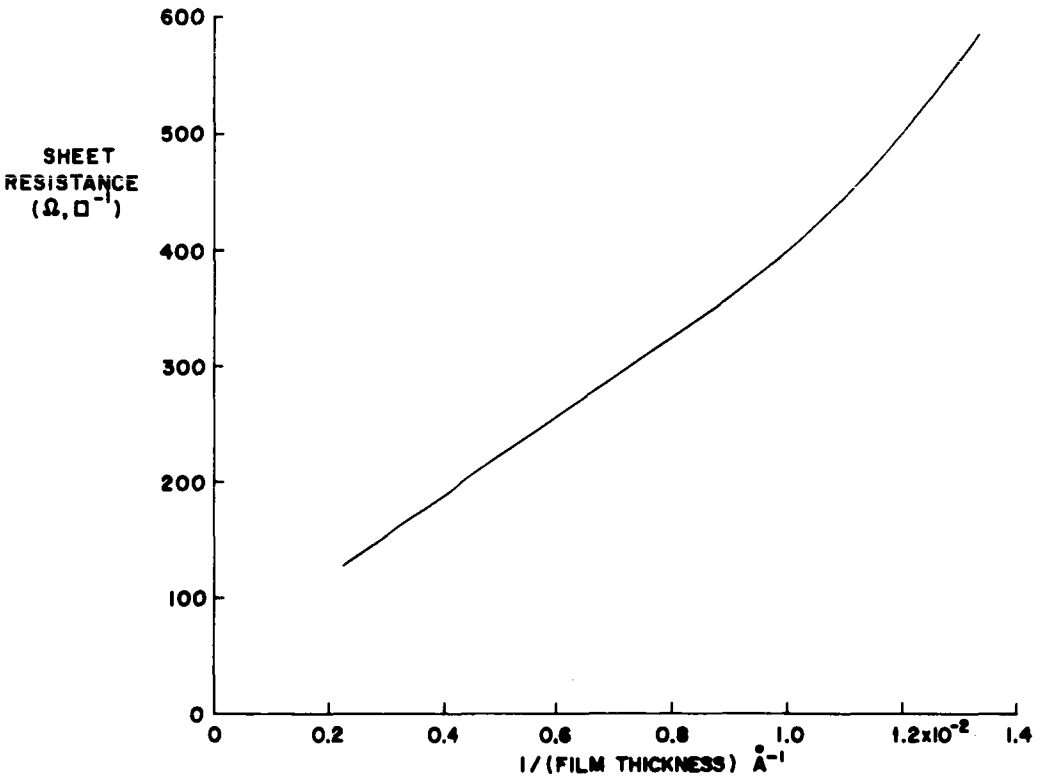

Figure 2. Sheet resistance of a Cu_2Se film as a function of 1/t

deposited film dropped sharply on exposure to air, and continued to decrease for some days. The latter process may be due to annealing in the film which results in an increase in carrier mobility.

Figure 3 shows a plot of ln (transmission to white light) as a function of film thickness for a typical flash-evaporated film on glass. The linearity of the relationship for film thicknesses greater than 100 Å suggests that the optical properties of a thin film can be described by an average absorption coefficient ($\overline{\alpha}$), whose value has been calculated, from the curve shown, to be $6.7 \times 10^4 cm^{-1}$. The spectral transmission of a 68% (at 1.5 eV) transmitting film on glass in the range 3000 to 9000 Å is shown in Figure 4. A broad transmission peak is observed in the range 6000 to 9000 Å. For wavelengths shorter than 6000 Å the transmission drops sharply falling to about 50% of peak transmission at 5000 Å. The sharp drop in transmission at short wavelengths adversely affects the spectral response of the cells as discussed in Section IV.

In view of this, it appeared necessary to investigate the possibility of minimizing the absorption at high energies by varying the stoichiometry of the cuprous selenide starting material. Films were deposited on quartz substrates, and the film thicknesses were determined by the conventional Tolansky technique.[4] The structure of the film

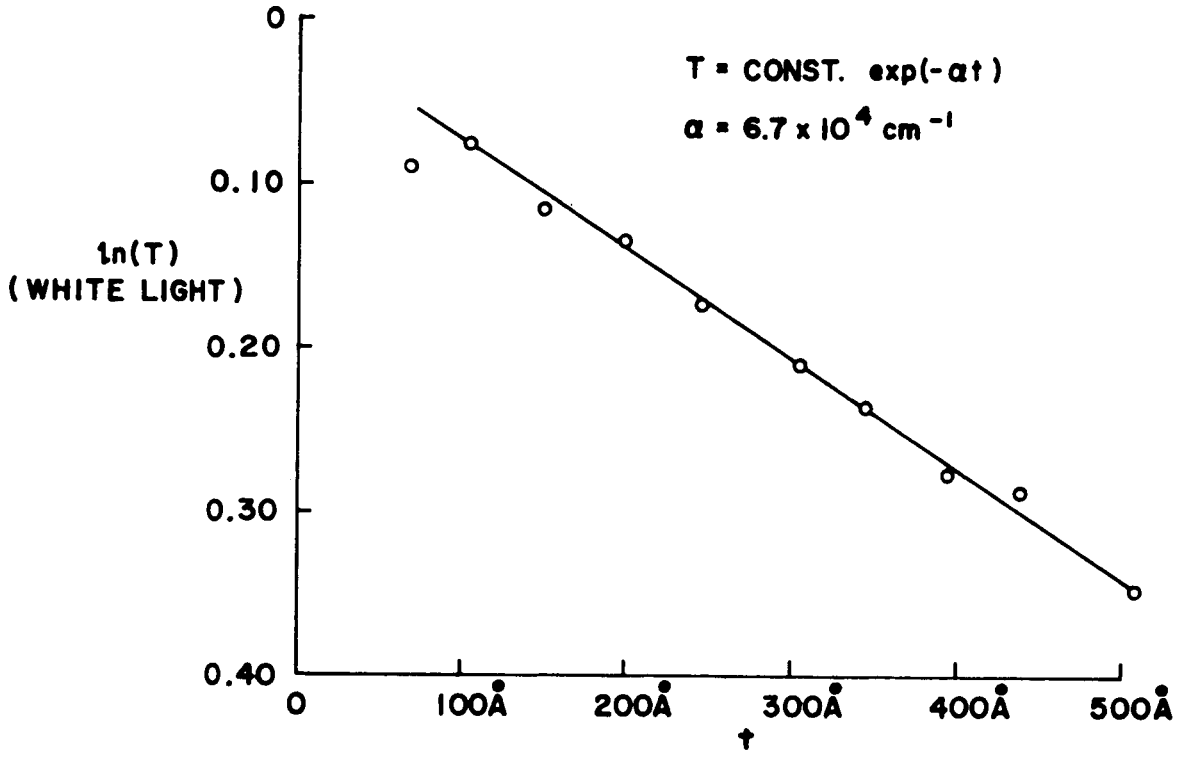

Figure 3. Logarithm of optical transmission of a Cu_2Se film as a function of t

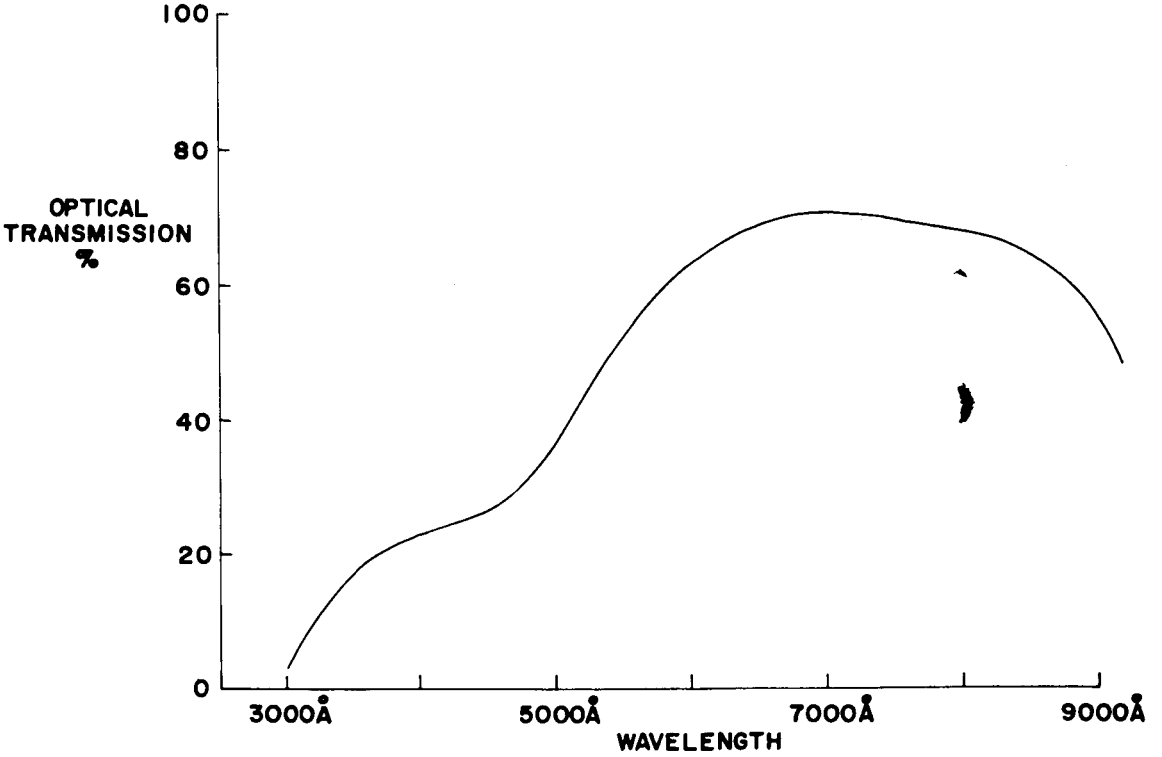

Figure 4. Spectral dependence of optical transmission of a Cu_2Se film on glass

was determined by x-ray diffractometry. Two highly oriented phases were observed in all samples. The results of x-ray diffraction measurements on the samples which were used for optical measurements are summarized in Table III.

The $Cu_{2-x}Se$ phase was characterized in all films by a (d) value of 5.740 Å. Using this value the composition of the $Cu_{2-x}Se$ phase has been estimated to be $Cu_{1.81}Se$.[5]

Transmission spectra of each sample were measured on a Cary spectrophotometer. Using a relation of the form

$$T = F(R) \exp(-\alpha t) \quad (1)$$

where T is the transmissivity,

t the sample thickness,

α the absorption coefficient, and

F(R) a function of the reflectivity R,

the use of transmission spectra of two samples of different thicknesses prepared during the same evaporation permits calculation of the absorption coefficient by elimination of F(R). In this way the absorption spectra were calculated, as shown in Figures 5 through 8 for samples of various compositions. An increase in α with increasing photon energy beginning at about 2 eV for all samples is observed. This shape is characteristic of a semiconductor in the region of the fundamental absorption edge.

TABLE III

CUPROUS SELENIDE FILM STRUCTURE

Film #	Source Ingot	Phase Ratio $Cu_{2-x}Se$:Cu_3Se_2	$E_{opt}(1)$ $Cu_{2-x}Se$ (eV)	$E_{opt}(2)$ Cu_3Se_2 (eV)
M_1	CS-3	16.3:1	2.17	—
M_2	CS-5	5.0:1	2.20	—
M_3	CS-4	3.5:1	1.96	1.42
M_4	CS-7	2.5:1	2.09	1.45

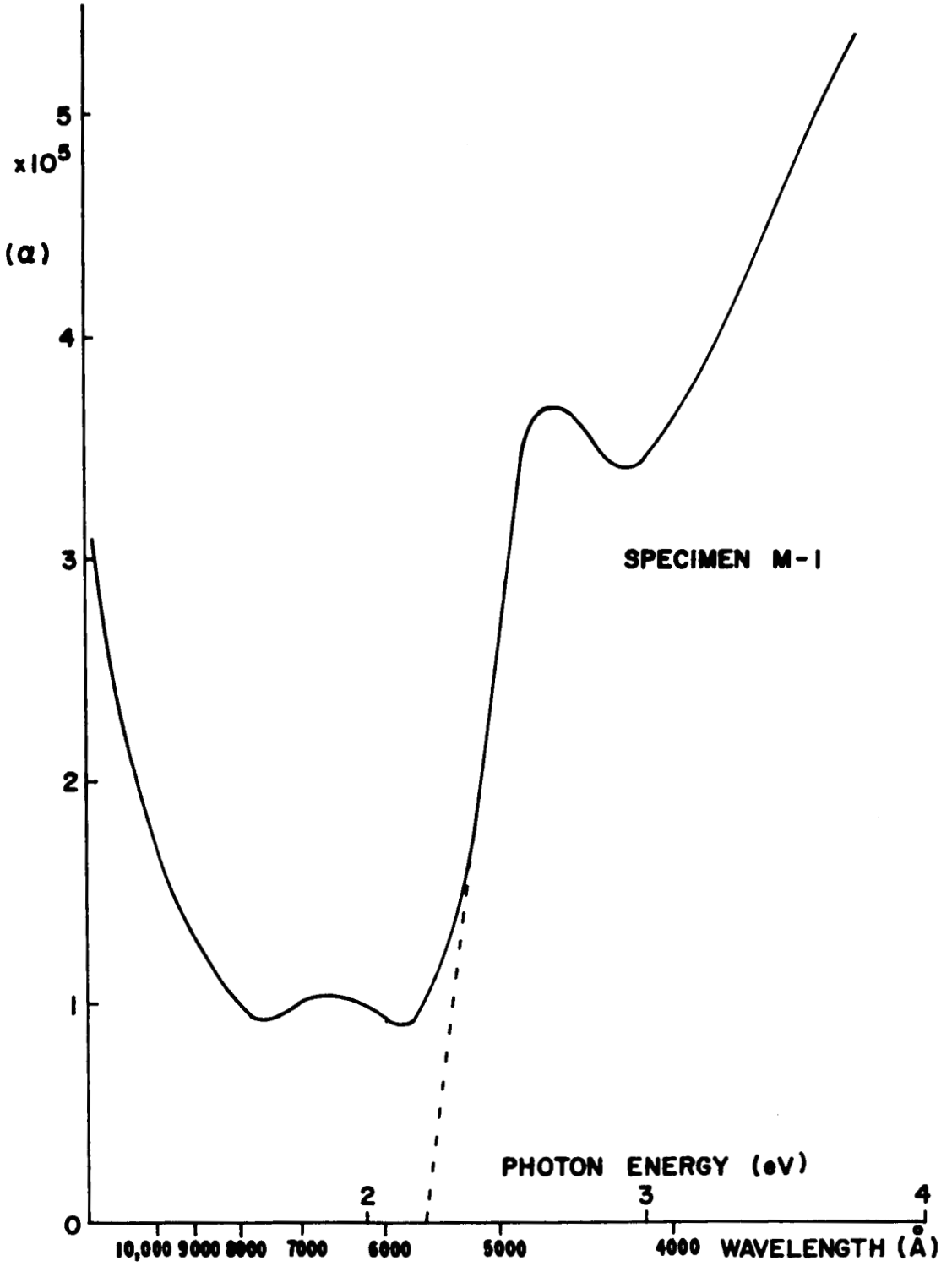

Figure 5. Optical transmission as a function of photon energy for cuprous selenide specimen M-1

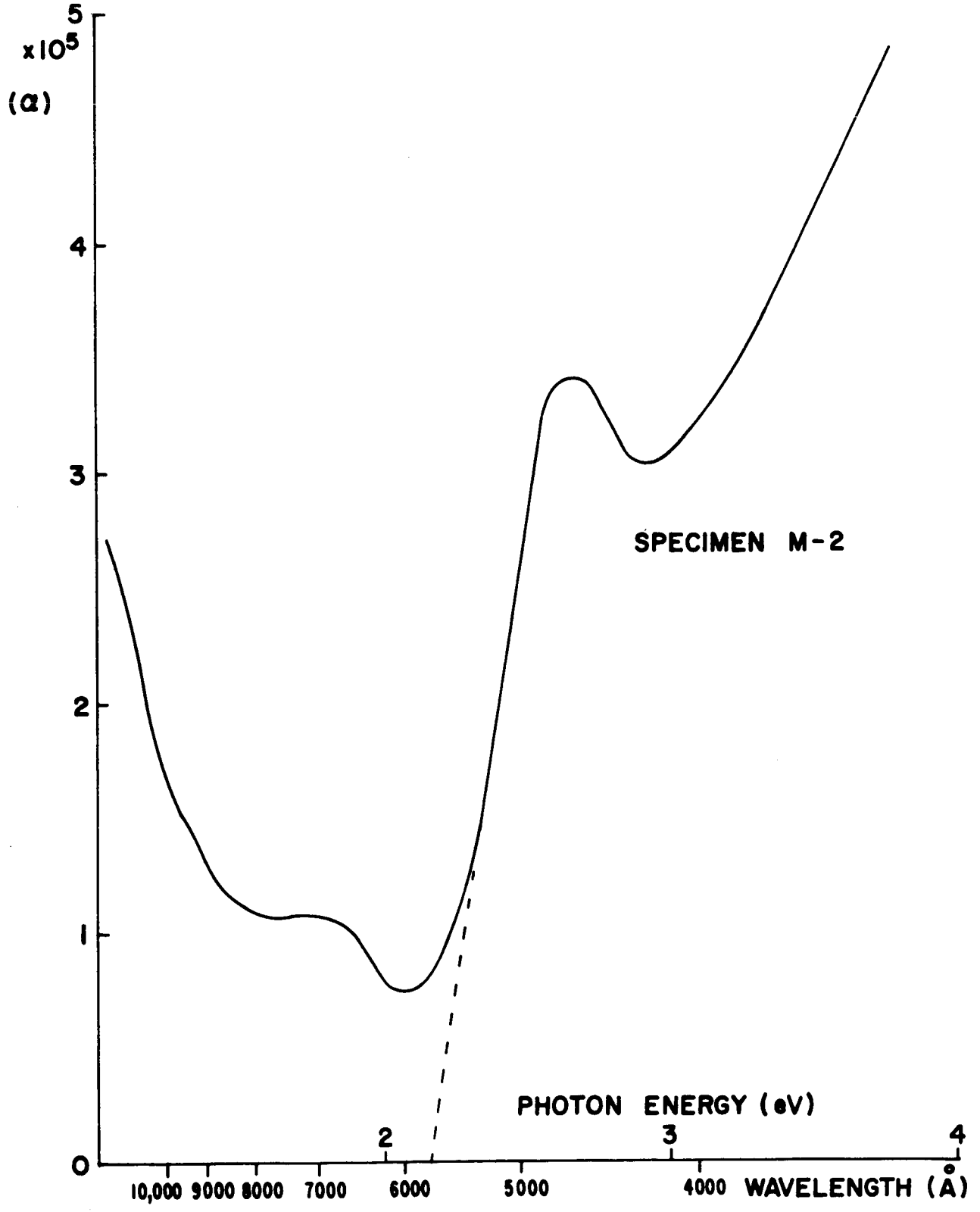

Figure 6. Optical transmission as a function of photon energy for cuprous selenide specimen M-2

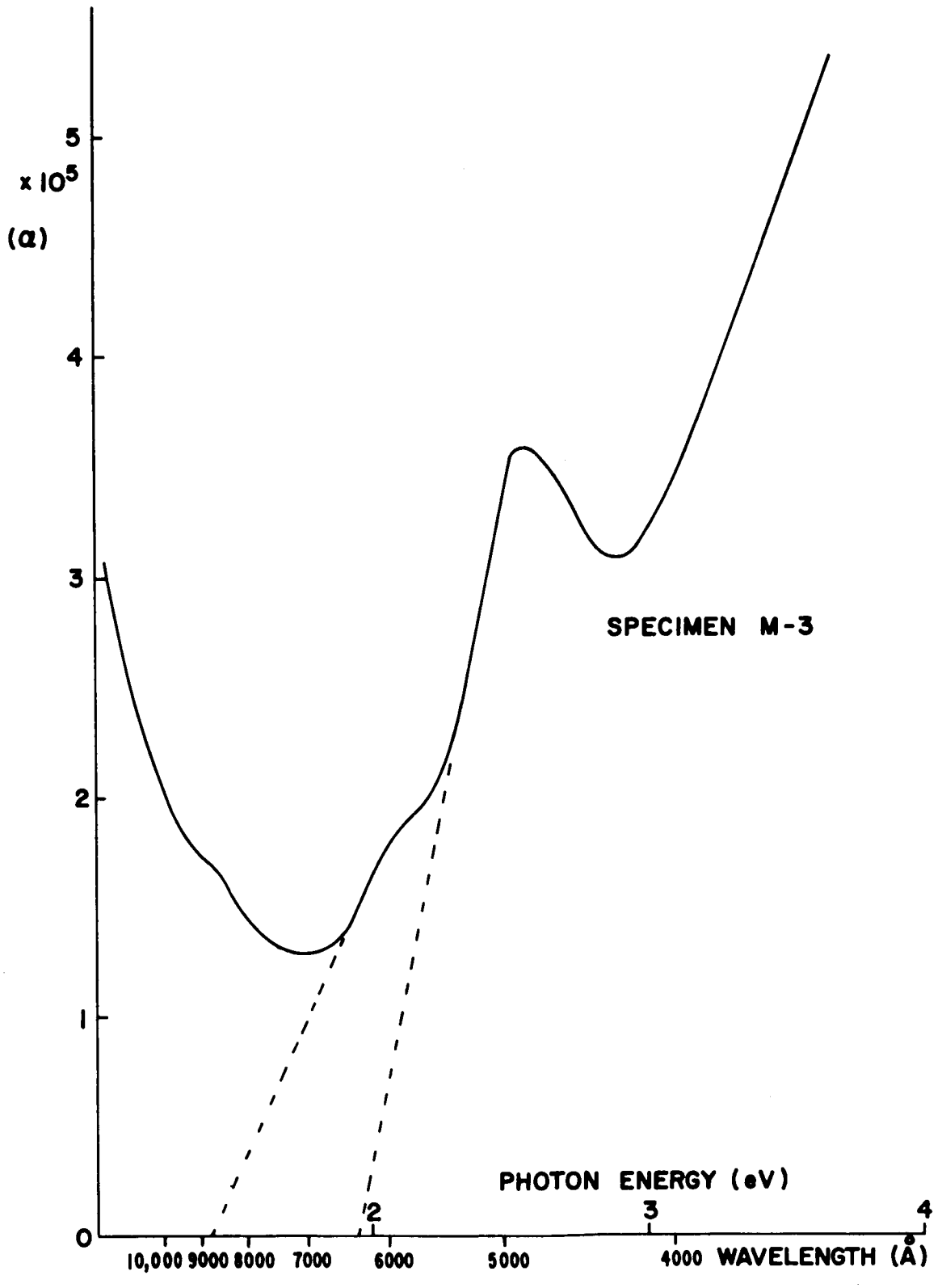

Figure 7. Optical transmission as a function of photon energy for cuprous selenide specimen M-3

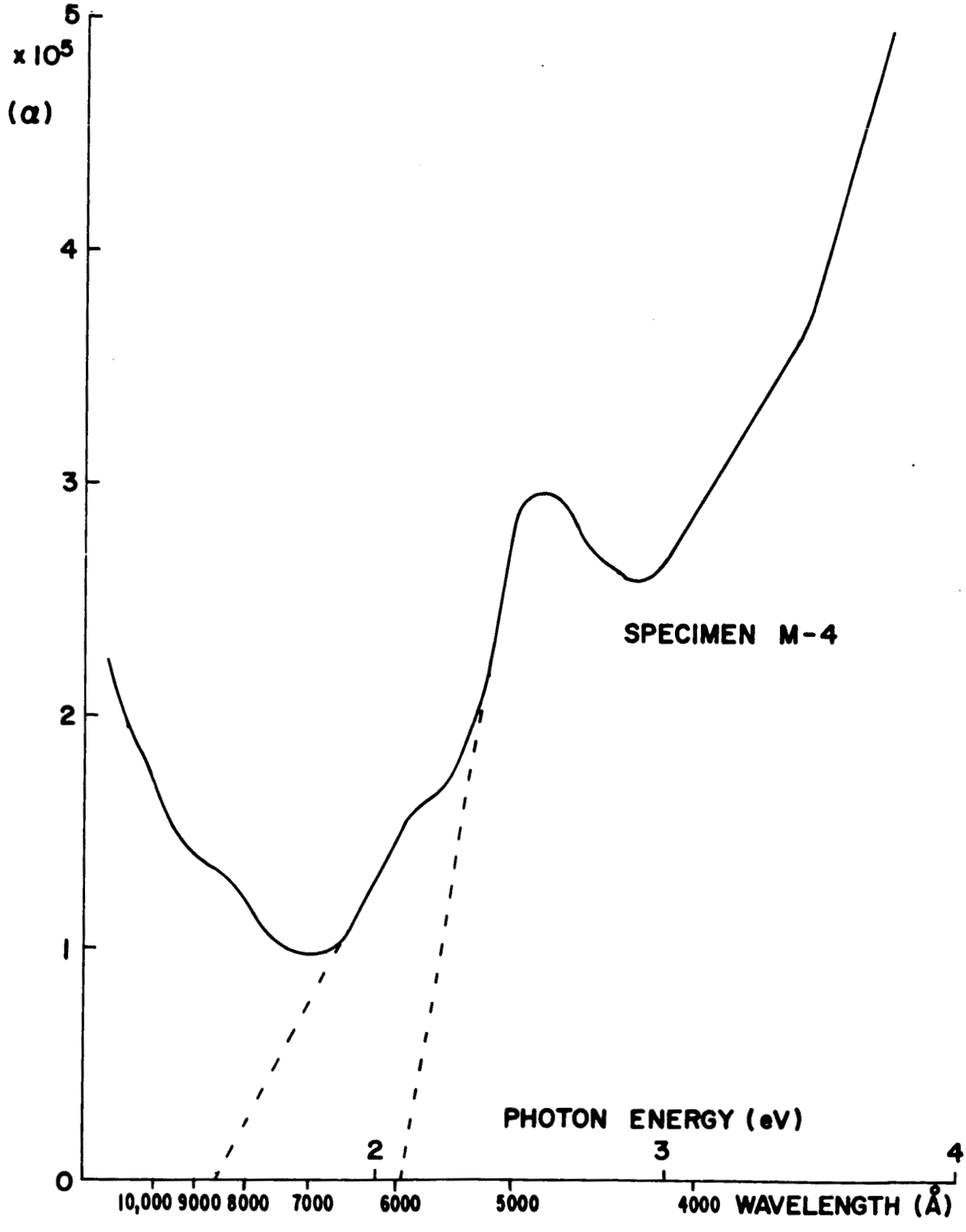

Figure 8. Optical transmission as a function of photon energy for cuprous selenide specimen M-4

Assuming this increase in α near 2 eV to be due to band-to-band transitions across the energy gap the absorption curve was extrapolated to $\alpha = 0$ to obtain a value of the 300°K optical energy gap $E_{opt}(1)$ which is believed to be associated with face-centered cubic $Cu_{1.81}Se$. The values of $E_{opt}(1)$ associated with materials M-1 and M-2 are believed to be more representative of $Cu_{1.81}Se$ since in these films the effects of the second phase (Cu_3Se_2) would be minimized. The shape of the absorption curve in the region of energies between 1.4 and 2.0 eV is believed to be dominated by the Cu_3Se_2 present in the films. The appearance of a sharp change in (α) near 8300 Å can be correlated with changes in the concentration of Cu_3Se_2 present. As for the $Cu_{1.81}Se$ phase, the absorption curve in this region was extrapolated to $\alpha = 0$ for materials M-3 and M-4. Hence, an optical energy gap $E_{opt}(2)$ at 300°K was obtained, which is believed to be characteristic of Cu_3Se_2. The results of this analysis are summarized in Table III. The increasing absorption for photons of energy less than 1.6 eV is due to absorption by free carriers. In Figure 9 a plot of absorption coefficient as a function of λ^2 is shown for material M-3, whose ratio of $Cu_{2-x}Se$ to Cu_3Se_2 was determimed to be 3.5. The curve is linear and extrapolates to $\alpha = 0$ at $\lambda = 0$, as is to be expected for free carrier absorption.

In summary, it has been found that the decrease in transmission for wavelengths less than 5500 Å, observed in the thin cuprous selenide films on glass, is fundamentally associated with the two phases which compose the films. No significant increase in transmission can be expected for small changes in the stoichiometry of the evaporant. To minimize losses in cell efficiency due to absorption in the cuprous selenide, thinner films should be used. Increases in cell performance by this technique were evaluated, with the results reported in Section IV. C. 3.

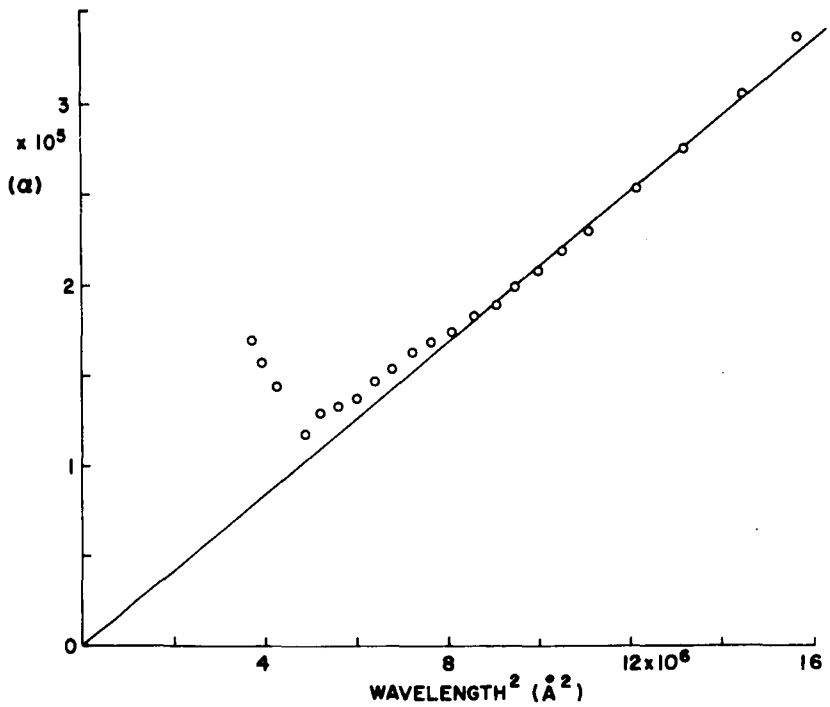

Figure 9. Optical transmission of cuprous selenide specimen M-3 in the region of free carrier absorption

SECTION III

BARRIER CHARACTERISTICS

A. SINGLE-CRYSTAL GaAs-Cu_2Se BARRIER

As part of the effort to increase the open-circuit voltage of the GaAs-Cu_2Se heterojunction thin-film solar cells, the effect of GaAs crystal orientation on open-circuit voltage was examined. This was measured under 100 $mW \cdot cm^{-2}$ equivalent tungsten illumination, for a number of n-type, small-area ($< 1\ cm^2$), single-crystal solar cells. The data on open-circuit voltage was supplemented by both I-V and differential capacitance measurements made on 1-mm^2 Cu_2Se barrier areas which were deposited adjacent to the cell to be studied.

The GaAs single-crystal wafers were cut from n-type ingots having donor concentrations between 1×10^{16} and $4.2 \times 10^{17}\ cm^{-3}$ and electron mobilities between 3000 and 4900 $cm^2\ (volt\text{-}sec)^{-1}$. The wafers were degreased and etched heavily in aqua regia to remove the work-damaged surface. Ohmic tin contacts were applied at about 400°C in a hydrogen atmosphere. The wafer was then given an additional light etch in aqua regia which was followed by a polish etch in methanol-Br or $3H_2SO_4$: $1H_2O_2$:$1H_2O$. The wafer was mounted in a vacuum system and barrier-contact layers for both the cell and a series of 1-mm^2 diodes were deposited simultaneously using appropriate metal foil masks. Following the evaporation of a gold grid onto the cell, both the cell and the small-area barrier were evaluated.

During the differential capacitance measurements on the small-area barriers it was frequently found that the ac capacitance continued to increase for about 30 to 60 seconds after the application of the reverse bias voltage. It was evident that during this period the total charge concentration within the barrier region was increasing and further that the shallow donors within this region were completely ionized. Hence, the increase in carrier concentration after application of the bias voltage could be associated with the ionization of deep donors lying below the Fermi level of deep electron traps which are normally full at 300°K. Williams[6] has recently discussed this effect with respect to deep donor levels in considerable detail. After ionization of deep centers has been completed the variation in capacitance with time ceases and the difference between the initial and final values of capacitance is a measure of the total concentration of deep centers. The relation between capacitance per unit area (C), applied dc voltage (V), and donor concentration (N), can be described at the instant of application of the dc bias as

$$N_d = \frac{2}{q\epsilon\epsilon_o} C^2 (V + V_d) \qquad (2)$$

and by

$$N_d + N'_d = \frac{2}{q \epsilon \epsilon_o} C^2 (V + V'_d) \tag{3}$$

after equilibrium has been established where

N_d = density of shallow donors

N'_d = density of deep donor centers

ϵ = dielectric constant

V_d = diffusion voltage. Typical results of this type are shown in Figure 10.

Theory indicates that

$$I = I_o \exp\left[\left(\frac{qV}{AkT}\right) - 1\right]$$

or

$$I = I_o \exp\left(\frac{qV}{AkT}\right) \quad \text{for } I \gg I_o \tag{4}$$

in the region 10^{-6} to 10^{-2} A · cm^{-2}. A curve of this form is shown in Figure 11 along with the values of I_o and A representative of this heterojunction, derived from the curve.

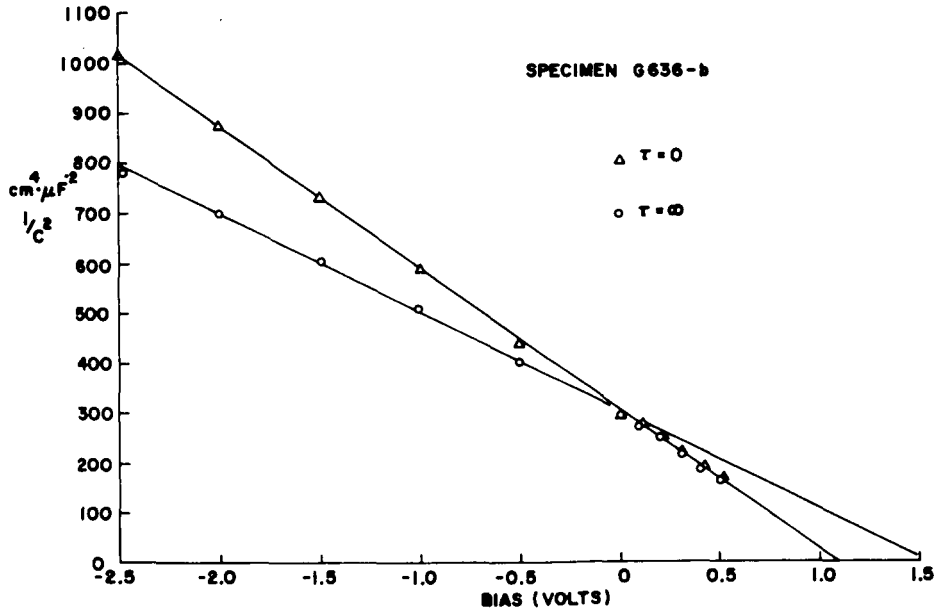

Figure 10. $(1/C^2)$ as a function of (V) for a cuprous selenide barrier contact to single-crystal GaAs

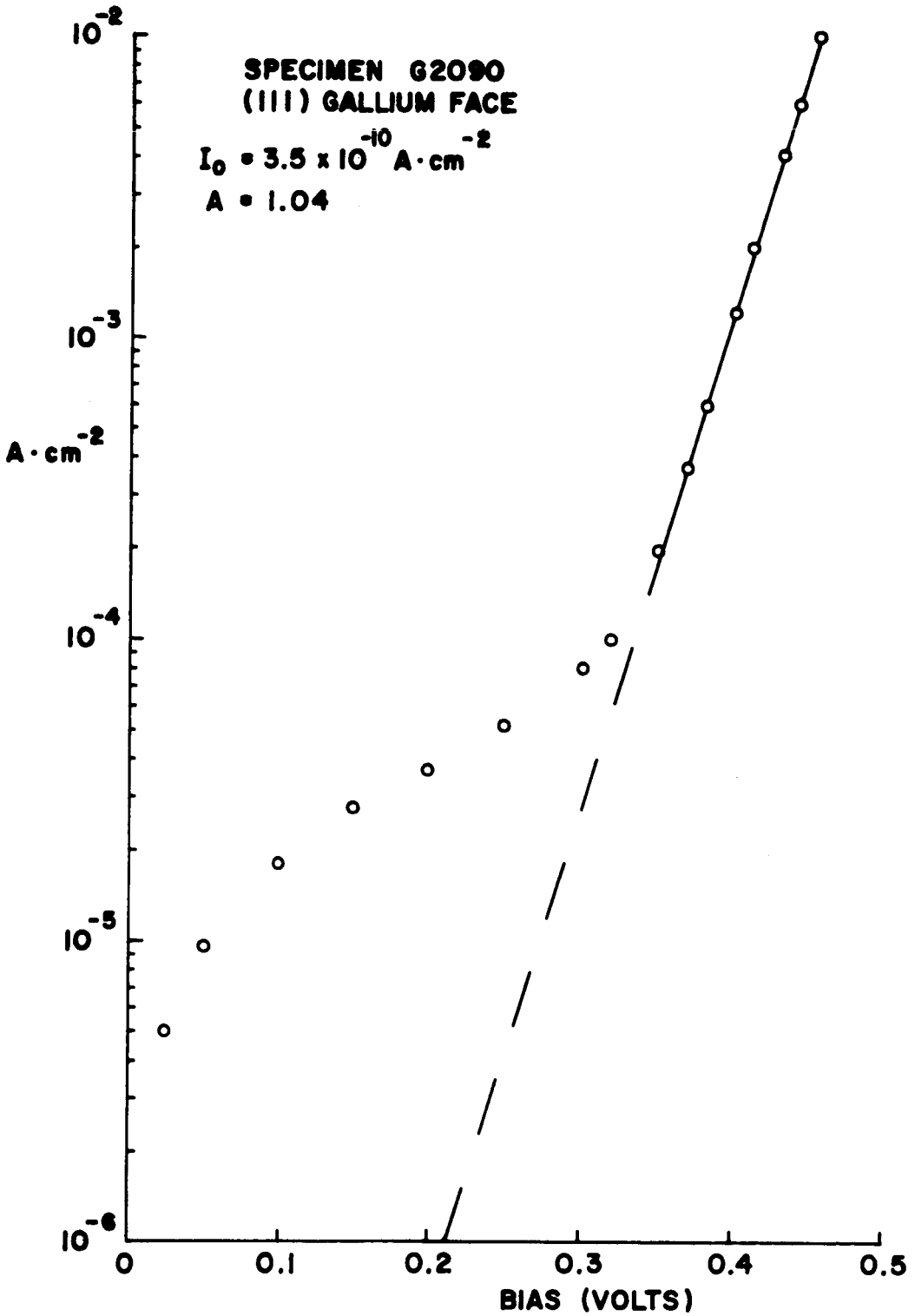

Figure 11. Log (I) as a function of (V) for a cuprous selenide barrier contact to single-crystal GaAs

The single-crystal solar cells were evaluated under 100 mW · cm^{-2} equivalent tungsten illumination to determine V_{oc} under normal testing conditions. Table IV summarizes the results of these experiments. Included also in the table are values of the shallow donor concentration (N_d), the deep donor or trap concentration (N_d'), the diffusion voltage V_d at t = 0 when available, the carrier density (N) and the crystal orientation and dopant.

As indicated by the results in the table the values of V_{oc} obtained on the Ga face (111) oriented single crystals is generally higher than that obtained on the other faces. This result indicates that the etch treatments which have been used are preferential to the (111) Ga face and does not eliminate the possibility that other etchants would maximize the open-circuit voltage on another face. These results are further discussed in Section VI.

B. POLYCRYSTALLINE GaAs-Cu_2Se BARRIERS

During evaluation of the modified growth process it was noted that a correlation existed between the ratio of "wet" to "dry" hydrogen entering the furnace, and the characteristics of the solar cells made from the films. In general, the series resistance (R_s), short-circuit current density (I_{sc}), and shunt resistance (R_{sh}) of the cells increased with increasing water vapor content in the ambient gas.

To obtain an understanding of this effect, small-area (1-mm^2) Cu_2Se barriers were evaporated onto GaAs films, which were grown under the conditions which yielded cells having the efficiency distribution described in Section IV. Both differential capacitance and I-V measurements were made on these barriers.

The results of the differential capacitance measurements were similar to those obtained on the small-area single-crystal barriers inasmuch as a deep donor or electron trap was detected. In this case the center is believed to be a deep electron trap associated with the oxygen impurities introduced into the GaAs films during the growth process. This hypothesis is supported by the work of Williams[6] who studied the properties of a deep neutral electron trap in single-crystal GaAs which he believed to be associated with oxygen impurities. The increases in short-circuit current, series resistance, and shunt resistance with increasing oxygen content in the ambient gas would result from the compensating effect of the traps in the GaAs films.

Interpretation of the C-V measurements indicated that the electron trap was present in a concentration which was comparable to, but less than, the shallow-donor concentration. A typical result obtained during this period is shown in Figure 12. The depletion region width, d_o, was determined from the zero bias capacitance by the relation

$$d_o = \frac{\epsilon \epsilon_o}{C} \qquad (5)$$

TABLE IV

RESULTS OF DIFFERENTIAL CAPACITANCE MEASUREMENTS ON SINGLE-CRYSTAL GaAs

Crystal	Orientation	Dopant	N (cm^{-3})	N_d (cm^{-3})	N_d' (cm^{-3})	V_d (volts)	V_{oc} (volts)
G 838-1	100	Te	$1\text{-}4\times10^{17}$	4.7×10^{17}	-	1.24	0.710
G 838-1	100	Te	$1\text{-}4\times10^{17}$	4.1×10^{17}	-	1.25	0.674
G 838-2	100	Te	$1\text{-}4\times10^{17}$	-	-	-	0.530
G 838-2	100	Te	$1\text{-}4\times10^{17}$	-	-	-	0.677
G 636	110	Te	$1\text{-}4\times10^{16}$	4.7×10^{16}	1.7×10^{16}	1.09	0.732
G 636	110	Te	$1\text{-}4\times10^{16}$	3.4×10^{16}	1.4×10^{16}	1.09	0.721
G 929-1	111Ga	Sn	$5\times10^{15}\text{-}3\times10^{16}$	4.7×10^{16}	2.1×10^{16}	1.00	0.770
G 929-1	111As	Sn	$5\times10^{15}\text{-}3\times10^{16}$	4.6×10^{16}	1.8×10^{16}	0.98	0.721
G 929-2	111Ga	Sn	$5\times10^{15}\text{-}3\times10^{16}$	-	-	-	0.750
G-2090	111Ga	Ge	$1\text{-}2\times10^{16}$	1.0×10^{17}	1.0×10^{16}	1.05	0.658
G-2090	111Ga	Ge	$1\text{-}2\times10^{16}$	8.5×10^{17}	0.7×10^{16}	0.98	0.448
G-881	111Ga	Ge	5.2×10^{16}	-	-	-	0.750

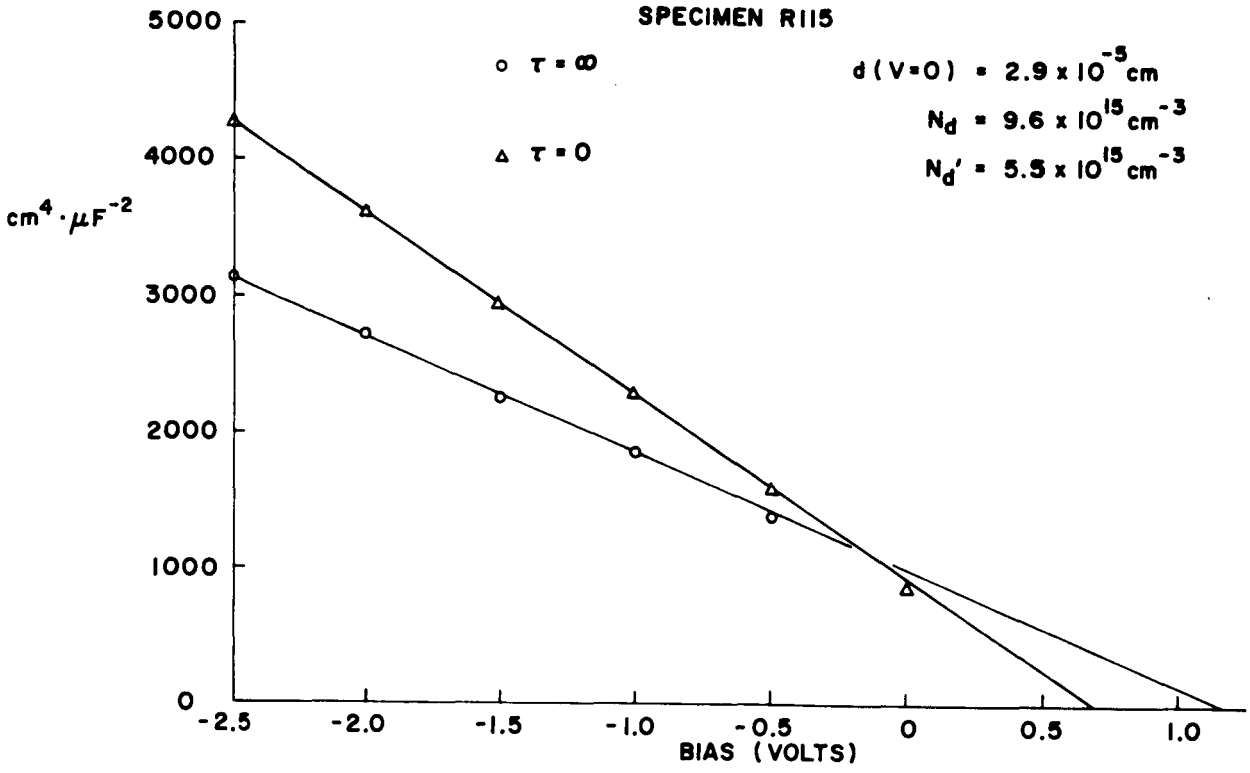

Figure 12. $(1/C^2)$ as a function of (V) for a cuprous selenide barrier contact to a polycrystalline GaAs layer

The highest value of d_o obtained at the center of a GaAs film was 0.29 μm. This can be used in a calculation of the expected short-circuit current, assuming:

(a) All carriers generated in the depletion region are collected.

(b) Minority-carrier diffusion governs the collection efficiency for electron-hole pairs created outside the depletion region.

Such a calculation shows that the experimental I_{sc} values which are observed are reasonable. This point is discussed further in Section VI.

The current-voltage characteristics of these small area barriers were examined in the range 10^{-6} to 10^{-1} A · cm^{-2}. A typical result is shown in Figure 13. Values of A and I_o obtained on these films varied between 3.1 - 3.5 and 2-10 x 10^{-6} A · cm^{-2}, respectively.

In order to better establish the effect of the ambient H_2 gas water vapor content on the GaAs films a series of films were grown under conditions in which all parameters except the water vapor content of the hydrogen were kept as nearly constant

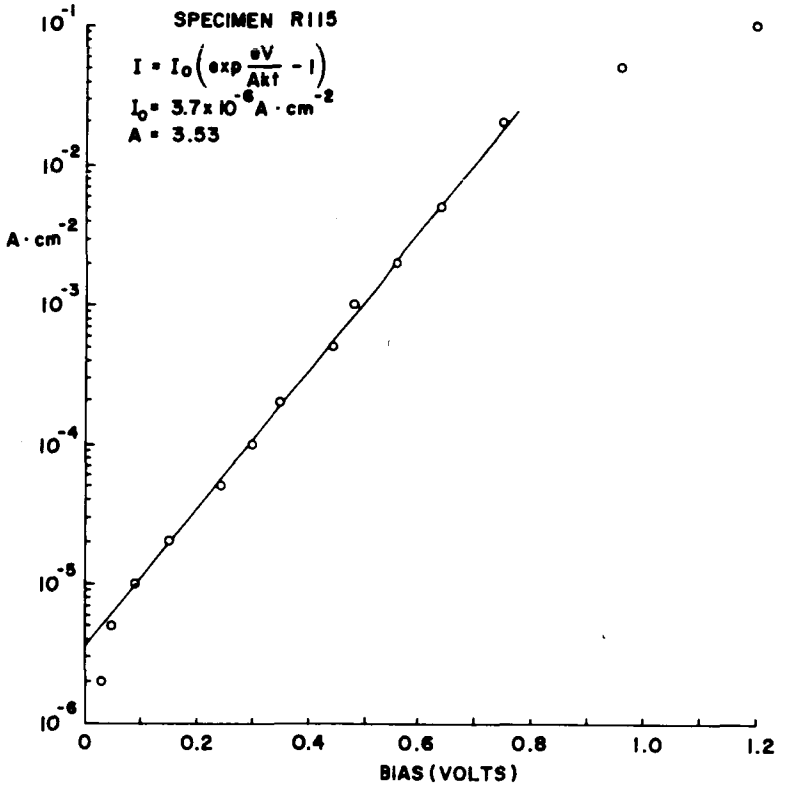

Figure 13. Log (I) as a function of (V) for a cuprous selenide barrier contact to a polycrystalline GaAs layer

as possible. The GaAs single-crystal source was n-type Ge-doped material containing 8×10^{16} -2.0×10^{17} electrons cm^{-3}. The source was (111) oriented with the Ga face toward the InAs-Al substrate. The results of both differential capacitance and I-V measurements made on small area Cu_2Se barriers which were evaporated onto these films are summarized in Table V. These results are consistent with the model of oxygen behaving as a deep trap or compensator in the films, the concentration and effect being related to the growth environment. Thus, as the oxygen content of the H_2 ambient increases:

1. the net donor density decreases,
2. the depletion region width increases,
3. the reverse bias breakdown voltage V_b increases, and
4. the trap density increases to a measurable quantity.

The effect of the increase in oxygen on both the reverse saturation current I_o, and the constant in the exponent in the diode equation (as shown in Table V) is not wholly understood.

TABLE V

RESULTS OF DIFFERENTIAL CAPACITANCE MEASUREMENTS ON Cu_2Se BARRIER CONTACTS TO POLYCRYSTALLINE GaAs FILMS

Film	Ratio of "wet" to "dry" H_2	N_d^* cm^{-3}	N_d' cm^{-3}	d_o μ m	V_d volts	I_o $A \cdot cm^{-2}$	A	V_b volts
R-198	1 : 2	5.4×10^{17}	-	0.053	1.20	2.6×10^{-6}	2.81	1.25
R-205	1 : 1	3.6×10^{17}	-	0.068	1.40	1.0×10^{-6}	2.40	1.7
R-202	2 : 1	1.31×10^{17}	2.0×10^{16}	0.085	0.80	2.0×10^{-7}	2.20	3.1
R-201	2 : 1	2.5×10^{16}	1.2×10^{16}	0.23	1.30	6.0×10^{-7}	2.78	7.1

*Because of the nature of the electron trap the donor concentration N_d obtained from the C^{-2} versus V relation at application of the DC bias is the uncompensated shallow donor concentration.

It appears from these data that both parameters pass through a minimum as the degree of compensation increases. The origin of this effect is not clear at this time, and additional experiments of the type described above would be required to substantiate its existence.

SECTION IV

CELL CHARACTERISTICS

A. FABRICATION

1. Processes

Since the processes used in cell fabrication were described in detail in reference (1), a summary only will be given of those processes which have not been altered during the reporting period.

All normal cells were formed on aluminum substrates, the exceptions being a group of six cells made on molybdenum foil for the stability tests. The aluminum foil was nominally 5 μm thick, and was precoated with 3 to 4 μm of InAs by the vapor transport process in a hydrogen ambient, using polycrystalline wafers of InAs as the source material. The thickness of the InAs was checked by weighing the substrate before and after deposition, and the same differential weighing technique was used for determination of the GaAs film thickness. The InAs growth process used hydrogen saturated with water vapor at 0 °C, and a growth rate of 2 μm per hour was normal.

The GaAs was grown on the substrate also by the vapor transport method, using single-crystal GaAs source wafers, with a net donor concentration in the low 10^{16} cc^{-1} range. The water vapor concentration in the hydrogen furnace ambient was controlled using the system described in Section I of this report, and a film growth rate around 0.7 μm per hour was normal.

The GaAs film was etched in a dilute solution of bromine in methanol. This etch acts as a polish and has been found to improve cell stability. Various etches have been used for this step, but it has been found that the Br-methanol solution provides the most consistent results, probably because it is considerably slower than acid etches such as aqua regia or H_2SO_4:H_2O_2 solutions. The stability tests described in Section V established the effectiveness of the Br-methanol etch, and it has been used as a standard process during the present reporting period.

The barrier contact film of cuprous selenide was deposited using the flash evaporation process. The starting material was of stoichiometry $Cu_{1.8}Se$ for the majority of the cells, and the material was prepared in ingot form by the methods described in Section II. The ingots were reduced to particles of 0.25 mm diameter and smaller by crushing prior to evaporation. Control of cuprous selenide film thickness was achieved using the measurement of optical transmission through a monitor film deposited simultaneously on glass, the evaporation being terminated when an indicated transmission of 70% was obtained.

The gold grid was applied to the cells by vacuum evaporation through a metal mask, with a quartz-crystal oscillator film thickness monitor to measure the gold layer thickness. Two grid geometries were used, with differing line-widths and spacings. However, the finer grid-spacing type, which should in principle lead to lower cell series resistance by reducing the effect of the sheet resistance in the barrier contact layer, was not found to lead to lower cell resistance in practice.

The cells were finally trimmed to size using either scissors or a scalpel, cell areas being within the range 0.7 to 1.1 cm^2. At no time were any short-circuits developed in the cells as a result of this cutting operation. Hence, cells were made with the entire cell area active, except for that covered by the grid. In measurements of cell efficiency, the grid area was not subtracted from the cell area.

2. Yield

For most of the contract period, cells were made with continuous small alterations in the processing parameters, such variations being normal and necessary in improving the cell efficiency. However, at various times during the contract, a number of cells were made with a fixed, standard process, sufficient to allow a yield curve for the process to be obtained.

The results of these curves are shown in Figure 14. During the period when these 13 cells were made, no nonworking cells were produced, although very occasionally short-circuited cells were obtained during other periods of the work. These short-circuits arose when abnormally thin GaAs layers (less than 8μm) were used.

B. ANTIREFLECTION COATINGS

1. General Considerations

The appearance of cells made with 70% transmitting Cu_2Se barrier layers has been considerably variable. Surface colorations seen range from the silver-grey characteristic of the untreated GaAs films, through pale-green, dark-green, and purple. The colorations indicate that interference effects are taking place in the barrier layer, and for some of the colors seen there is no doubt that some antireflection effects are present.

To evaluate the possibilities for employing an antireflection coat, the refractive index of the Cu_2Se film material was measured. The technique employed was an adaptation of Tolansky's multiple-beam interference method for measuring film thickness. A specimen was prepared by the usual flash-evaporation technique, on a microscope slide which had been silver-coated prior to the deposition of the Cu_2Se. A mask

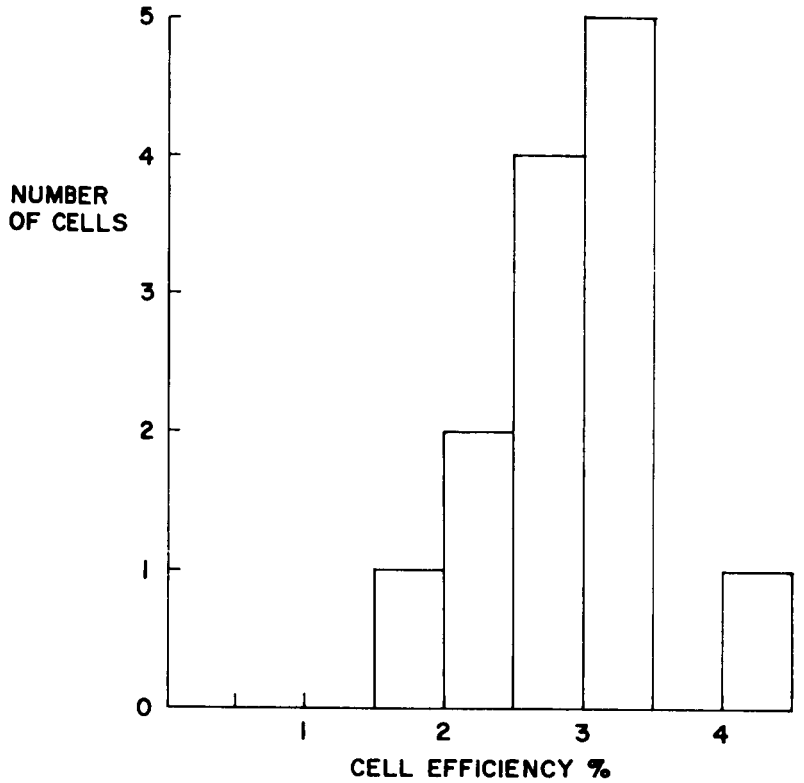

Figure 14. Efficiency distribution for thin-film cells

was employed to create a sharp edge on one side of the Cu_2Se deposit. Half of this specimen was then silvered again, and the usual Tolansky technique used to determine the thickness of the Cu_2Se film. The region of the step without the second (overlying) silver layer was then used to measure the refractive index of the Cu_2Se film. The principle of the method is illustrated in Figure 15; a full exposition has been given by Heavens.[7] The measurements showed a refractive index of 2.4 in a film of about 650-Å thickness.

If the Cu_2Se film were to be used as an antireflection coating alone on GaAs, the geometry would be as shown in cross section in Figure 16(a). The conditions for antireflection in this and the two-layer coating described later are discussed by Holland.[8] For the single-layer case, the well-known result is

$$t_2 = \lambda/4\mu_2 \tag{6}$$

$$\mu_2 = \sqrt{\mu_1 \mu_3} \tag{7}$$

with the symbols as indicated in Figure 16(a). For GaAs, with a refractive index of 3.34, it is seen that the antireflection condition cannot be satisfied by Cu_2Se. It should be noted, however, that it is common experience that some antireflection

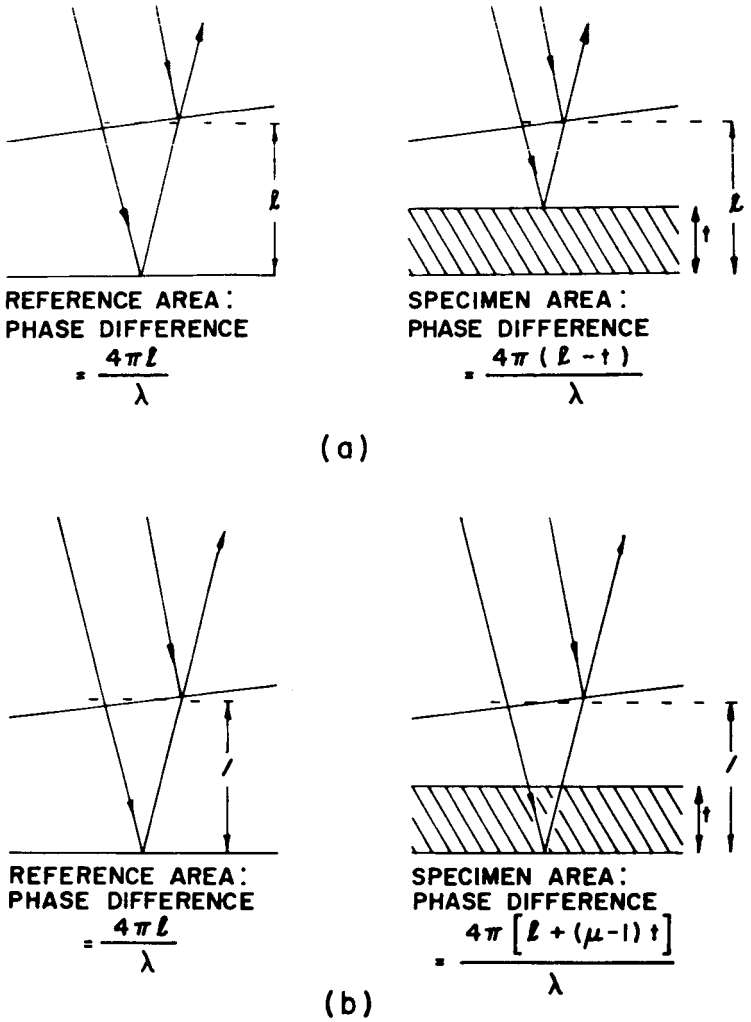

Figure 15. (a) Tolansky multiple-beam interferometry method for measuring film thickness
(b) Multiple-beam interferometry method for measuring film refractive index

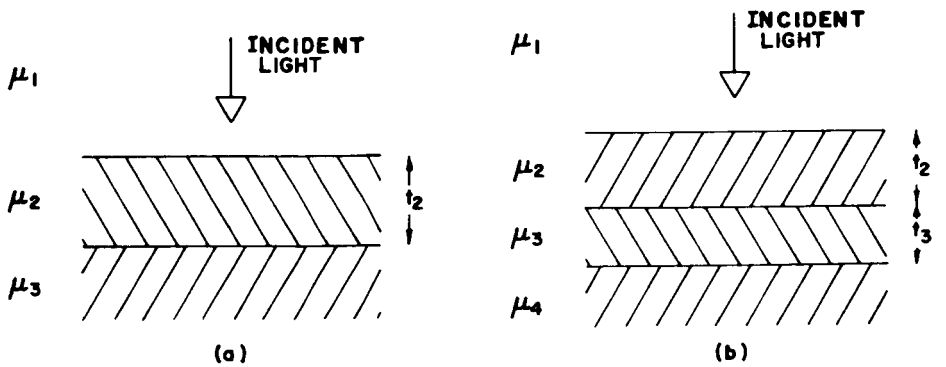

Figure 16. (a) Cross section of single-layer antireflection coating
(b) Cross section of double-layer antireflection coating

effects can be obtained even under conditions not close to the optimum defined by Eqs. (6) and (7). Thus, it is not unreasonable that some antireflection appearance should arise when Cu_2Se is deposited on GaAs, as noted above. One also notes that the thickness of the Cu_2Se films usually deposited to be 70% transmitting (600 Å) comes near the quarter-wavelength condition (560 Å). Small variations in this thickness are presumably the cause of the color changes noted in the introductory paragraph of this section.

To obtain better antireflection conditions, two approaches have been explored, as described below.

2. Two-Layer Antireflection Coatings

A two-layer antireflection coating is shown in cross section in Figure 16(b). The conditions for antireflection are

$$t_2 = \lambda/4\mu_2, \quad t_3 = \lambda/4\mu_3 \tag{8}$$

$$\mu_2 = \mu_3\sqrt{\frac{\mu_1}{\mu_4}} \tag{9}$$

Hence, to satisfy the conditions for light of wavelength 5460 Å, on a GaAs surface:

$$\mu_2 = 1.31$$

$$t_2 = 1000 \text{ Å}$$

$$t_3 = 564 \text{ Å}$$

An optical coating material with $\mu_2 = 1.3$ is MgF_2. Facilities were established for the vacuum deposition of this material, and as a preliminary evaluation of the effectiveness of the coating, two cells on one single-crystal GaAs slice were made. These had a Cu_2Se film thickness of 560 Å, and the cell characteristics were measured. 1000 Å of MgF_2 was then deposited on one of the cells, and the characteristics were again measured. The results showed that the I_{SC} was improved by 28% on the test cell, whereas the control cell current remained the same within measurement error.

Following this initial success, quarter-wavelength MgF_2 coatings were evaporated onto several thin-film cells. Efficiency measurements were made before and after the deposition. Typical results are shown in Table VI. In each case it is seen that an increase in I_{SC} was obtained, but that a smaller proportional efficiency increase was seen because of loss in fill-factor and V_{OC}. These losses were larger

TABLE VI

RESULTS OF MgF_2 ANTIREFLECTION COAT ON THIN-FILM GaAs CELLS

Before A-R Coat				After A-R Coat		
Cell #	V_{oc}	I_{sc}	Power	V_{oc}	I_{sc}	Power
1	0.43V	9.0mA	1.94mW	0.43V	9.6mA	2.04mW
2	0.44V	11.0mA	2.46mW	0.43V	11.8mA	2.40mW

in earlier experiments, and were found to be much reduced by the provision of heat shields around the evaporation source to minimize the rise in temperature of the cell during the MgF_2 deposition. However, the losses could not be eliminated, and the gains in I_{sc} were much smaller than would be expected.

Because of this lack of effectiveness, an experiment was performed in which I_{sc} was monitored continuously while the MgF_2 coating was being deposited. This was done using a cell with a completed barrier-layer and grid, illuminated at very close to normal incidence by a mirror and microscope lamp. MgF_2 film thickness was monitored using a quartz-crystal film-thickness monitor, and an x-y plotter was used to provide a curve showing I_{sc} as a continuous function of film thickness. The experimental arrangements are shown schematically in Figure 17(a), and the results in Figure 17(b). As is seen from the curve, the maximum in I_{sc} occurs a little to the high side of the expected region of film thickness, but again the actual improvement in I_{sc} is very small indeed.

The extra thickness of MgF_2 indicated as optimum by this experiment is thought to arise from two causes:

(a) The polycrystalline surface of the thin-film cells has an effective area considerably greater than the geometrical cell area, as was shown by the sectioning experiments described in Section I of this report.

(b) The spectral distribution of the illumination was such as to favor wavelengths longer than the 5460 Å for which the optimization calculation was performed.

Two reasons may be advanced for the poor performance of the antireflection coat:

(a) The rough surface of the thin-film cells has antireflection properties of its own. This argument is apparently disproved by the positive results obtained with the single-layer coating described below.

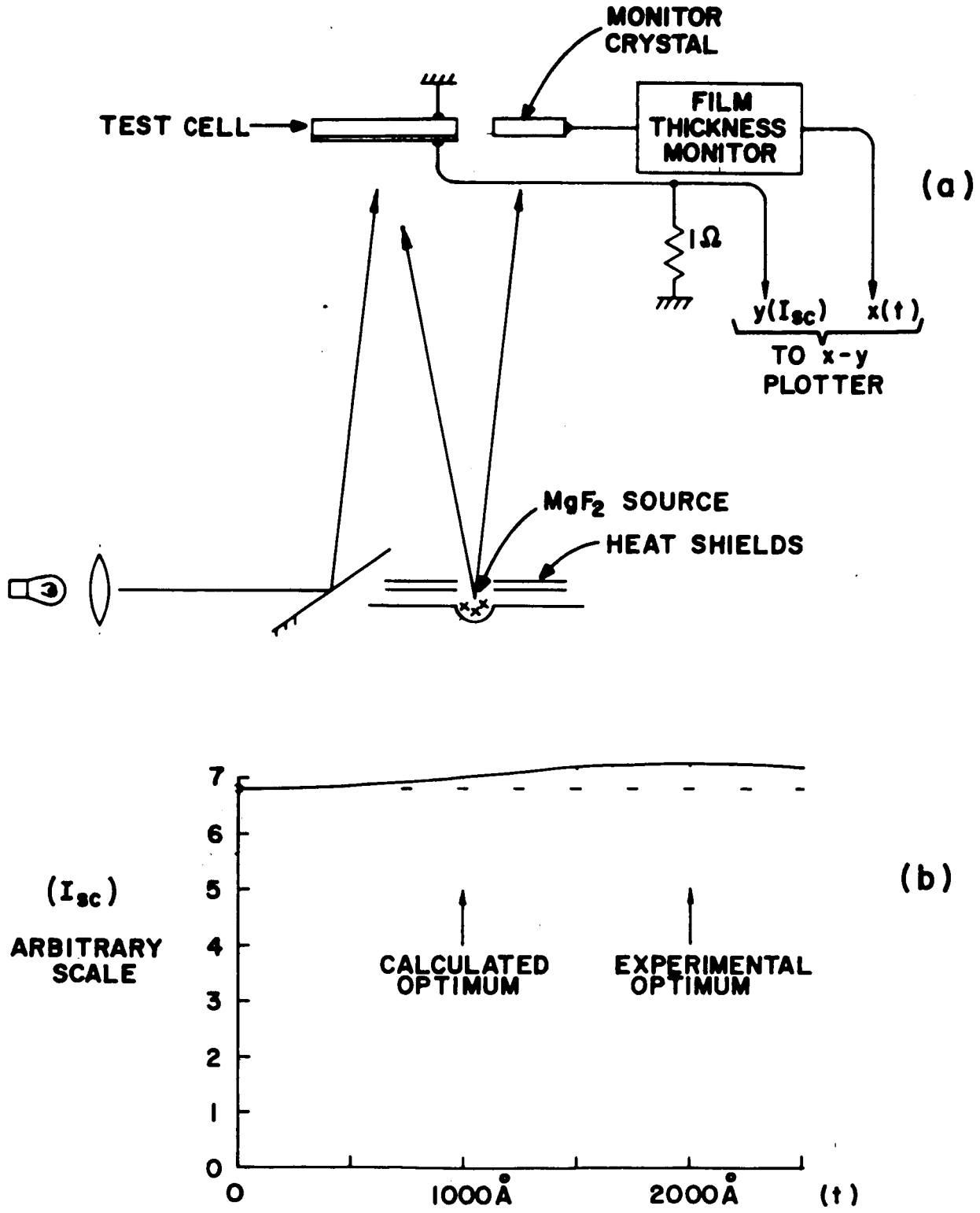

Figure 17. (a) Experimental arrangement for monitoring I_{sc} as a function of t
(b) I_{sc} as a function of MgF_2 thickness for a thin-film cell

(b) The Cu_2Se film absorbs strongly in the spectral region for which the antireflection effect was optimized. The positive result from the single-crystal cell experiment appears to run contrary to this argument.

It is felt that the results which were obtained may have arisen from combinations of these effects, together with other factors, such as reactions between the MgF_2 and the Cu_2Se. In view of the positive results obtained with the simpler coating described below, it did not appear profitable to pursue the matter further.

3. Single-Layer Antireflection Coatings

The results with measurements on cell characteristics as a function of Cu_2Se film thickness (Section IV.C.), and the optical data on Cu_2Se films (Section II), indicated that a cell with improved characteristics could be achieved by using a very much thinner Cu_2Se film than had been used in the past.

Now if this Cu_2Se were to be made much less than 1/4 wavelength thickness, it could be neglected in calculating the requirements for an antireflection coat, which would then in effect be applied to the GaAs surface. The requirements for this coating are as discussed above and given by Eqs. (6) and (7).

For GaAs ($\mu_3 = 3.34$), a suitable coating material is silicon monoxide SiO, with a refractive index of 1.97, which is not optimum, but is near enough for practical purposes. Experimental arrangements for vacuum deposition of this material were accordingly made.

Two thin-film cells were prepared with thin (95% transmitting) Cu_2Se layers. The thickness of these layers was measured, using monitor specimens deposited simultaneously on glass, by the Tolansky technique. An indication only of the thickness could be obtained, because with the simple preparation and measuring arrangements used, the film thickness was close to the limit of the method. The Cu_2Se film thickness was 100 ± 20 Å. The cells were completed with a gold grid, and their characteristics measured. On depositing the calculated required thickness of SiO on one cell, a good deep-blue coloration was obtained, and the I_{SC} improved by 24%, with a smaller improvement in efficiency (12%): the curves are reproduced in Figure 18. It is seen that losses in both V_{OC} and fill-factor occurred, and it is thought that these arose from heating of the cell during the SiO deposition.

An experiment similar to that performed on the MgF_2 antireflection coating, in which I_{SC} was plotted as a function of layer thickness, was performed using the second cell. The result is plotted in Figure 19, and it is seen that for this cell an I_{SC} increase of 33% was obtained.

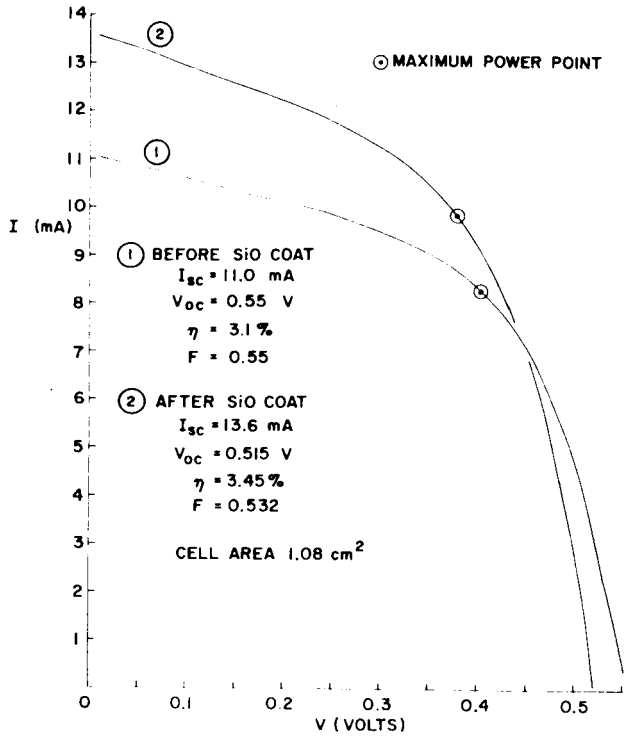

Figure 18. I-V curves of a thin-film cell before and after deposition of SiO antireflection coating

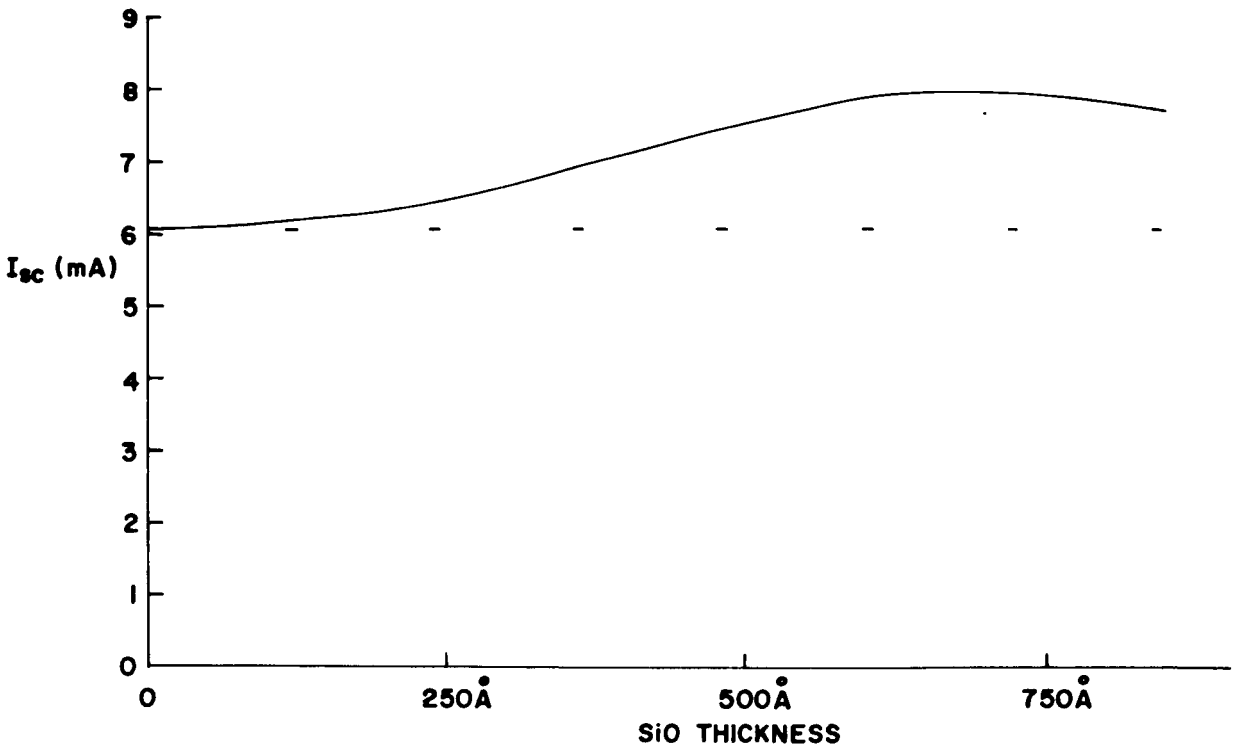

Figure 19. I_{sc} as a function of SiO thickness for a thin-film cell

4. Conclusions

Termination of effort under this contract prevented further experimental evaluation of this approach. However, it is felt that the work has demonstrated the feasibility of a promising method for improving cell efficiency. It should also be noted, however, that the short-circuit current in the cells is a sensitive function of the details of the structure of the depletion region at the cell surface. Thus, several of the most efficient cells made during the work have shown higher I_{SC} densities than those obtained in the cells having an antireflection coat. Since the occurrence of the high collection efficiency cannot be controlled completely at the present stage of the work, it is not surprising that it was not obtained with either of the cells having SiO coatings.

C. OPERATING CHARACTERISTICS

1. General Considerations

In this section of the report are discussed two groups of experiments in which factors bearing on the series resistance of the cells were examined. The simplest equivalent circuit of a photovoltaic cell is shown in Figure 20. The shape of the operating characteristic in a cell of reasonable efficiency is, of course, dominated largely by the diode characteristic. For the present cells, experimental work on this has been reported in Section III. The reverse characteristics have also typically shown low shunt conductance in the cells, and this factor has not been examined in detail. However, appreciable effects of series resistance, R_S, are frequently seen in the cells. Since loss in efficiency can quickly result from even small amounts of series resistance, as was shown by the work of Wysocki,[9] it was felt to be important that these effects be examined closely.

In the present cell structure, series resistance can be associated with the following regions:

(a) The substrate-to-GaAs interface: this is minimized, though not entirely eliminated, by the InAs intermediate layer.

(b) The bulk of the GaAs: may arise either from conduction across grain boundaries, or from true bulk resistance effects in the crystallites.

(c) The Cu_2Se barrier layer: the sheet resistivity of the layers is low compared with most semitransparent films, but cannot be neglected. The collector grid is intended to minimize this effect.

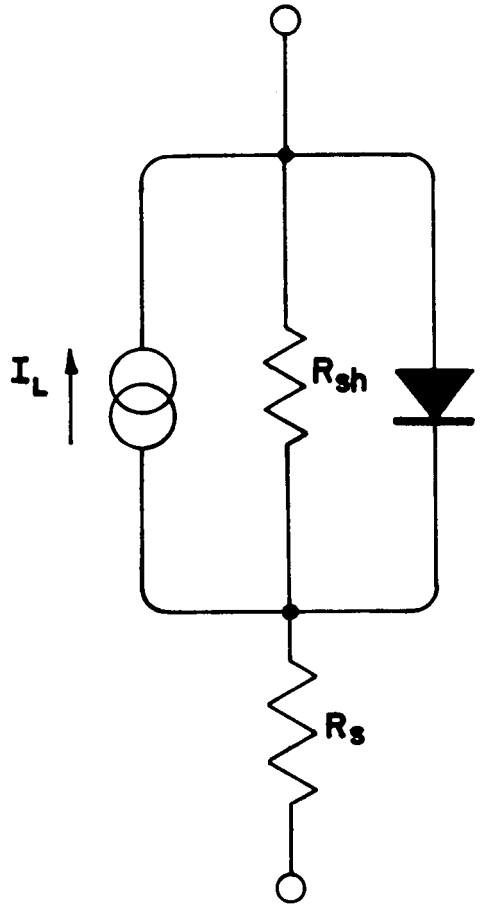

Figure 20. Equivalent circuit of a photovoltaic cell

(d) Gold grid, and cell contacts: losses in these can be made very small compared with those in other resistances present.

Two groups of experiments have been performed, one pertaining to (b) above, the other to (c).

2. GaAs Resistivity Effects

A typical thin-film cell I-V characteristic is reproduced in Figure 21(a). It will be noted that the curve shape is "rounded", compared with that of a barrier-layer cell on single-crystal GaAs, shown in Figure 21(b). Since the Cu_2Se layer and grid structures were identical for these two cells, it was concluded that the rounded effect in the thin-film cell was arising from series-resistance effects in the GaAs film.

Now the effect of adding increasing values of R_S in the simple cell equivalent-circuit of Figure 20 can be simulated by using a variable external series resistance with a conventional silicon cell. This was done, and a family of I-V curves were generated and are shown in Figure 21(c). It was clear that none of these curves looked like those obtained with the thin-film cell.

Occasionally, thin-film cells have been seen with a characteristic showing two breakpoints, as reproduced in Figure 21(d). Analysis showed that a curve of this type could be simulated using two silicon cells in the circuit shown in Figure 22(a). The I-V curve reproduced in Figure 21(e) was obtained with such a circuit, using two silicon cells. The agreement with the analysis is seen to be good.

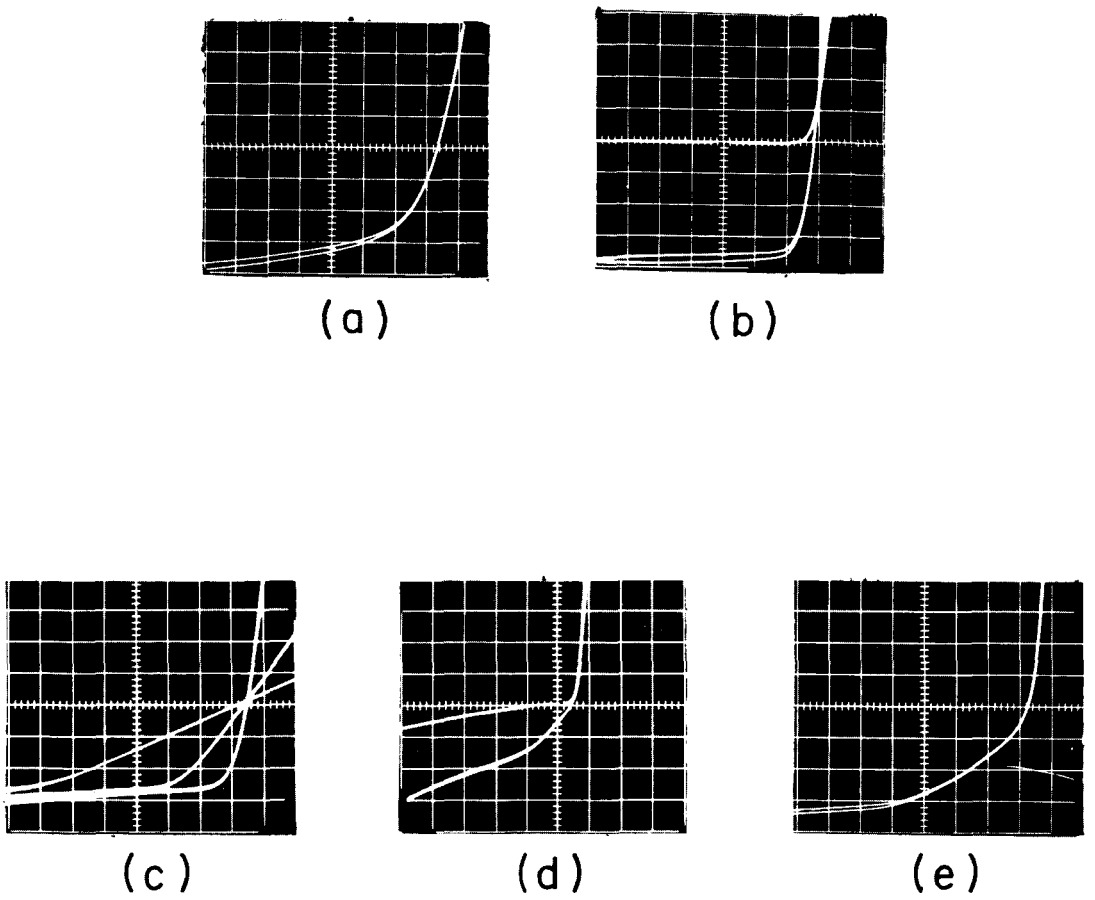

Figure 21. (a) I-V characteristic of a typical thin-film cell
(b) I-V characteristic of a barrier cell on single-crystal GaAs
(c) Family of I-V curves, showing effect of increasing values of R_S
(d) I-V characteristic of a thin-film cell, showing two breakpoints
(e) I-V characteristic obtained from silicon-cell circuit giving two breakpoints

From these results, it is concluded that the rounded I-V characteristics of the thin-film cells can be accounted for by nonuniformity of resistivity of the GaAs over the cell surface. Such a nonuniformity would lead to a distributed equivalent circuit being needed for cell analysis, as is shown in Figure 22(b). With a range of series-resistance values present, multiple breakpoints would occur in the I-V characteristic, leading to the rounded shape of the curve seen for most cells. The occasional curve of the type in Figure 21(d) arises when only two well-defined areas of different effective series resistance values happen to occur in a cell, with comparable I_L values in the two regions. The effect of this on cell performance is further discussed in Section VI.

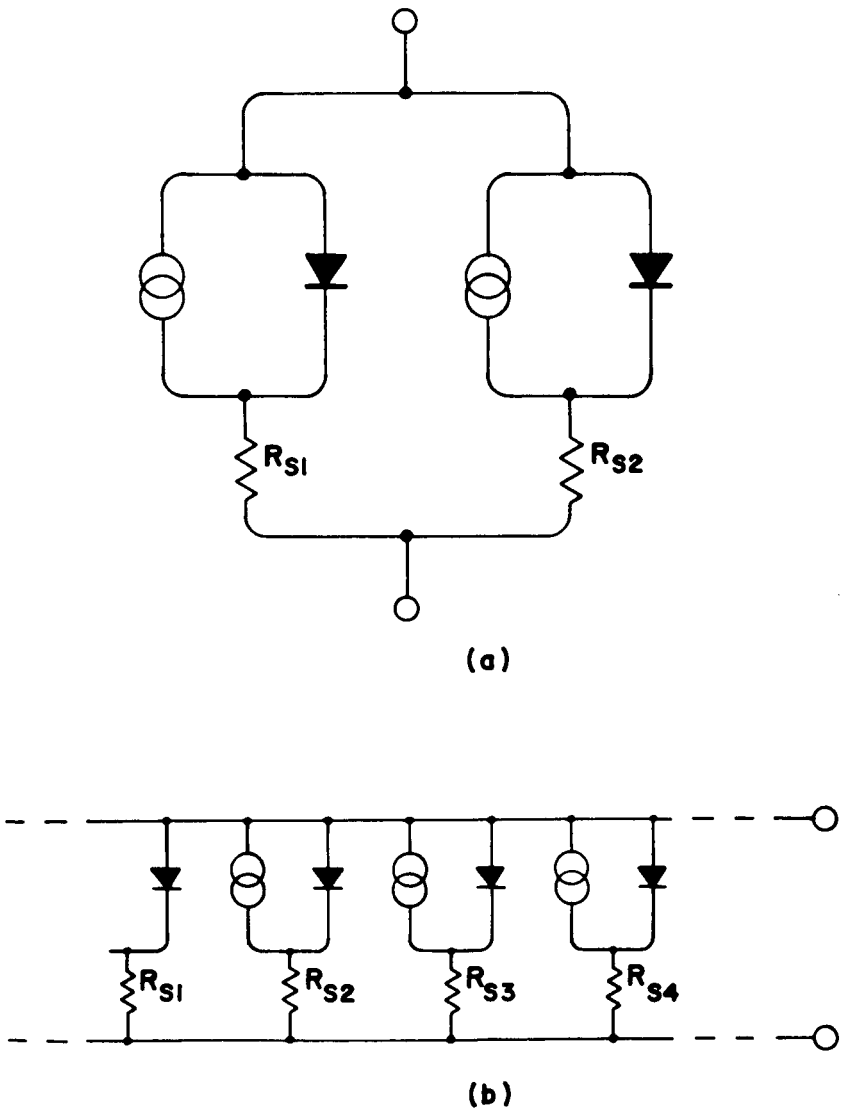

Figure 22. (a) Equivalent circuit of cell, giving characteristic with two breakpoints
(b) Distributed equivalent circuit of thin-film cell

3. Cu_2Se Film Resistivity Effects

Two experiments were performed to discover the effect on cell performance of the use of Cu_2Se films of various thicknesses.

A gold grid was deposited directly on the surface of a GaAs film, and the photovoltaic response was measured. The gold provided a good blocking contact to the GaAs surface, but the photocurrent available was very small (about 200μA). The film was mounted in a vacuum system, with external connections and an illumination system essentially similar to that shown in Figure 17(a). In this case, however, the x-y recorder was used to plot I_{SC} as a function of Cu_2Se film thickness. The resulting curve is shown in Figure 23. It is seen that a good I_{SC} value is achieved very rapidly once the film thickness has exceeded an indicated 10 Å, implying that the Cu_2Se film achieves coherency very rapidly indeed. The maximum in I_{SC} is also seen to be broad, in the range 150 to 180 Å.

The rapidity with which I_{SC} was found to rise was unexpected. A second experiment was performed to check on this, using the same type of specimen and equipment. However, rather than recording only I_{SC}, total I-V curves were obtained in between the sequential deposition of increments of Cu_2Se film thickness. In this way, some estimate could be made of the variation of cell series resistance with Cu_2Se film thickness. Some of the results obtained are shown in Figure 24. The first picture (a), shows both the illuminated and unilluminated curves for the grid-GaAs contract. The photocurrent is so small that the curves are superimposed. In (b) are shown the illuminated and unilluminated curves for a cell with Cu_2Se film thickness of 70 Å, and (c) shows the same cell with 500 Å of Cu_2Se. The film optical transmission values were 92.5% and 70.9% for the two cells, respectively, as measured on a specimen film deposited simultaneously on glass.

This experiment confirmed the result obtained previously, and also showed that Cu_2Se films with thicknesses greater than 70 Å did not reduce significantly the cell series resistance, the slope of the I-V curve in (b) and (c) being the same at high forward bias voltage values. The results from the two experiments also showed that increasing the thickness of the Cu_2Se film in the range 90% to 70% optical transmission did not change the I_{SC} value by a corresponding amount. It is possible that the Cu_2Se film acts as an antireflection coat in this thickness range, so as to partially compensate for increasing absorption in the film.

The primary conclusion drawn from these results was that thinner Cu_2Se films could be used without materially affecting the cell performance, though there would be negligible advantage per se in doing so. This conclusion was used in proposing the SiO antireflection coating described earlier in this Section.

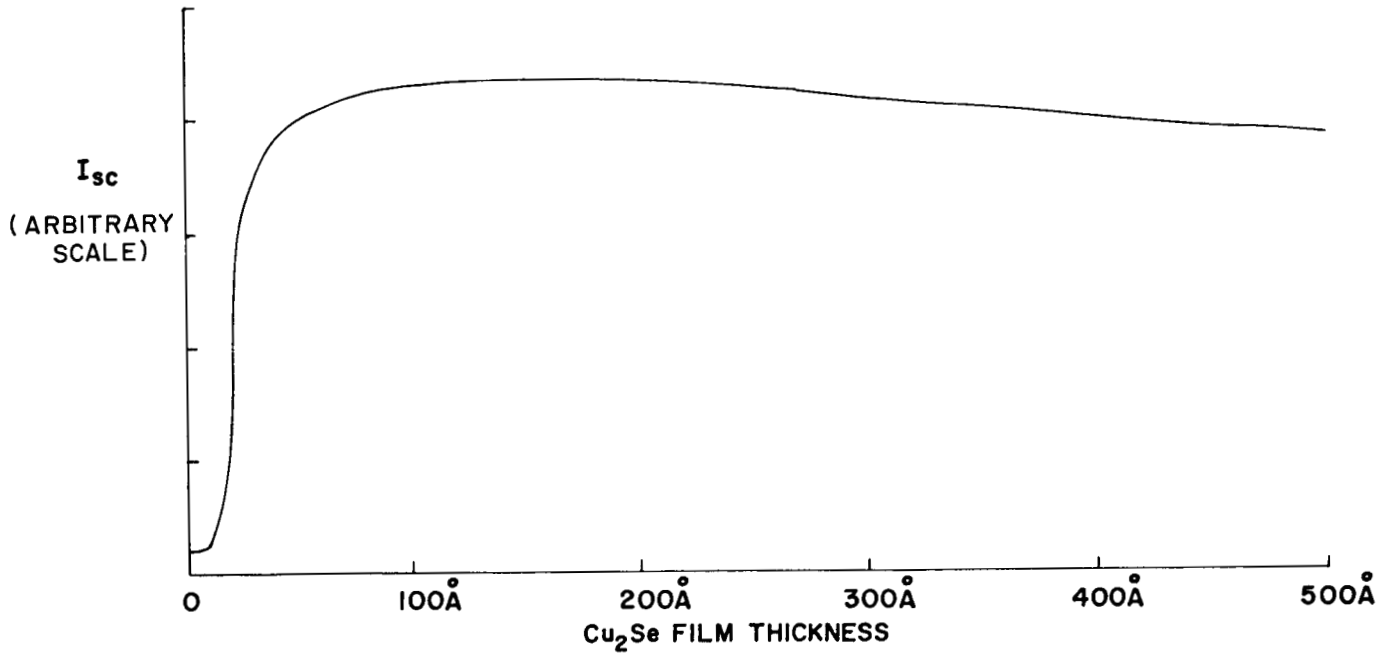

Figure 23. I_{sc} as a function of Cu_2Se film thickness

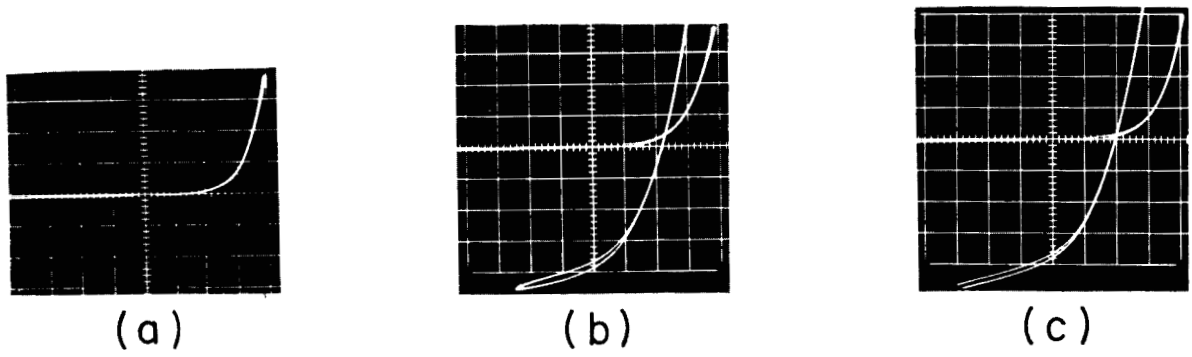

Figure 24. (a) I-V curves for grid-GaAs contact
(b) I-V curves for cell with Cu_2Se thickness of 70 Å
(c) I-V curves for cell with Cu_2Se thickness of 500 Å

D. SPECTRAL RESPONSE

1. Measurement Technique

Since spectral response measurements can be of great diagnostic and analytical value, a considerable number of such measurements have been made during the reporting period.

The equipment used is unique, in that it enables measurements to be made with a constant illumination intensity falling on the cell under test, but maintains a constant resolving power throughout the spectral range. Rather than using the analyzer slit width in the monochromator to control the illumination, an optical wedge (a continuously variable neutral density filter) is used. The equipment provides a continuous recording of cell I_{SC} as a function of illumination photon energy, at constant illumination. A computer then converts this recording to normalized quantum yield.

2. Results: Short Wavelength Cut-Off

The normalized spectral response curve for a typical cell is shown in Figure 25, along with a curve for another thin-film cell made with a thin platinum film in place of the Cu_2Se film in the test cell. The differences between the curves are noticeable. At the high-energy end, the Cu_2Se cell response drops more rapidly, and this portion of the curve was found to be highly reproducible. In particular, the same sharp cut-off was seen for cells in which an antireflection coat was used, implying that the effect was not due to interference in the Cu_2Se film.

The optical measurements on Cu_2Se films, showing the transmission as a function of wavelength, revealed the cause for the rapid drop in cell response beyond 5500 Å.

As discussed in Section II, absorption in the Cu_2Se increases rapidly at wavelengths shorter than 5500 Å, which correlates well with the observed cell performance, and it is concluded that the shape of the spectral response curve in this region arises from optical absorption in the Cu_2Se film. This was confirmed by the results shown in Figure 26, which show the spectral response curves obtained from cells made with barrier layers of various thicknesses. It is seen that the blue response of the cells is progressively lost as the Cu_2Se film thickness increases.

3. Results: Long Wavelength Cut-Off

The curve for a Cu_2Se cell shown in Figure 25 shows anomalous behavior over the wavelength region 6000 to 8500 Å. The response of the Pt-film cell is much closer to what is expected from a cell of the barrier type, with a broad response maximum

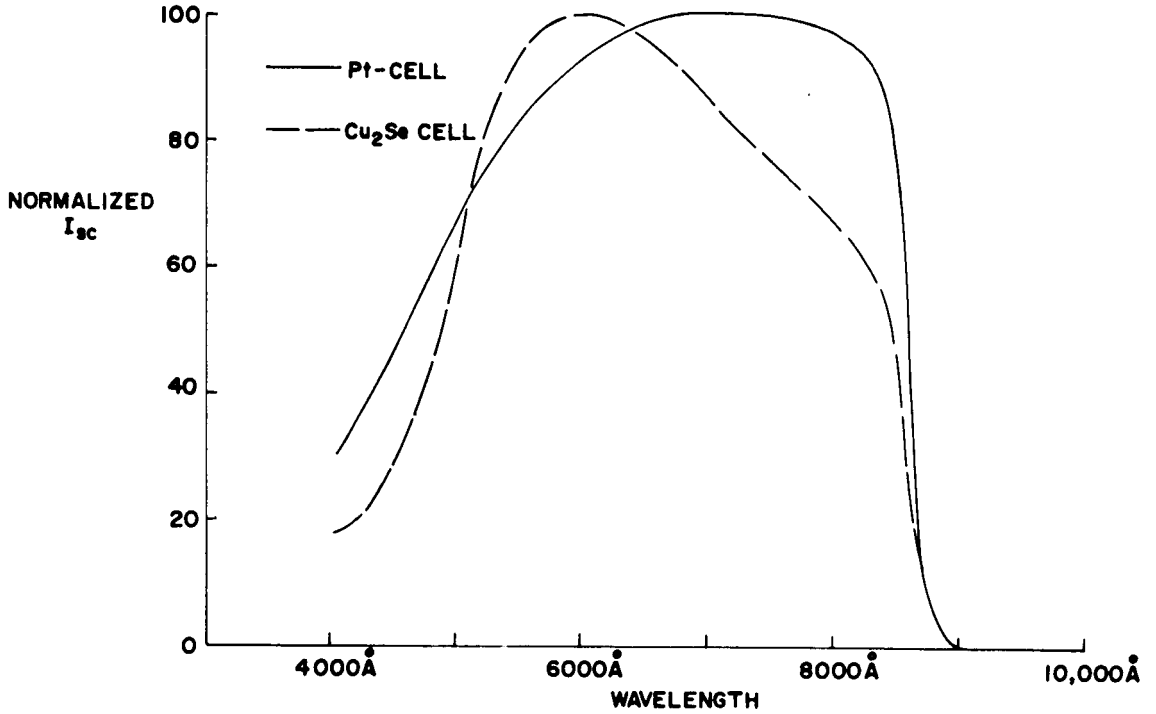

Figure 25. Spectral response for thin-film cells with Pt and Cu_2Se barriers

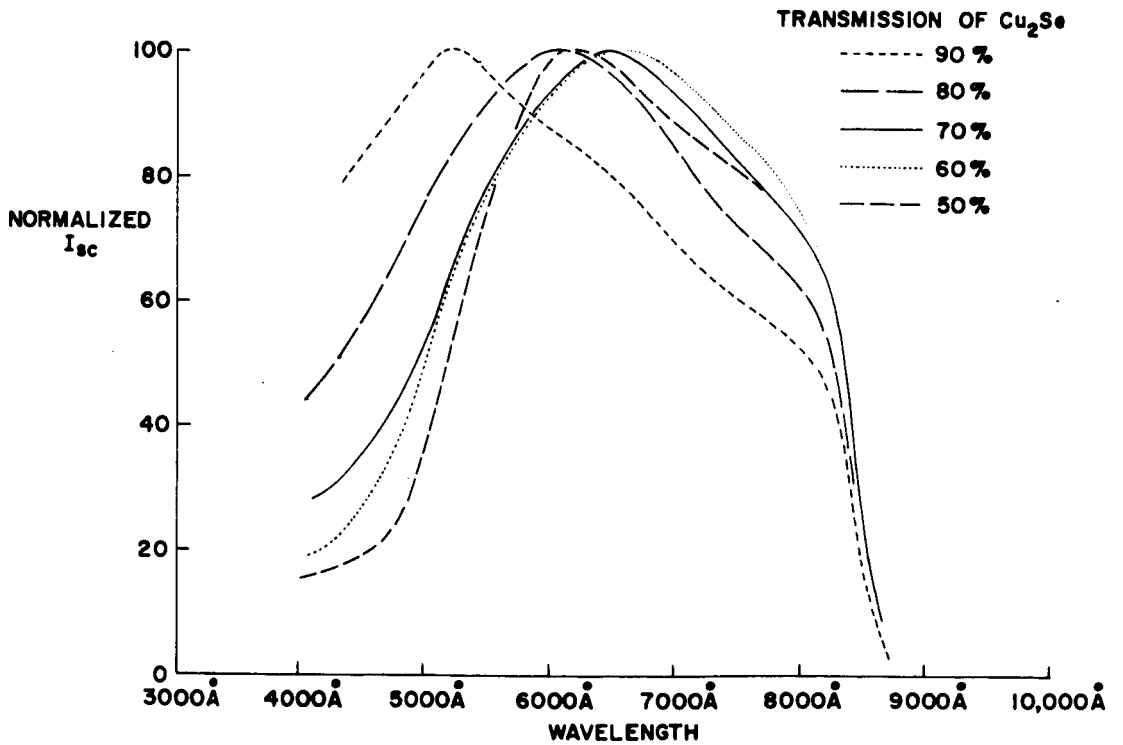

Figure 26. Spectral response of a Cu_2Se barrier cell on single-crystal GaAs, with progressive thickness increments of Cu_2Se

at wavelengths somewhat shorter than the band-edge for the GaAs. An explanation of this anomaly appeared desirable, especially since the possibility appeared to exist that the peak at 6000 Å may have been due to the Cu_2Se film playing an active part in the cell operation. However, a more likely explanation was optical interference in the Cu_2Se causing an antireflection effect of increasing effectiveness through the range 8500 to 6000 Å. To check on these hypotheses, three groups of experiments were performed.

In Figure 26 are shown a group of spectral response curves obtained from a cell made on a single-crystal wafer of GaAs, by deposition of successive increments of Cu_2Se. It is seen that the behavior of the curves in the region of wavelengths between the band-edge and the response peak, and the position of the peak itself, is strongly dependent on the Cu_2Se film thickness. This is consistent with the effects in this region being caused by optical interference in the Cu_2Se film.

As a test of the alternative hypothesis, that the Cu_2Se was contributing actively to the cell output, a group of spectral response measurements were made on cells made on silicon single-cyrstal wafers. These are shown in Figure 27, the curves being for cells with the following structures:

(a) A regular diffused junction n-p cell.

(b) A barrier-layer cell with a 70% transmitting evaporated platinum film.

(c) A barrier-layer cell with a 70% transmitting evaporated Cu_2Se film.

Since the index of refraction for Si is close to that for GaAs, it would be expected that any optical interference effects would be comparable in the Cu_2Se cells made on Si and GaAs. However, because the intrinsic response for the silicon extends to longer wavelengths than that for GaAs, any interference filter effects should be visible over a wider wavelength range. This is in fact the case, as is shown by the curves of Figure 27. The response curve for the Cu_2Se-Si cell with a 70% transmitting Cu_2Se film is seen to peak at the same wavelength as does that of the similar Cu_2Se-GaAs cell shown in Figure 26, which confirms that the effects giving rise to the sloping response between the band-edge and the peak response are due to an interference filter action in the Cu_2Se film.

As a final, direct check on the hypothesis that a varying reflectance from the cell was the mechanism giving rise to the slowly rising curve between the band-edge and the peak response, the diffuse reflectivity of the cell was measured as a function of wavelength. The results are shown in Figure 28, as obtained from a cell made on polycrystalline GaAs by deposition of a 70% optically transmitting film of Cu_2Se.

A calculation was then performed to predict the cell spectral response over a limited range, under the assumption that the quantum efficiency per photon absorbed in the GaAs was constant over the spectral range of interest. Thus, the change in response

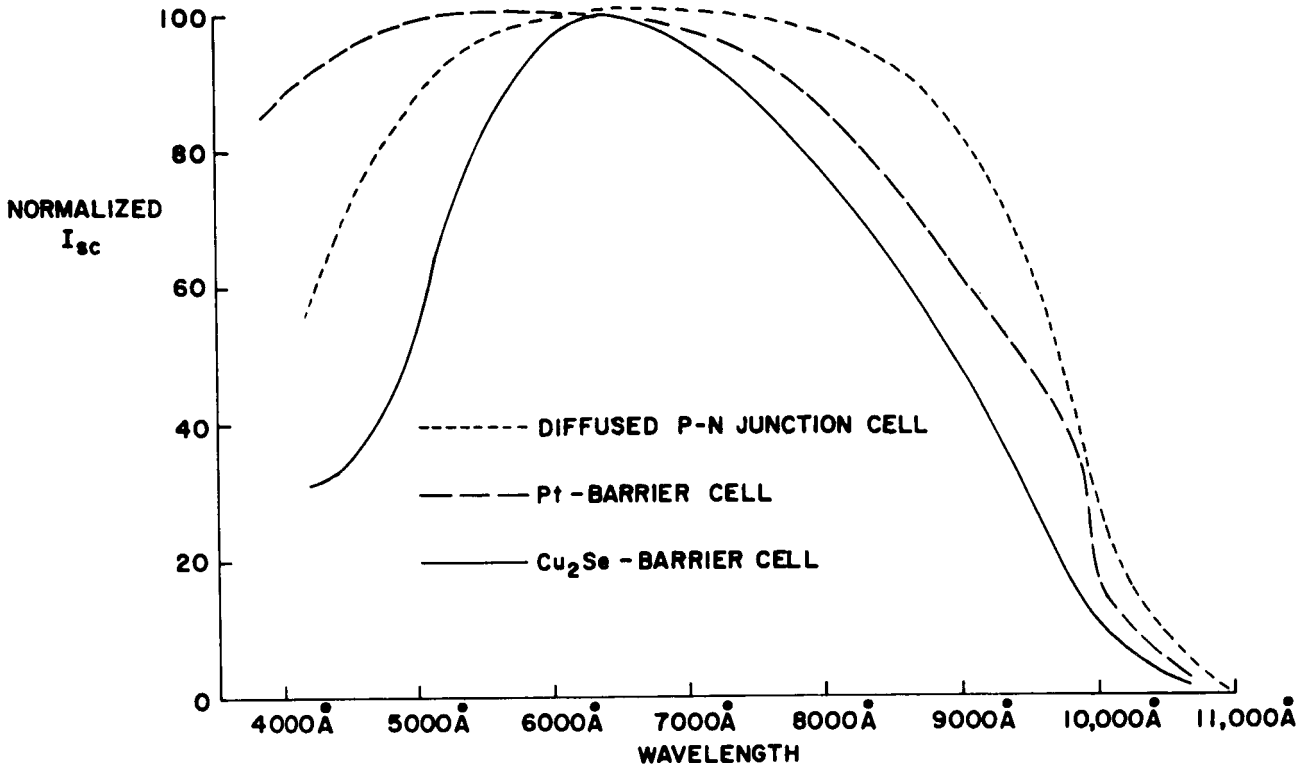

Figure 27. Spectral responses of various types of Si cells

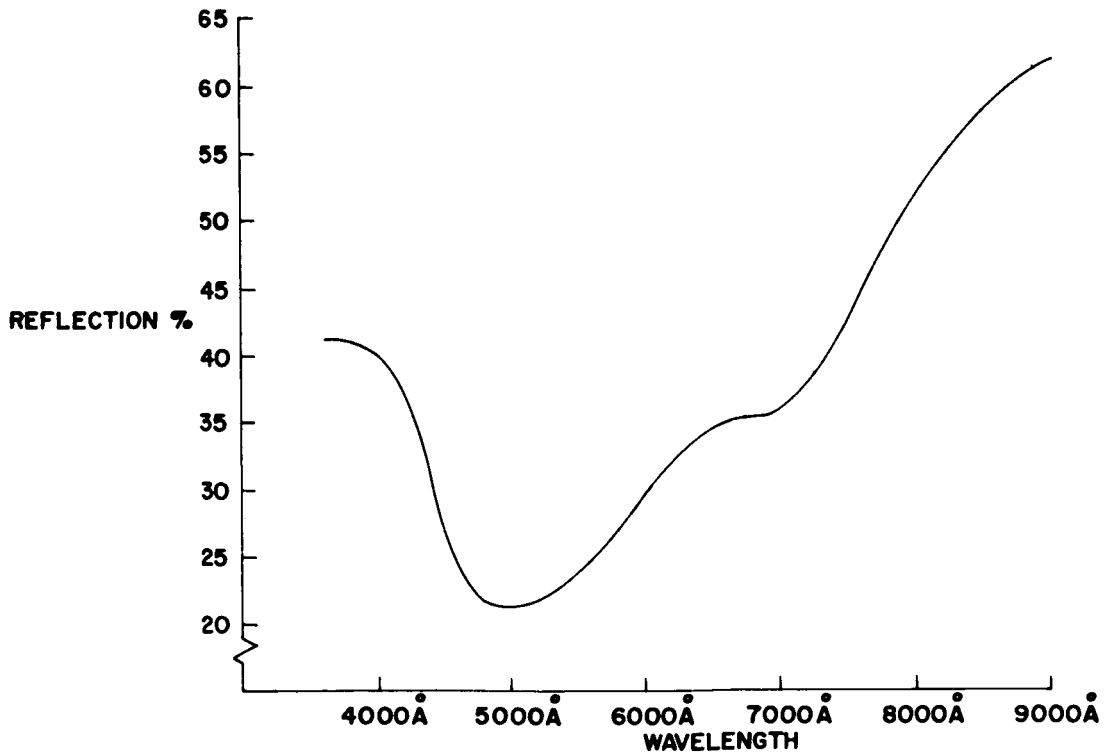

Figure 28. Diffuse reflectivity of a thin-film cell as a function of wavelength

would arise wholly from the reflectance change with wavelength. The result from the calculation is shown in Figure 29, together with experimental points obtained from a cell identical in structure to the one on which the reflectance measurements were made. It is seen that the curves are in good agreement, except near the GaAs band edge, where low optical absorption may be expected to reduce the photogenerated carrier collection efficiency.

From the foregoing experimental evidence, it was concluded that the long-wavelength response of the cell was due wholly to the normal photovoltaic effect in the GaAs, with a spectral response governed principally by reflectance from the Cu_2Se film acting as an interference filter on the front surface of the cell.

E. Cu_2Se – SINGLE-CRYSTAL GaAs SOLAR CELLS

During the study of the effect of the crystallographic orientation of single-crystal GaAs on the open-circuit voltage of the Cu_2Se - GaAs solar cell, a number of single-crystal cells, up to 1 cm^2 in area were made. Typically, the efficiency of these cells under 100mW•cm^{-2} equivalent tungsten radiation was between 5 and 7%. However, one cell having an efficiency of 8.0% was fabricated. The I-V characteristic of this cell under test is shown in Figure 30. This cell's performance is further discussed in Section VI.

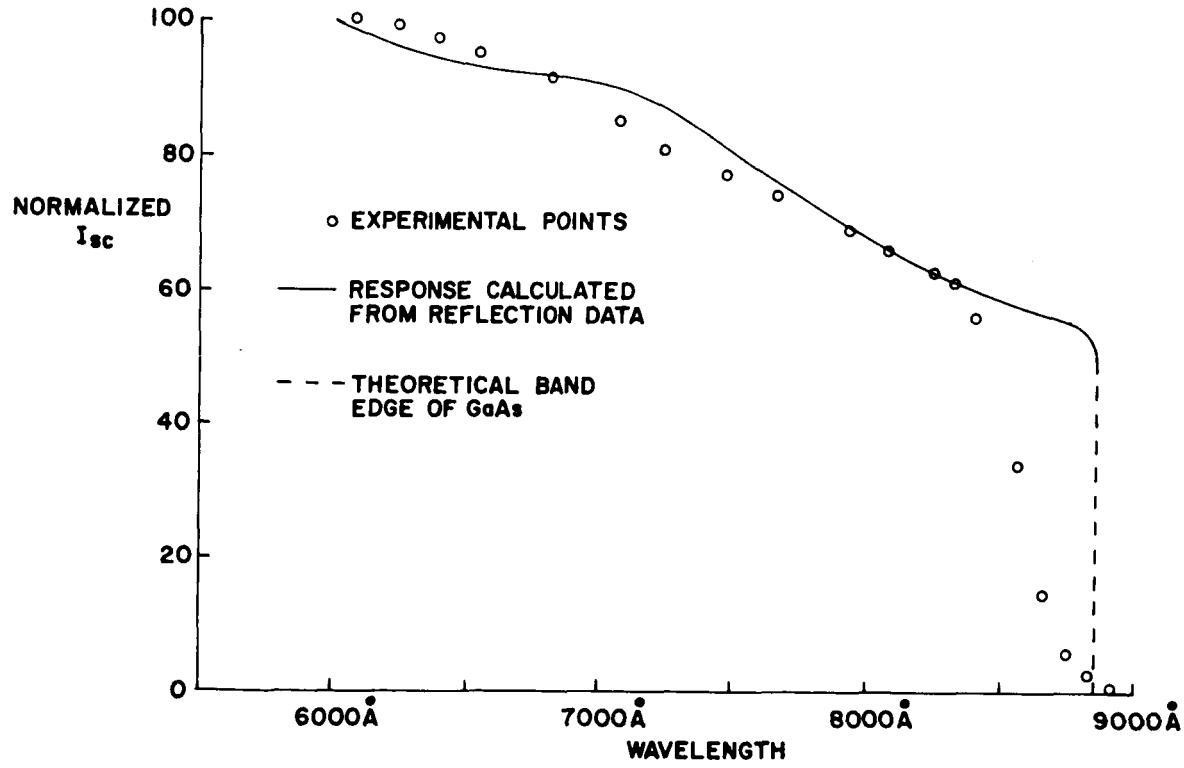

Figure 29. Comparison of the calculated and experimental spectral response of a thin-film cell

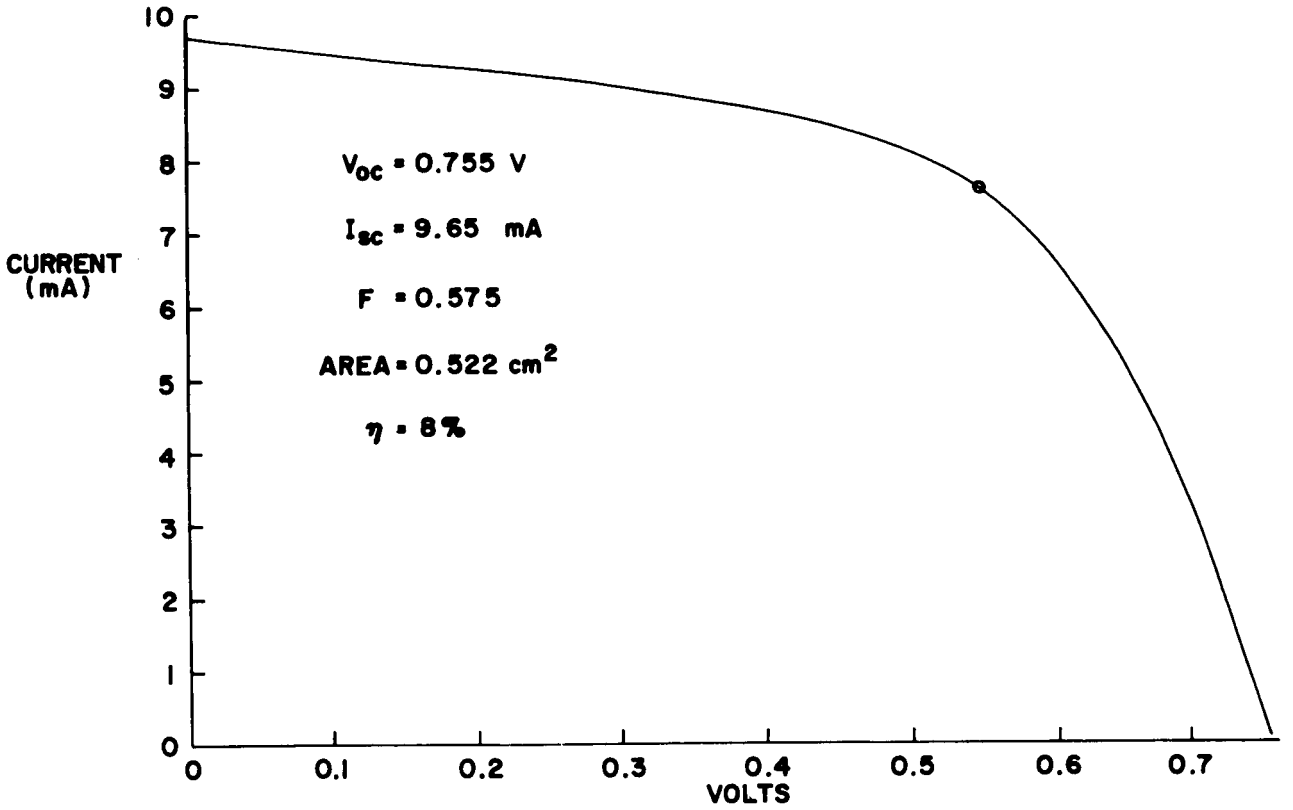

Figure 30. I-V curve of barrier cell on single-crystal GaAs, with 8% efficiency

SECTION V

STABILITY TESTS

A. OBSERVED INSTABILITIES

Cells with the structure Al-InAs-GaAs-$Cu_{1.8}Se$ have been observed to degrade when stored under laboratory ambient conditions. The nature of the degradation is such as to lead to a loss in fill-factor and I_{SC}, apparently caused by a back-to-back diode effect. A typical degraded I-V characteristic is shown in Figure 31(a).

It was found that etching the cell with dilute nitric acid solution for some minutes removed the unwanted diode, restoring the cell characteristic to its original form. The result of progressive etching treatment is shown by the I-V curves of Figures 31(b) and 31(c), which are from the same cell as 31(a).

It was postulated that the degradation occurred by oxidation of the cuprous selenide film surface. The sequence of events leading to degradation by this process were thought to be:

(a) During deposition of the cuprous selenide film, the starting composition ($Cu_{1.8}Se$) may not necessarily be the final film composition, especially for thin films, because of accommodation coefficient differences for Cu and Se on the deposition surface. In particular, it could be expected that the film would be Cu-rich compared with the evaporant, because of the relatively high vapor pressure of selenium.

(b) The stable form of cuprous selenide has stiochiometry $Cu_{1.8}Se$,[5] and there is also evidence that copper is relatively mobile in $Cu_{1.8}Se$.[3]

(c) Given (a) and (b), it follows that there will be a tendency for excess Cu to migrate to the surface of the cuprous selenide film, where it will be oxidized to Cu_2O, a process leading to the situation shown in Figure 32.

(d) The degrading diode then occurs by the formation of a barrier either at the gold-Cu_2O or the Cu_2O-$Cu_{1.8}Se$ interface.

(e) The Cu_2O may be etched off the cell surface by the HNO_3, restoring the cell to its original state.

This model does not account for the fact that the gold grid was not removed from the cell during etching, as might be expected. However, it did account for the fact that an etch in dilute HNO_3 immediately after completion of the cell apparently prevented degradation, presumably by removing the excess copper from the $Cu_{1.8}Se$ film.

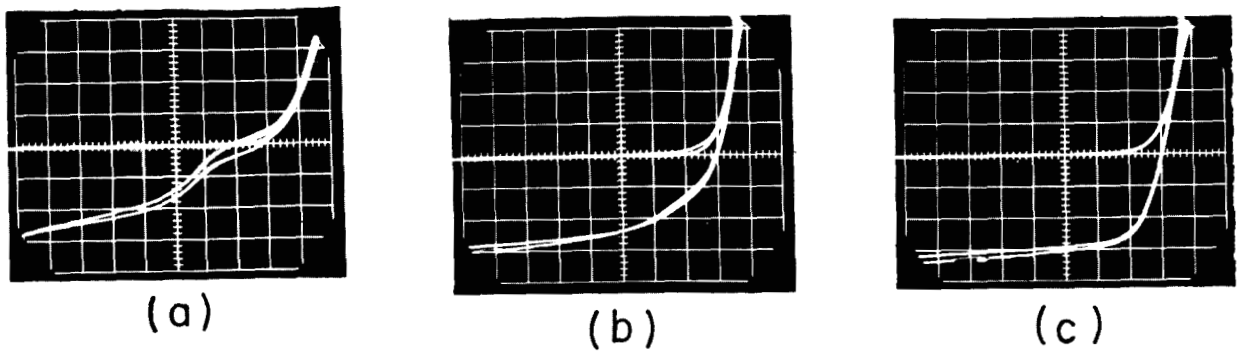

Figure 31. (a) I-V curve of a degraded barrier cell
(b) I-V curve of a degraded cell, showing partial recovery
(c) I-V curve of a degraded cell, showing complete recovery after etching

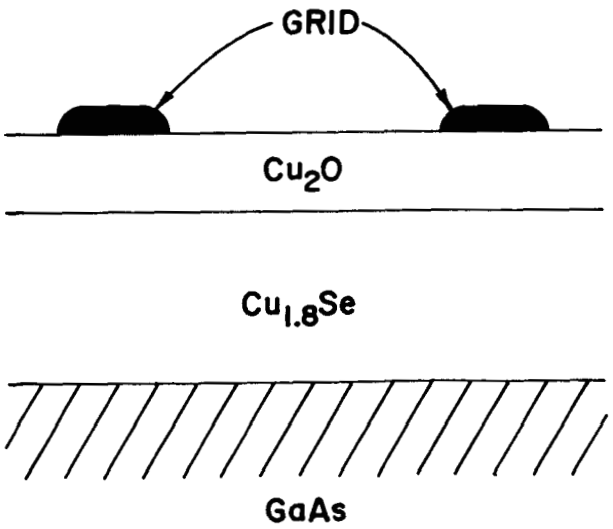

Figure 32. Cross section of degraded barrier-contact cell

To test this hypothesis, and to evaluate cell stability, two groups of tests have been performed. The first of these examined the intrinsic stability of the device, using cells stored under inert gas ambient, without illumination. The second group of tests examined the behavior of the cells when stored under various environments which could be expected to react with the cell materials to cause degradation.

B. PRIMARY STABILITY TESTS

1. Preparation

Twelve cells were fabricated using two different substrate materials and three different etching procedures, as shown in Table VII. These cells were sealed into individual glass envelopes, and leads were attached by use of conducting adhesive, with external connections through Kovar pins sealed through the tube base. The tubes were evacuated prior to backfilling with dry helium at 1 atmosphere pressure. The cells were stored at room temperature and were not illuminated during storage.

2. Testing

The cells were tested under tungsten illumination giving an I_{sc} value for a test cell equivalent to that obtained under 100 mW cm^{-2} sunlight. All cells were tested at four- or five-day intervals, and at each test a complete I-V characteristic was plotted. From this, the maximum power point was determined graphically, and the cell efficiency calculated.

TABLE VII

CELL TYPES USED IN PRIMARY STABILITY TEST

Structure	Number	Etch Before Barrier Formation	Etch After Barrier Formation
Cu_2Se/GaAs/InAs/Al	2	no etch	no etch
Cu_2Se/GaAs/InAs/Al	2	methanol-Br	2.5% HNO_3
Cu_2Se/GaAs/InAs/Al	2	2.5% HNO_3	2.5% HNO_3
Cu_2Se/GaAs/InAs/Mo	2	no etch	no etch
Cu_2Se/GaAs/InAs/Mo	2	methanol-Br	2.5% HNO_3
Cu_2Se/GaAs/InAs/Mo	2	2.5% HNO_3	2.5% HNO_3

Testing began in early December 1966, and cells were added progressively as they were fabricated. When the test ended, in mid-April 1967, each cell had been tested for a minimum of two months, and some cells had been tested for as long as four months.

3. Results

Figures 33(a) and 33(b) show cell efficiencies plotted as a function of time. The performances are shown as percentages of the initially measured efficiency. A detailed analysis of each cell is presented in Table VIII. Table IX shows the final state of the cells.

TABLE VIII

CELL PERFORMANCES IN PRIMARY STABILITY TEST

Cells on aluminum substrates:

Etches	Behavior	Period (days)
None-none	Initial loss, then steady at 93%; color change	132
None-none	Gradual 40% loss; color change	75
Br-HNO_3	No loss; no color change	122
Br-HNO_3	Initial loss, then steady at 95%; no color change	81
HNO_3-HNO_3	No loss; color change	80
HNO_3-HNO_3	Initial loss, then steady at 88%; color change	80

Cells on molybdenum substrates:

Etches	Behavior	Period (days)
None-none	No loss; no color change	93
None-none	Variable efficiency,* loss up to 40%	60
Br-HNO_3	Initial loss, then steady at 80%	89
Br-HNO_3	Initial loss,* then stable at 50%	60
HNO_3-HNO_3	No loss	103
HNO_3-HNO_3	No loss	73

* Believed to be associated with pin-cleaning operation.

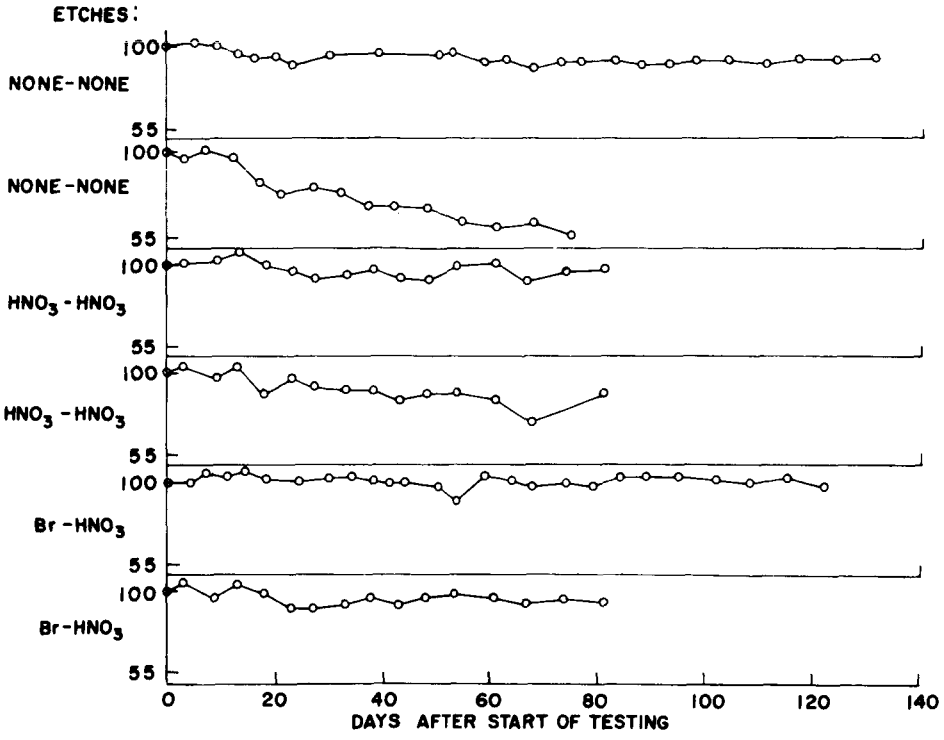

(a)

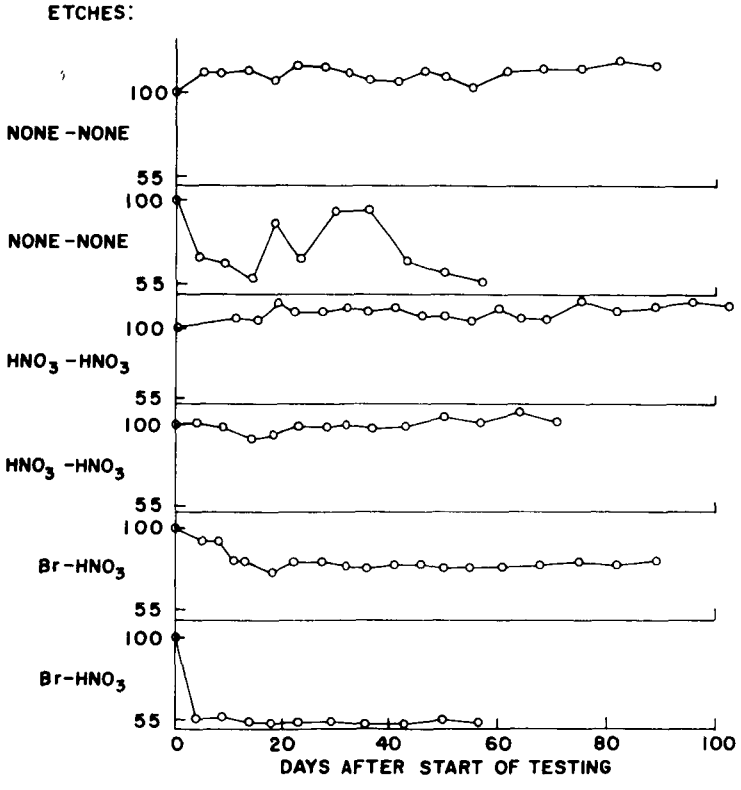

(b)

Figure 33. (a) Efficiencies as a function of time for cells on aluminum substrates, primary stability test
(b) Efficiencies as a function of time for cells on molybdenum substrates, primary stability test

TABLE IX

PRIMARY STABILITY TEST RESULTS

Substrates:	#1	#2	#3
Al	93	100	100
	60	95	88
Mo	100	80	100
	60	50	100

Etches

Etches: #1 None-none
#2 Br-HNO_3
#3 HNO_3-HNO_3

The pin-cleaning operation mentioned in Table IX, was performed on the cell envelopes after completion of the sealing operation. The Kovar pins showed evidence of oxidation which led to variable contact resistances. These pins were cleaned by etching, and after completion of this process the cell efficiencies were found to have been reduced. Only with two tubes was this cleaning procedure found to be necessary, and in both cases the cell outputs were degraded by the operation. The cause for the effect is not immediately clear, since the cells were hermetically sealed in the envelopes, and were thus not exposed to the etches; the process did not involve any high-temperature operations. A conjectural possibility is that electrolytic effects on the Kovar pins caused the cells to be electrically stressed.

Visual examination of the cells indicated that of the twelve cells, four on aluminum substrates showed surface color changes. The usual pale grey-green or blue coloration of the cells as initially fabricated, changed to a dark-brown or purplish shade. A correlation was seen between this color change and the loss in cell efficiency, for the cells on aluminum. The mechanism of the color change is unknown, although it presumably is due to a change in the interference effects in the film, which give rise to the surface color. This may be a thickness change, with the film material remaining the same (which seems unlikely), or a change in refractive index of the film perhaps arising from a phase change in the film material. This phase change may be catalyzed by the aluminum substrate, by the following process. The GaAs film growth occurs at a temperature very close to the melting point of the aluminum substrate,

and thus there appears to be a good possibility that the aluminum is sufficiently mobile to be able to enter the GaAs. It is inactive electrically, since AlAs is also a III-V semiconductor, although with a wide bandgap. Thus, small amounts of aluminum, sufficient to catalyze a phase change in the cuprous selenide, may be present at the GaAs-Cu_2Se interface. Without further work, however, this must remain a conjecture.

Analysis of I-V characteristics showed that V_{oc} values remained constant regardless of changes in cell efficiency. Losses in cell efficiency were due to drops in I_{sc} and fill-factor.

4. Conclusions

Three types of cell behavior were observed:

(a) An initial drop in efficiency, followed by stable operation (6 cells).

(b) Stable output (5 cells).

(c) Progressive loss in efficiency (1 cell).

Of the cells on aluminum, the most stable ones were shown to be those with the Br-methanol GaAs etch and the 2.5% HNO_3 Cu_2Se etch. The Br-methanol appears to be effective for this application mainly because it provided a polishing effect on the GaAs layer. Other polish etches (3 H_2SO_4:1H_2O_2:1H_2O, and to a lesser extent aqua regia) are too fast in their rate of removal of material to be applied to the thin GaAs layers in use. The HNO_3 etch used on the Cu_2Se film may induce stability by removing copper from the film, as discussed in Section V.A.

C. SECONDARY STABILITY TESTS

1. Preparation

Three glass envelopes were prepared, each of the geometry shown schematically in Figure 34. Each envelope contained five cells of Al-InAs-GaAs-$Cu_{1.8}Se$ structure, with Br-methanol and HNO_3 etches used during cell fabrication. The cells were mounted using adequate conducting adhesive to provide both electrical and thermal low-resistance contact between the aluminum substrate and the gold-plated glass temperature-controlled surface. Top connections were made using flexible tungsten tungsten contacts, with conducting adhesive to ensure low-resistance contact. External connections were made by Kovar pins sealed through the envelope base, as shown.

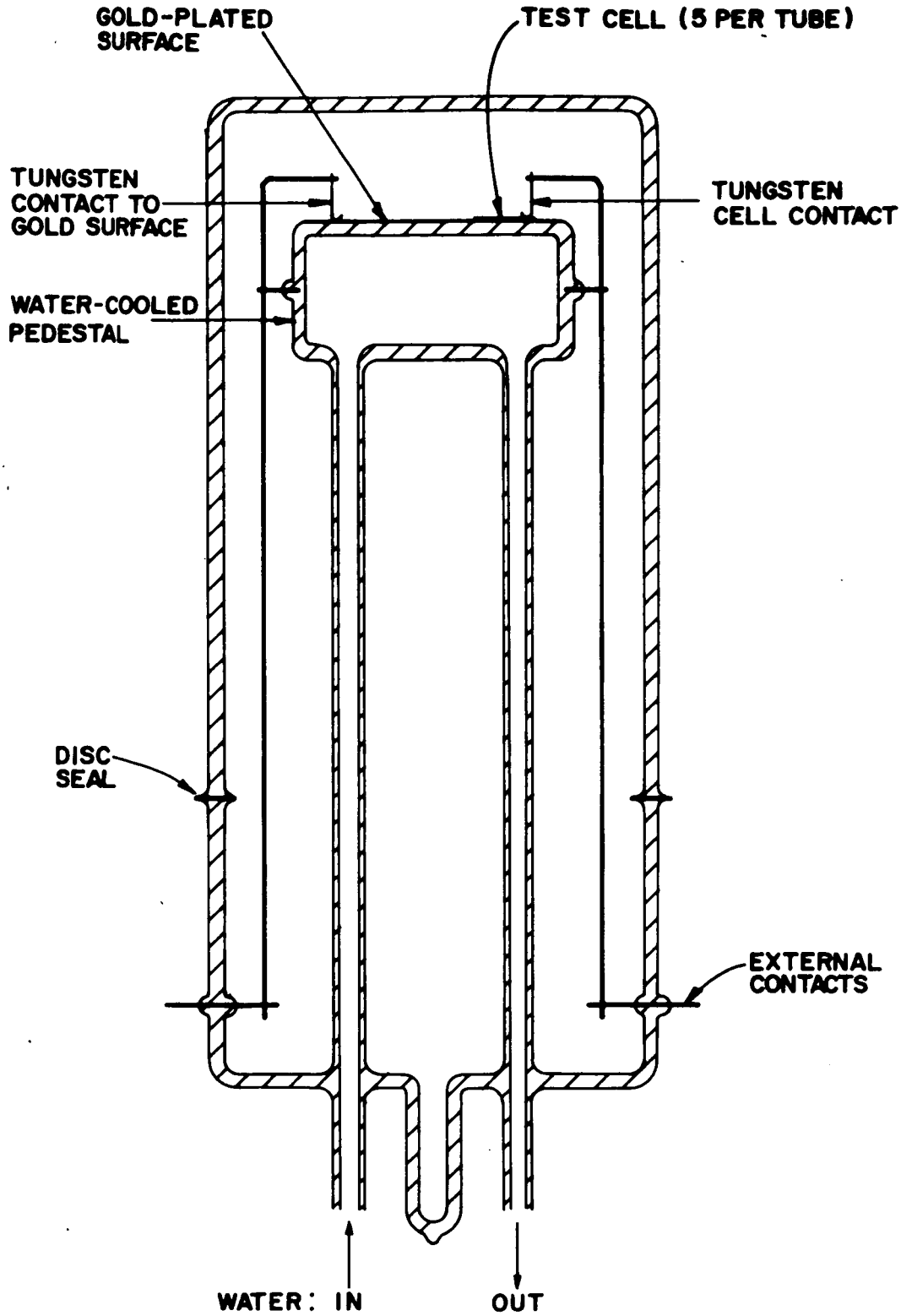

Figure 34. Cross section of envelope for cell mounting, secondary stability test

After the mounting of the cells, the tubes were sealed using a two-step process. In the first step the upper window-and-envelope portion was sealed to the base-and-stem portion, using a disc seal made by rf induction heating. During this process, dry ultra-pure nitrogen was flushed continuously through the tube, using a fine inlet pipe passed through the pumping tube in the base. This process was used to minimize heating of the cells, which had been found to cause problems during sealing of the tubes used in the primary stability test. In the second step of the process, the pumping tubulation was used to evacuate the tube. One of the envelopes was then sealed; the other envelopes were backfilled with the desired ambient gas, and then sealed. One of these tubes was filled with dry oxygen at one atmosphere pressure, the other with air with 80% humidity at 25°C and one atmosphere pressure. The 80% humidity was attained by filling the tube with air saturated with water vapor at 21°C by passing the gas through a water bubbler maintained at this temperature, the vapor pressure of water at 21°C being equal to that of water vapor in 80% humid air at 25°C.

2. Testing

The cell efficiencies and spectral responses were measured individually immediately after sealing. From the I-V curve obtained, the matching load resistor was calculated for each cell. The cells were then illuminated continuously for the test duration with tungsten light giving output equivalent to that of 100-mW·cm^{-2} sunlight, with the matched load resistor connected. Water at 25°C from a controlled constant-temperature source was circulated through the cell mounting. Power output from the cells, and V_{oc}, were measured daily with a digital voltmeter; the I-V curves were made at weekly intervals to determine changes in efficiency, fill-factor, and I_{sc}.

The spectral response of each cell was measured at the conclusion of the test and compared with that obtained at the start of the test.

3. Results

Figures 35(a), (b), and (c) show $\frac{\text{Power Output}}{\text{Initial Output}} \times 100$ for the three groups of cells, and the spectral responses are shown in Figures 36(a), (b), and (c).

Visual examination of the cells showed that the tube-sealing operation for the cells in oxygen and air ambients caused a change in surface coloration of the cells. The efficiencies of the cells immediately after this sealing were found to be less than those measured before the operation. However, during the first part of the test, the cell color returned to the normal green-blue appearance, and the efficiencies recovered to their original values. This improvement appears in the performance data shown in Figures 35(b) and (c).

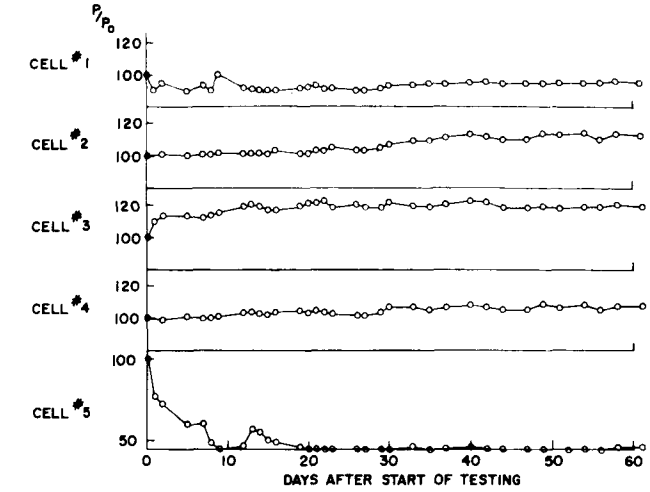

(a)

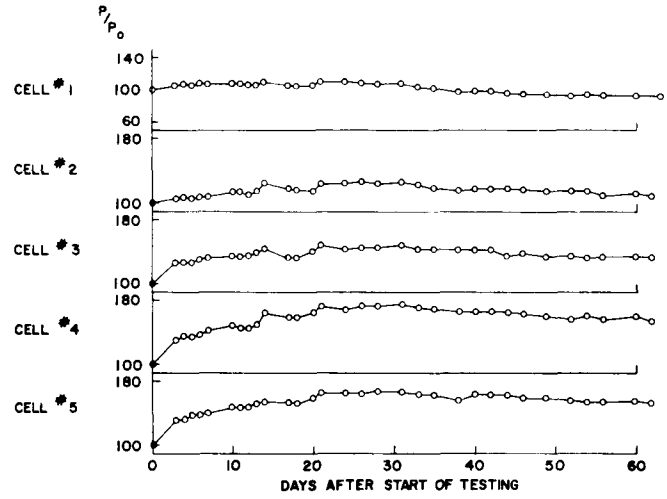

(b)

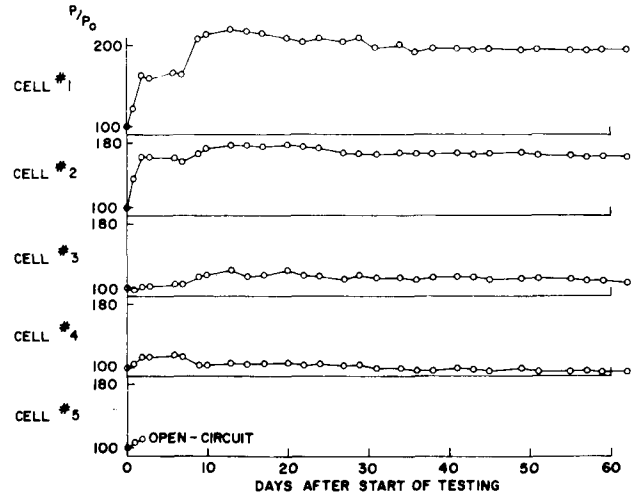

(c)

Figure 35. (a) Power output as a function of time, cells in vacuum, secondary stability test
(b) Power output as a function of time, cells in oxygen, secondary stability test
(c) Power output as a function of time, cells in 80% humid air, secondary stability test

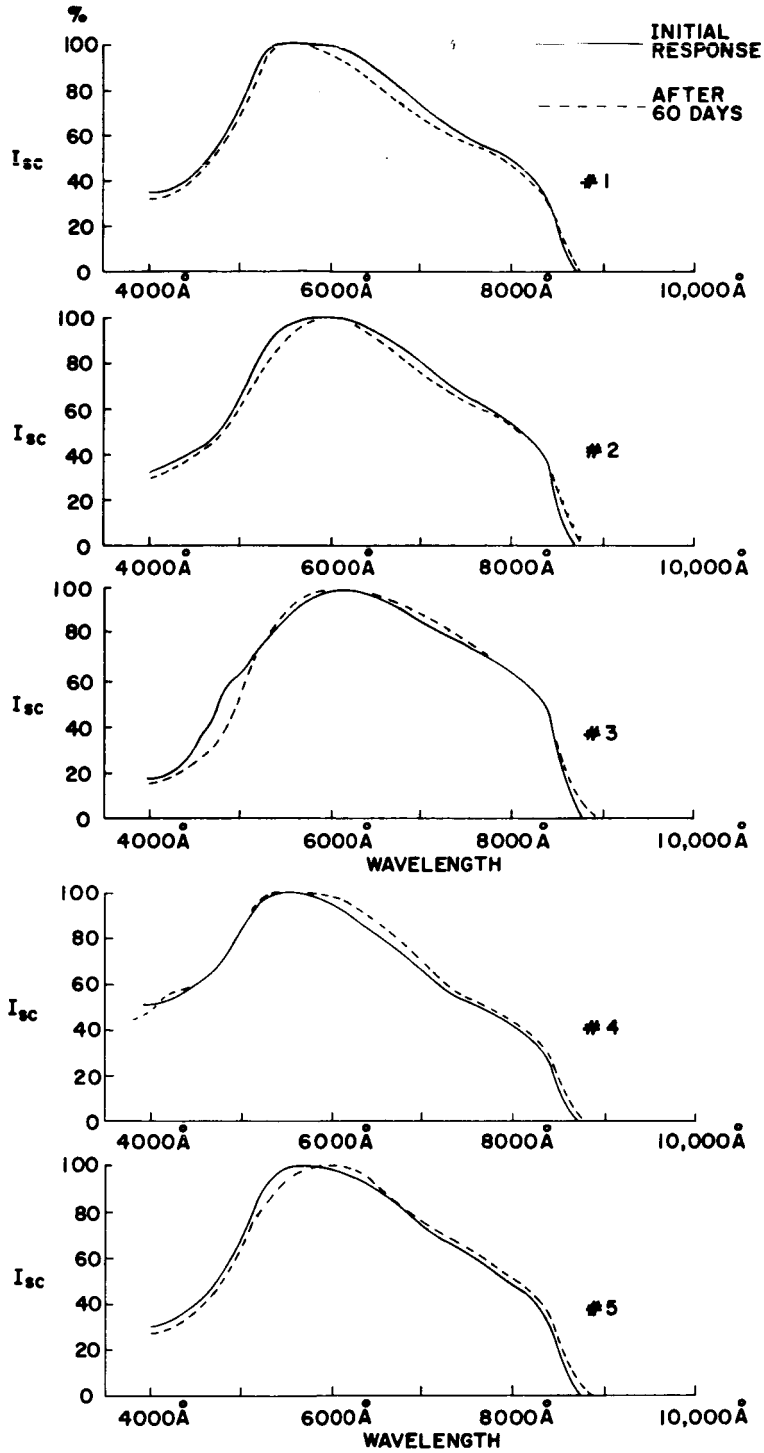

Figure 36. (a) Spectral responses of cells in vacuum, secondary stability test

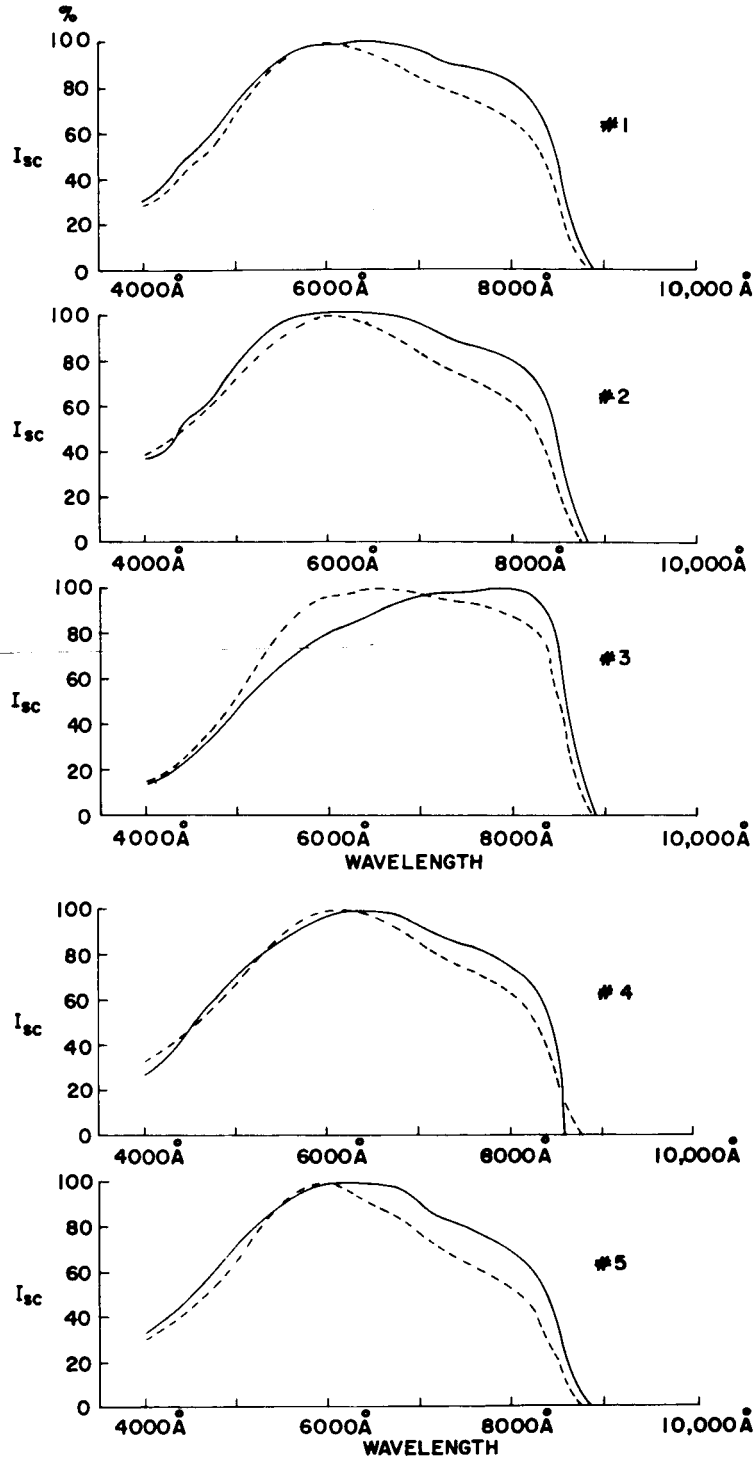

Figure 36. (b) Spectral responses of cells in oxygen, secondary test

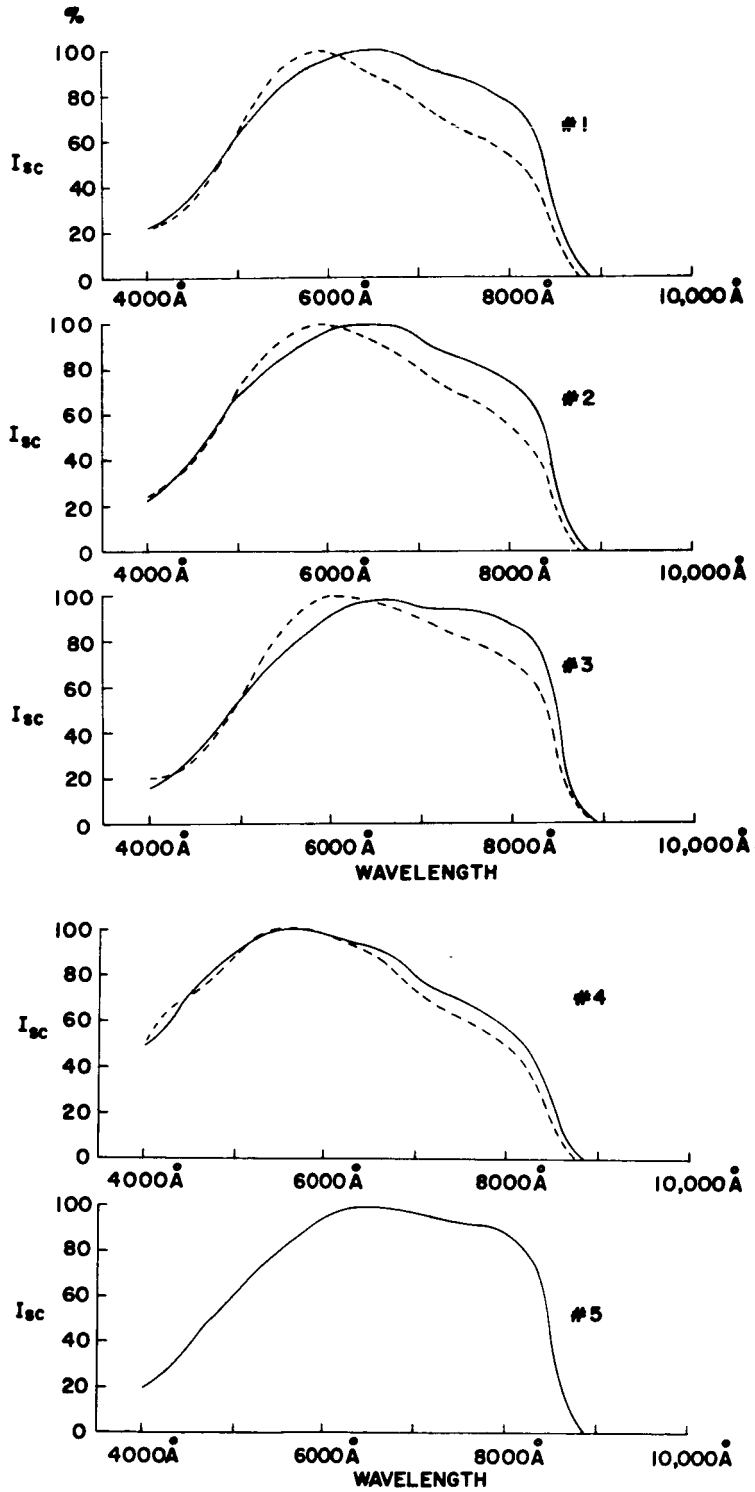

Figure 36. (c) Spectral responses of cells in 80% humid air, secondary stability test

It is seen that aside from this increase in efficiency at the start of the test, the cell performances were stable within the indications of the present data. Exceptions to this are (a) one of the cells in vacuum, which degraded to 45% of its initial power, by losses in I_{sc} and fill-factor, and (b) one of the cells in oxygen, whose output fell abruptly to zero, apparently because of an open-circuit in the contact to the cell.

D. CONCLUSIONS

The test data confirm that the present fabrication processes yield thin-film cells which are stable under operation in vacuum and humid-air environments. The limited duration of the tests is a qualification of this result, but in comparison with results seen in other types of thin-film cells, the outcome appears to be encouraging.

This test program has also emphasized the need for further development of the methods used for making connections to the cells, since in many cases the performance degradation was associated with poor electrical contacts.

SECTION VI

ANALYSIS OF CELL EFFICIENCY

A. ANALYSIS OF PRESENT CELL PERFORMANCE

A major barrier to further use of this type of cell is its present efficiency limitation of about 4%. Hence, it has seemed worthwhile to analyze the observed characteristics of the cell to determine the ways in which the experimental cells depart from ideal cells, which have theoretical efficiencies rather higher than 22% under AMO conditions.[10]

1. The Ideal Solar Cell

The equivalent circuit for the ideal solar cell is shown in Figure 37. The cell characteristic is

$$I = I_D - I_L$$

$$= I_o \exp\left(\frac{qV}{kT} - 1\right) - I_L \tag{10}$$

The value to be used for I_o depends on whether the diode is a p-n junction, or a metal-semiconductor barrier. For the p-n junction, using the diffusion theory[11]:

$$I_o = A \exp\left(\frac{E_G}{kT}\right) \tag{11}$$

with $$A = \frac{b}{(1+b)^2} \, kT \, (\mu_n + \mu_p) \left(\frac{1}{\sigma_n L_p} + \frac{1}{\sigma_p L_n}\right) (N_C \cdot N_V)^{1/2} . \tag{12}$$

(The symbols used are conventional, and may be found in the list of symbols at the beginning of this report.) Substitution of appropriate values into Eqs. (11) and (12) shows that in theory, for the GaAs p-n junction at room temperature, $I_o = 4.1 \times 10^{-16}$ A · cm^{-2}. This is dependent on carrier density, but the order of magnitude is the significant factor for the purposes of this analysis.

For the metal-semiconductor barrier case, according to the isothermal diode analysis[10]:

$$I_o = n_{pn} q \left(\frac{kT}{2\pi m^*}\right)^{1/2} \left(\exp \frac{-qV_D}{kT}\right) , \tag{13}$$

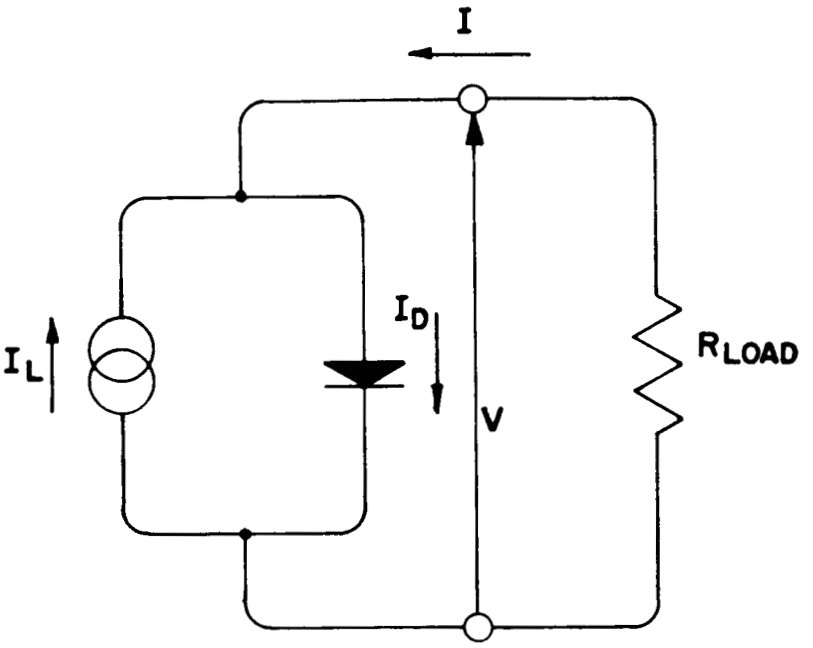

Figure 37. Equivalent circuit of ideal solar cell

where the symbols are again conventional. This equation neglects image forces and tunneling, but for diodes with low carrier concentrations, the expression is sufficiently accurate for the purposes of this analysis. Substituting appropriate values and assuming $V_D = 1.38$ eV for GaAs at room temperature, $I_o = 2.2 \times 10^{-19}$ A · cm^{-2}.

It follows that under 135-mW·cm^{-2} AMO illumination, $I_L \gg I_o$, and Eq. (10) can be reduced to

$$I = I_o \exp \frac{qV}{kT} - I_L . \tag{14}$$

It is convenient to characterize a cell's curve by quoting the open-circuit voltage (V_{oc}), the short-circuit current (I_{sc}) and the fill-factor (F). The latter is defined by

$$F = \frac{V_m \times I_m}{V_{oc} \times I_{sc}} , \tag{15}$$

where (V_m , I_m) is the maximum power operating point of the cell, i.e., matched load condition. From Eq. (14) it can be shown that an approximation for the fill-factor is*:

$$F = \frac{(\ln B - \ln\ln B)\ (\ln B - 1)}{(\ln B)^2}, \tag{16}$$

where $B = \frac{I_L}{I_o}$.

Hence, it remains necessary only to obtain a value for I_L, to determine the theoretical efficiency. An absolute theoretical maximum can be arrived at by assuming unity quantum efficiency for the cell operation, and integrating the solar radiation spectrum over the range of energies greater than the intrinsic absorption edge of the material. For GaAs, with an absorption edge at 1.38 eV, this gives a value for I_L = 46 mA · cm^{-2}. From this figure, the parameters for a theoretical GaAs cell operating under AMO illumination were derived, as shown in Table X.

TABLE X

THEORETICAL OPERATION PARAMETERS FOR GaAs SOLAR CELLS

	p-n Junction Cell		Barrier Cell	
Illumination	135 mW·cm^{-2}	100 mW·cm^{-2}	135 mW·cm^{-2}	100 mW·cm^{-2}
I_{sc}	46 mA·cm^{-2}	34 mA·cm^{-2}	46 mA·cm^{-2}	34 mA·cm^{-2}
V_{oc}	0.84 V	0.83 V	1.0 V	1.0 V
F	0.86	0.86	0.87	0.87
η	25%	24%	30%	30%

The efficiencies for the p-n junction cell are rather higher than those given by Loferski,[10] because of the simple assumptions which have been made concerning I_o. It may come as somewhat of a surprise to see theoretical efficiencies for the barrier cell rather higher than those for the junction cell. However, the assumptions made in the calculation are so simple as to render the result of little practical significance,

* This approximation was obtained under work on a different research contract (NASW-1427); the approximation produces F values differing from precise calculations by less than 1% over the range of conditions considered here.

for reasons which are discussed below. Before going on to discuss deviations from theoretical behavior, it may be of some help to the reader to summarize the assumptions underlying the calculations giving the parameters shown in Table X:

(i) In the p-n junction cell, the electrical behavior follows the characteristic derived by the diffusion theory analysis.

(ii) In the barrier cell, the electrical behavior follows the characteristic derived for the simplest isothermal diode, with tunnelling and image forces neglected, and a barrier height equal to E_G for GaAs.

(iii) There is no series resistance in the cell equivalent circuit.

(iv) There are no reflection losses from the cell.

(v) All photons with energy greater than the bandgap value (1.38) are absorbed with unity quantum efficiency.

(vi) The collection efficiency for generated carriers is unity (i.e., only radiative recombination occurs, and all photons generated by this process are re-absorbed and contribute to cell output; also the diffusion length is infinitely larger than the reciprocal of the optical absorption constant).

2. Comparison with Experimental Cells

The theoretical treatment above departs from the experimental behavior even for cells made with p-n junctions in single-crystal material, and the departures from the theory seen for barrier cells on polycrystalline semiconductor material are even larger.

Analytical solution of the general equation of the cell characteristic, accounting for departures from theoretical behavior of the diode, and including the effects of R_S and R_{Sh}, is not possible. The behavior of the system may be analyzed numerically, but such an analysis is beyond the scope of this work. However, it is possible to arrive at an estimate of the effects on the cell performance of the various factors tending to lower the cell efficiency, if some simplifying assumptions are made.

In the p-n junction, it is found experimentally that the diode in the equivalent circuit has a characteristic of the form.

$$I = I_o \exp\left(\frac{qV}{AkT} - 1\right), \tag{17}$$

where A ranges from the expected unity up to values as high as 10 or 20, though it is usually less than 4. Large values of A lead apparently to increased values of V_{oc} for the cells. However, the physical processes leading to increases in A, such as recombination in the junction region, lead also to increases in the value of I_o in the diode characteristics. The increases in I_o might typically be to 10^{-9} A · cm^{-2}, where the theory indicates 10^{-16} A · cm^{-2}.

In the barrier cell, the same effects on the diode characteristic are also seen. For the present cells, values of A are typically between 2 and 4, while values for I_o are in the 10^{-6} A · cm^{-2} range for the cells on polycrystalline GaAs films. For cells on single-crystal GaAs, considerably smaller values of I_o are found, leading to higher efficiencies for these cells, in particular, better V_{oc} values.

Processes leading to an experimental I_{sc} value lower than the theoretical value are:

(i) Reflection from the front surface of the cell.

(ii) Absorption in the barrier-contact film.

(iii) Absorption in the grid electrode structure.

(iv) Collection efficiencies less than unity.

Table XI shows estimates for the values realized in practice for these processes, and gives the I_{sc} values found in practice for two cells, one an average cell of 3.0% efficiency, the other the most efficient cell made, with 4.2% efficiency. The figures given in the table are factors by which each process affects the I_{sc} value, and hence the experimental I_{sc} is the product of the theoretical I_{sc} and the four factors involved.

The value of collection efficiency found here correlates well with what can be expected from a diffusion analysis. If a flux of N_1 photons of energy greater than the bandgap are incident on the junction region in the GaAs, the depletion region width is d, the optical absorption constant for GaAs beyond the band edge is α, and the diffusion length for minority carriers is L, it can be shown that:

$$I_{sc} = qN_1 \left[1 - \frac{1}{1+\alpha L} \exp -\alpha d \right] \qquad (18)$$

For $\alpha = 10^4$ cm^{-1}, the expression shows that for d = 0.29 μm and I_{sc} value of 11.8 mA · cm^{-2} (both as measured for the 3.0% efficient cell), then L = 0.3 μm.

TABLE XI

EFFECT OF LOSS PROCESSES ON I_{sc}

	Theory	3.0% Cell	4.2% Cell
Theoretical I_{sc} ($mA \cdot cm^{-2}$)	34	34	34
Absorbance of surface	1.0	0.60	0.70
Transmittance of barrier film	1.0	0.70	0.70
Transmittance of grid	1.0	0.95	0.95
Collection efficiency	1.0	0.87	0.95
Realized I_{sc} ($mA \cdot cm^{-2}$)	34.0	11.8	15.0

Notes:
(i) Surface absorbance estimated from curve in Figure 28.
(ii) Transmittance of barrier film taken to be that of monitor film on glass.
(iii) Grid transmittance obtained from geometry of deposition mask.
(iv) Collection efficiency derived from other factors and known I_{sc} value (see text).

Now $$L = \sqrt{D\tau} = \sqrt{\frac{\mu q}{kT}} \quad . \qquad (19)$$

where μ = carrier mobility

q = electronic charge

k = Boltzmann's constant

T = absolute temperature

τ = carrier lifetime

Hence the experimental results indicate a mobility-lifetime product of 2.3×10^{-9} $cm^2 \cdot V$. This is reasonable for polycrystalline material since the value of this parameter for single-crystal bulk GaAs is around 4×10^{-5} cm. This also brings out the difference in quality between the polycrystalline film GaAs, and bulk single-crystal GaAs.

Combining experimental values for I_{sc}, A, and I_o, it is possible to obtain a value for the expected cell efficiency, using Eqs. (16) and (18). The results of these calculations for the 3.0% and 4.2% efficient cells are shown in Table XII. The remaining factor leading to loss in cell efficiency is series resistance, since it has been found that shunt resistances may be neglected for the cells under discussion.

The difference between the fill-factor indicated by calculation from the I_{sc} and I_o values, and that obtained in practice, has been assumed to arise from series resistance effects. The measured value of series resistance is generally between 10 and 20 ohms for typical cells, and this value appears reasonably to account for the loss of performance, as calculated by Wysocki.[6]

The results of the foregoing calculations are summarized in Table XIII. The figures given are the factors by which the theoretical efficiency must be multiplied to give the realized efficiency because of departures from the ideal value for the four parameters shown.

The data show that the second cell has a higher efficiency mainly because of increases in I_{sc} and F. It should, however, be pointed out that cells with average efficiencies have frequently shown V_{oc} values in excess of 0.55 V. In this respect, the behavior of the cell on single-crystal GaAs, whose characteristic is reproduced in Figure 30, is especially interesting. The V_{oc} value for this cell is 0.755 V, implying a very low value for I_o. This is consistent with the I_o values as determined by the I-V measurements, and shown in Figures 11 and 13 for single-crystal and polycrystalline specimens.

B. CONCLUSIONS

The results of the above analysis indicate that no single major factor accounts for the observed reduction of cell efficiency below the theoretical value. However, the two largest contributors to the loss in efficiency are the presently observed V_{oc} and I_{sc} values. Hence, it is appropriate that the major research effort during the reporting period should have concentrated on these two areas.

The parameter which experimentally departs most from the theoretical value is I_o. While it appears to be possible to control this to some degree (see Section III), it would be necessary to reduce the experimental value by some three or four orders of magnitude to significantly improve the cell performance. It appears that the present values of I_o may arise from the polycrystalline nature of the semiconductor, so that improvements in this direction may be difficult to obtain. This is an area which at the present time can only be approached empirically, and it is found to be a major factor in determining the efficiencies of other polycrystalline solar cells.

TABLE XII

OPERATING PARAMETERS AND CALCULATED EFFICIENCY FOR EXPERIMENTAL CELLS

	3.0% Cell	4.2% Cell
I_o ($A \cdot cm^{-2}$)	3.7×10^{-6}	$15. \times 10^{-6*}$
A	2.34	2.0*
I_{sc} ($=I_L$) ($A \cdot cm^{-2}$)	11.8×10^{-3}	15.0×10^{-3}
V_{oc}	0.49	0.49
F (calculated)	0.65	0.68
F (measured)	0.51	0.57
*estimated		

TABLE XIII

SUMMARY OF THE EFFECT OF LOSS PROCESSES ON CELL EFFICIENCY

	3.0% Cell	4.2% Cell
Combined effect of I_o and A on V_{oc}	0.49	0.49
I_o effect on F	0.81	0.83
R_s effect on F	0.75	0.84
I_{sc}*	0.35	0.44
*This factor is analyzed in more detail in Table XI.		

SECTION VII

REVIEW OF ALTERNATIVE CELL TYPES

A. CELL STRUCTURES

The cuprous-selenide-on-GaAs barrier layer cell which has been investigated during the present contract period represents the results of considerable exploratory work done under previous contracts.* Hence, a review of this earlier work is in order, to indicate the rationale underlying the present research.

The original work used GaAs as the active semiconductor component of the cells. This choice was based on several factors:

1. Loferski[10] had shown that the energy gap of GaAs was close to the optimum for conversion of sunlight into electrical energy.

2. The material has a high optical absorption constant[13]; therefore, complete absorption of incident light can be accomplished by a very thin layer of GaAs. This high optical absorption constant arises from the direct bandgap of GaAs, which contrasts with the case for silicon. In silicon, the indirect gap results in a softer absorption edge, so that a loss in efficiency is noted in silicon cells whose thickness is less than about 6 mils.[14]

3. Methods for forming thin films of GaAs had been under active investigation for some years, and satisfactory approaches had been developed, suitable for application to solar cell fabrication for research purposes.

However, research results with the CdS cell had shown that calculations of the type performed by Loferski were based on assumptions not necessarily valid in practice. Hence, it was felt worthwhile to investigate a material with bandgap wider than the calculated optimum, for solar-cell use. GaP films were grown and investigated for this reason, and these films were later applied to an alternative cell structure (see Section VII. B.).

A novel cell structure was also investigated during early phases of the work. This was based on an aluminum substrate into one surface of which a layer of fine GaAs particles was impressed. The soft aluminum surface held the GaAs, and the remaining exposed surface of the substrate, in the interstices between the particles,

---

*Contracts NAS7-202, NAS3-2796 and NAS3-6466.

was anodized to provide electrical isolation. Application of a barrier to the exposed surface of the GaAs particles would then create a cell in the desired thin-layer geometry. (The entire approach closely resembles that investigated at Hoffman Electronics for the fabrication of large-area solar cells using silicon spheres.[15]) Initial evaluation of the electrical characteristics of GaAs pressed into aluminum foil indicated that a high contact resistance existed: pre-coating the foil might have eliminated this problem. However, the packing density of the particles on the substrate could not be expected ever to exceed 70% of area utilization, so that when more promising approaches to cell fabrication appeared, this work was discontinued.

B. JUNCTION-FORMING PROCESSES

The initial objective in cell fabrication was to develop methods for forming p-n junctions in the GaAs layers. Processes investigated were:

1. Successive growth of layers of different conductivity type, using doped source wafers to control the majority carrier type in the GaAs in the vapor growth technique, and using the halide growth technique (see Section VIII of this report for more information on these processes).

2. Diffusion of Zn, Mn, Cu, Sn, Se, and Te into the polycrystalline n-type layers to form a p-type surface.

In all cases, the diodes made by these methods showed high shunt conductances, which severely degraded the photovoltaic performance of the cells.

Application of these methods to forming p-n junctions using single-crystal wafers in place of the polycrystalline base layers showed that good (low-leakage) diodes could be made. The difficulty with the layer-base diodes was presumed to be due to the polycrystallinity, and it was thought that rapid impurity diffusion along the grain boundaries probably provided the shunt conductivity paths. This conclusion was later verified by "mapping" photovoltaic performance over the surface of a polycrystalline wafer of GaAs. A localized sharp drop in V_{oc} was found to occur at a region where three crystallites met at a point.

Diffusion of impurities along grain boundaries was possible because of the necessity for high temperatures in the junction formation processes. A low-temperature junction formation process was sought. Two possibilities were investigated:

1. The deposition of a thin layer of GaAs by sputtering, using an argon ambient and wafers of GaAs source material.

2. The formation of thin films of GaAs under high vacuum, by flash evaporation of particles of GaAs.

(More information on these processes will be found in Section VIII.).

In each case, the resulting GaAs films were found to exhibit anomalous optical properties and to have high electrical resistivity. The high resistivity would degrade the cell performance because of the resulting large value of series resistance, so that these two processes appeared to be impractical for cell fabrication.

One other junction structure was evaluated for cell manufacture. The processing knowledge acquired during earlier work on growth methods for GaP layers was applied to the formation of heterojunction cells. N-type GaP layers between 20 and 250 microns in thickness were deposited on p-type GaAs single-crystal wafers. In some cases a drop in V_{OC} value which decreased with increasing GaP layer thickness was observed, to a degree which could not be explained by simple heterojunction formation. It seemed that the junction depth increased more rapidly than the GaP layer growth rate, which may have been caused by phosphorus diffusing into the GaAs to displace arsenic, which would diffuse outwards, during the GaP growth process. Similar experiments were also performed using polycrystalline GaAs layers as the base material, but good rectification ratios could not be obtained, so that the method was shown to be unsuitable for application to thin-film solar cell fabrication.

Following these difficulties with attempts to make p-n junctions and heterojunctions in polycrystalline GaAs layers, it was decided that the most promising approach to cell fabrication lay in barrier-layer cells. These depended on the formation of an inversion layer at the GaAs surface, and the deposition of a semi-transparent conducting layer on the GaAs surface which would make contact with the inversion layer. The band structure of such a layer is shown schematically in Figure 38, part (a) of which shows the maximum band-bending case, and part (b) of which shows the case when a partially filled set of surface states exists. The maximum V_{OC} value would be obtained in case (a) when V_O is a maximum, but the more usual case is as in (b). Since the existence of the surface states, and their density and energy value, can only be determined empirically, and is also very sensitive to changes in surface treatment, it followed that an experimental program was needed to evaluate a range of candidate materials for the barrier-contact layer.

Suitable materials included both metals and compounds, but because of the high optical absorption coefficients for metals, primary emphasis was placed on those compounds which could be formed in electrically conducting thin films. These compounds are, in general, semiconductors with wide bandgaps, thus allowing optical transmission of photons in the energy range in which GaAs shows photosensitivity. However, as prepared in thin-film form, these materials are often degenerate, having a large carrier concentration caused either by departures from stoichiometry or by the presence of impurities. Consequently, these compounds behave in many ways as metals, particularly in forming contacts to semiconductors. For this reason it is proper to regard the photosensitive junctions made by these materials with a semiconductor as being barrier junctions (as described above) rather than heterojunctions. The degeneracy of the compounds does, however, lead to more free-carrier absorption for photons with energies less than the bandgap, than would be the case for a true semiconductor.

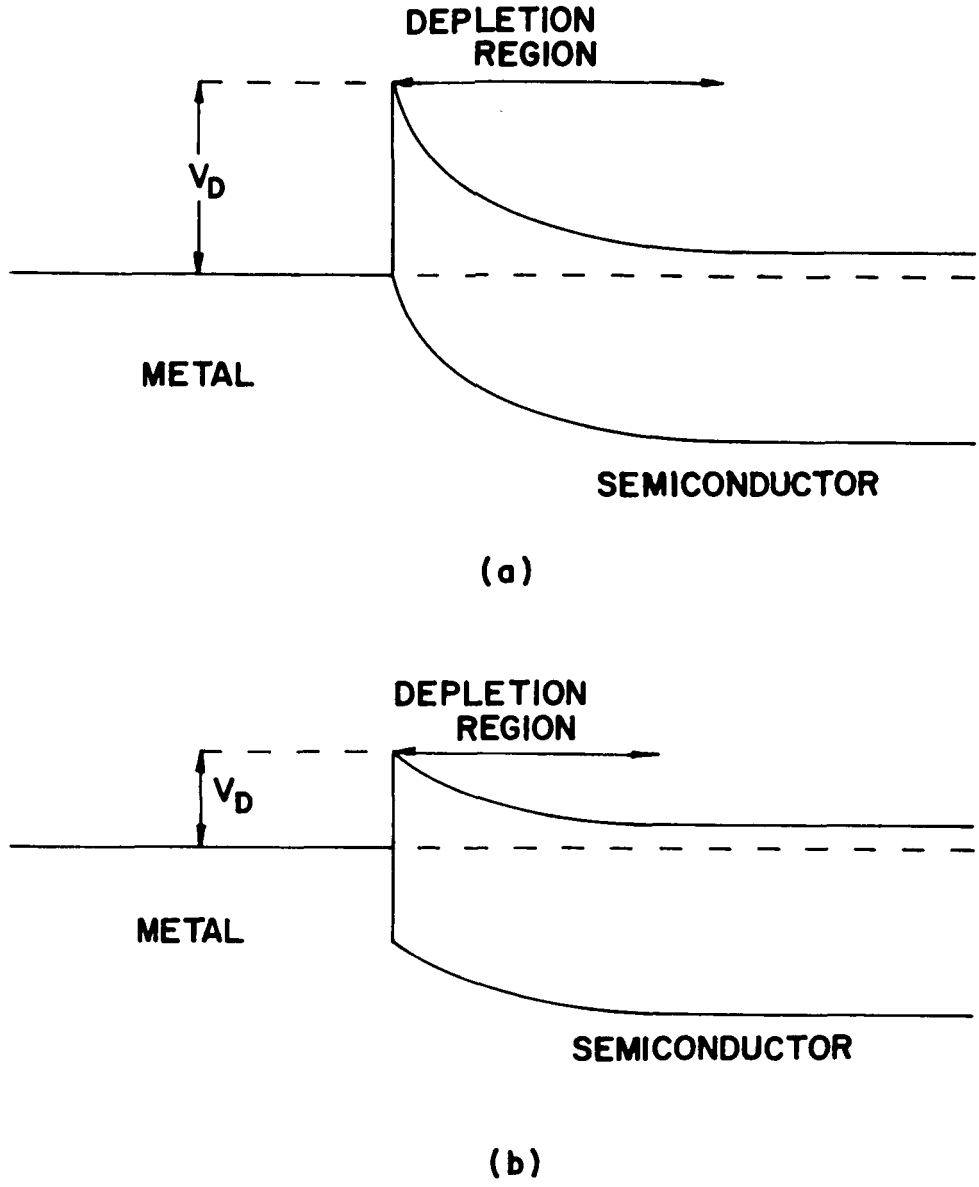

Figure 38. (a) Band structure of inversion layer, maximum band-bending case
(b) Band structure of inversion layer, surface state present

Materials investigated and results obtained are summarized in Table XIV. These results are from initial survey experiments, and give only an indication of the potentialities of a given material, rather than a definition of the ultimate performance. In addition to copper, silver and aluminum were also examined as barrier layers, with small photoresponses being seen. Tin oxide was also evaluated, with similar results.

TABLE XIV

SUMMARY OF RESULTS WITH VARIOUS BARRIER-FORMING MATERIALS

Material	Fabrication Method	Result
Cu	Electrodeposited on polycrystalline GaAs	High leakage and high series resistance
Ag	Electrodeposited on polycrystalline GaAs	Low photoresponse
Al	Vacuum evaporated	Low photoresponse
CuI	Electrodeposited Cu, exposed to I vapor, on single-crystal GaAs	V_{oc} = 0.79V, sheet resistance increases with time
Cu_2S	Electrodeposited Cu, reacted with H_2S or S in CS_2, or vacuum evaporated	V_{oc} = 0.6V, sheet conductivity-transmission product low
Cu_2Se	Electrodeposited Cu, reacted with Se in benzene, or vacuum	V_{oc} = 0.75, stable film
Cu_2Te	Electrodeposited $TeBr_4$ reacted with $CuSO_4$, also vacuum evaporated	V_{oc} = 0.6V, high sheet resistance high shunt conductance
CdS	Electrodeposited Cd exposed to H_2S or anode in $(NH_4)_2S$ soln., on single-crystal GaAs	No photovoltage on n-type GaAs
ZnTe	Vacuum deposited with Cu dopant on GaAs single crystal	V_{oc} = 0.43V
In_2O_3	$InCl_3$ sprayed onto substrate at 350°C in air	Transparent films, sheet resistance < 100 Ω sq^{-1}, ohmic contact
Bi_2O_3	Vacuum evaporated	V_{oc} = 0.15V
MoO_3	Vacuum evaporated	Sheet resistance > 10^8 Ω sq^{-1}
NiO	Decomposed on evaporation	-
PbO	Decomposed on evaporation	-
NiS	Decomposed on evaporation	-
SnS	Vacuum evaporated	Sheet resistance 10^7 Ω sq^{-1} small photovoltage

TABLE XIV

SUMMARY OF RESULTS WITH VARIOUS BARRIER-FORMING MATERIALS (Cont'd.)

Material	Fabrication Method	Result
Cu_3P	Vacuum evaporated	V_{oc} = 0.4V
SnO		Low photoresponse
NiS	Electrodeposited Ni reacted with H_2S, on crystal GaAs	V_{oc} = 0.35

Following this evaluation, work was concentrated on the copper-sulphide barrier layer system, and considerable development effort was put into forming thin films of this material.

Vacuum evaporation was employed for forming the films, with a fresh charge of Cu_2S being used for each evaporation. The films as immediately prepared showed a resistivity of 200 ohm-cm, but this dropped on exposure to air. A very much more striking decrease in resistance was obtained when the film was exposed to the vapor over ammonium polysulphide, resistivities of 6.5×10^{-4} ohm-cm being obtained. The optical transmission of the films was measured as a function of wavelength, and from these measurements and the conductivity results it was concluded that the deposited films absorbed sulphur during the vapor treatment, to form copper vacancies, thus increasing the electrical conductivity, since Cu_2S is a deficiency semiconductor. I-V measurements on Cu_2S films deposited on single-crystal GaAs wafers indicated that the contact behaved electrically like a metal-semiconductor junction, confirming that the Cu_2S was degenerate.

Cells made with Cu_2S exhibited 1.5% efficiencies over areas of 0.72 cm^2, with V_{oc} = 0.5 volt. The main efficiency limitation was found to be cell resistance, which severely degraded the fill-factor.

The initial survey results also indicated that cuprous selenide was a potential alternative to Cu_2S; so a development effort was made with this material. A vacuum evaporation technique was evolved which led to films being deposited which were 70% transmitting to 1.5-eV radiation at 175-Å thickness, and gave a sheet resistivity of 93 ohms per square at this thickness. This result was encouraging, and thin-film GaAs cells on Mo substrates made with cuprous selenide showed indications of efficiencies close to 4% over small areas with this as a barrier layer. With further development, described elsewhere in this report, this material is still the most promising for this application.

With development of better growth techniques for GaAs films, resulting in more uniform layers, attempts have been occasionally made to produce junctions by diffusion. In all cases, however, high shunt conductances have been obtained, and the barrier-layer type of cell has been demonstrably superior.

SECTION VIII

REVIEW OF ALTERNATIVE MATERIALS

A. SEMICONDUCTORS

Theory indicates that for solar energy conversion using the photovoltaic effect, GaAs should be more efficient than GaP. However, in practice the limitations on conversion efficiency are not those considered in the theoretical treatment, so that it appeared worthwhile to consider GaP as an alternative material to GaAs for cell fabrication. Layers of GaP were formed on quartz, molybdenum, tungsten and germanium-coated tungsten, using the vapor-transport technique with source and substrate close to 1000°C. Good adherence and uniform layers were found. N-type layers were obtained from both n- and p-type starting material, with resistivities in the range 30 to 300 ohm-cm.

Some success was obtained in forming a p-type surface layer by diffusion of zinc into GaP polycrystalline layers. However, these junctions always exhibited a large shunt conductance which severely degraded the photovoltaic performance. For this reason, the use of GaP as a base material for cells appeared impractical. Hence attention was shifted to the GaP-GaAs heterojunction type of cell, for which the results reviewed in Section VII of this report were obtained.

Some results of exploratory-type experiments in which barriers of cuprous iodide and cuprous sulphide were applied to other semiconductors are summarized in Table XV.

In a wider context, the results with cadmium sulphide are interesting, especially in view of the recent successes which have been achieved with this material. However, at the time they were obtained the results shown in Table XV did not warrant the discontinuance of interest in GaAs as a base material. This was mainly because the CuI barriers were highly unstable, the output degrading completely over a period of a few days.

B. GaAs LAYER FORMATION METHODS

1. The Vapor Transport Method

For the entire time that the work on GaAs cells has been in progress, the principal method used to form the GaAs layers has been the vapor transport system developed originally by F. H. Nicoll of RCA Laboratories. The starting material is

TABLE XV

RESULTS WITH ALTERNATIVE BASE MATERIALS

Base Material	Form	Barrier Material	Illuminated Surface	V_{oc} Volts	Remarks
n - Ge	s.c.*	CuI	CuI	0.04	-
p - Ge	s.c.	CuI	CuI	0.11	-
n - Si	s.c.	CuI	CuI	0.4	-
p - Si	s.c.	CuI	CuI	zero	-
CdS	s.c.	CuI	CuI	0.30	very good rectification ratio obtained
CdS	s.c.	CuI	CdS	0.29	very good rectification ratio obtained
CdS	p.c.*	CuI	CuI	0.60	-
CdS	p.c.	CuI	CdS	0.30	smaller sensitivity than CuI-illuminated case
CdS	p.c.	Cu_2S	Cu_2S	0.41	-
CdS	p.c.	Cu_2S	CdS	0.41	smaller sensitivity than Cu_2S-illuminated case
CdTe	s.c.	CuI	CuI	0.62	linear I-V characteristic, high photosensitivity
CdTe	p.c.	CuI	CuI	0.30	less sensitivity than s.c. cell

* s.c.: single-crystal

p.c.: polycrystal

bulk GaAs, which has usually been in the form of a single-crystal wafer. This is maintained at a high temperature in a hydrogen furnace, with the substrate at a rather lower temperature in the same furnace. The reversible reaction

$$2\ GaAs + H_2O \rightleftharpoons Ga_2O + H_2 + As_2$$

is believed to occur, the forward direction being favored by higher temperatures. GaAs is thus transported onto the cooler substrate, at a rate determined by the concentration of oxygen present, and the temperatures of the source and substrate. Further details of this process and the results achieved recently are to be found in Section I of this report.

2. Vacuum Deposition Methods

Two approaches to achieving GaAs film growth under vacuum were investigated during earlier phases of this work. These were flash evaporation and sputtering. Both gave similar results.

The sputtering deposition system used GaAs wafers as the source material, these being mounted by conducting epoxy cement on a tantalum sheet. Typical deposition conditions were:

Discharge current	10 - 15 mA
Voltage	1900 - 2300 V
Argon pressure	55 - 65 microns
Substrate temperature	250 - 600°C
Cathode-substrate distance	3 cm
Deposition rate	160 - 240 Å min^{-1}
Argon flow rate	1 - 3 ml min^{-1}

The argon was passed through a dessicant before use.

The flash evaporation system employed particles of GaAs 10 to 14 mils in diameter, which were fed into a tungsten boat heated to 1600°C. The vacuum during deposition was of the order 10^{-5} Torr, and most films were grown at about 1000 Å min^{-1}. Substrate temperatures between 200 and 600°C were used, and GaAs films were successfully grown on glass, molybdenum, single-crystal GaAs, vapor-grown layers of GaAs, and calcium fluoride.

Results from both methods showed that amorphous films were obtained on substrates at room temperature, and that crystallinity in the deposits increased with increase of temperature. Single-phase GaAs was in general obtained, as evidenced by x-ray diffraction studies.

Measurements showed that the films obtained at low substrate temperatures had anomalously high optical absorption for wavelengths longer than the band edge, compared with single-crystal material. With increasing substrate temperatures, this anomalous effect became less pronounced, but even the best films obtained did not show the sharp absorption edge and low long-wavelength absorption characteristic of single-crystal material. In this respect, vapor-grown GaAs layers showed behavior much closer to bulk single-crystal material. The optical properties of the vacuum-deposited layers were not of direct significance, but were an indication that the film material differed considerably from bulk and vapor-deposited GaAs.

If not intentionally doped, the vacuum-deposited films were p-type. To produce n-type material, high doping concentrations (0.1 to 1.0% Sn) were found to be necessary. Undoped p-type films exhibited resistivities of 10^3 to 10^5 ohm-cm. Heavy doping with manganese (more than 0.1% Mn) reduced the resistivity of the p-type films to between 10 and 10^3 ohm-cm, but n-type films always had resistivities of 10^4 to 10^6 ohm-cm. Some evidence for a correlation between increasing substrate temperature and higher resistivity was found. These electrical measurements definitely indicated that the vacuum-deposited GaAs would be unsatisfactory for cell fabrication. These results all correlated with those published by other workers.[16]

3. Halide Transport Method

Another chemical system for forming GaAs layers is described by the reactions:

$$2\,Ga + 6\,HCl \longrightarrow 2GaCl_3 + 3H_2$$

$$2\,AsH_3 + 4\,GaCl_3 \longrightarrow 2GaCl_2 + 6HCl + Cl_2$$

The first reaction is obtained by passing HCl (diluted with H_2) over the metal at about 700°C. The resulting vapor is mixed with arsine and passed over the substrate at 600 to 650°C where the second reaction proceeds. The method has been shown to produce very high-quality epitaxial GaAs films on Ge and GaAs single-crystal substrates.[17]

Equipment specially designed for use with thin metal foil substrates was built and operated during 1965.* The design was such that InAs and GaAs films could be deposited sequentially (the reactions above are valid if In is substituted for Ga).

*Contract NAS3-6466.

Various difficulties with the equipment were encountered and solved, but a persistent problem proved to be cracking and curling of the aluminum foil substrate, under attack by the HCl in the gas mixture. Some satisfactory films on small areas of the substrate were obtained, but the effort was discontinued to allow concentration of effort on other areas of research. This method remains a potentially valuable approach to large-area cells and is felt to be ultimately the best method for growing GaAs layers.

4. Vapor Growth from the Elements

An approach combining the principles of the vapor transport technique and halide transport system was also evaluated. Gallium was transported from the metal by the oxide reaction described above, and arsenic was introduced as arsine. Layers of GaAs were formed on molybdenum substrates, but difficulty was encountered in obtaining uniform deposits free of gallium precipitations. The work on this method was discontinued to allow concentration on other problems.

C. SUBSTRATES

Early work on GaAs thin-film cells employed substrates of tungsten and molybdenum. These were chosen to permit high substrate temperatures to be employed during the GaAs layer growth process. It was found that GaAs layers grown directly on these substrates showed a high-resistance and non-ohmic contact with the substrate.

It was concluded that the non-ohmic effects were due to the metal-semiconductor junction, and that the high-resistance effects arose at the crystallite interfaces in the initially deposited GaAs. This initial growth region was shown to consist of a large number of very small crystallites. As growth proceeded, some of these crystallites grew faster than others, so that later growth produced fewer but larger crystallites. Thus the initial growth region provided a large number of inter-crystallite boundaries, which hence localized resistance arising from the boundaries in the region of the GaAs adjacent to the substrate.

To overcome both of these problems, methods for heavily doping the GaAs during the period of initial growth were devised. These consisted of either depositing the desired impurity on the GaAs source wafer surface prior to film growth, or of precoating the substrate with an impurity which would produce a high carrier concentration in the initially grown material. Both of these approaches obtained the desired objective, though the precoated substrate technique was found to give more uniform and reproducible results. However, with cells made using these methods of obtaining ohmic and low-resistance back contacts, the diode characteristics showed a tendency to high shunt conductance, which may have been due to diffusion of the substrate coating material along the grain boundaries to the front face of the cell.

Although the molybdenum and tungsten substrates were satisfactory from the cell fabrication viewpoint, the weight penalties which would be imposed by these materials made the use of a lighter alternative very attractive. Aluminum was the most promising candidate material, particularly since it was readily available in thin foil form. Initial evaluation was done with 25-μm-thick foil, but this material curled after the GaAs layer had been grown on it, presumably because of coefficient of thermal expansion mismatch between substrate and GaAs. With thinner foils, however, the problem was less severe, and with the thinnest foil which could be handled satisfactorily (5 μm) no curling was seen. This was presumably due to the ability of the aluminum to yield plastically when used in such a thin section.

Once again, high-resistance non-ohmic contacts between aluminum substrates and GaAs layers were obtained, and it was found that precoats of flash-evaporated InAs, vacuum evaporated Sn-Ge alloy, and Sn-Ag alloy, did not eliminate the problem, as they had done with the molybdenum substrates. This problem was solved by the discovery that a substrate precoat of vapor-deposited InAs eliminated both the high resistivity and nonlinearity in the contact. The technique has been used consistently throughout the remainder of the work. A discussion of the principles on which the technique is believed to operate, and results of recent work in this area, is to be found in Section III of this report.

The aluminum substrates limit the temperatures which can be used during GaAs film growth to being below the melting point of Al (640°C). This is a drawback, in that it limits the growth rate which can be attained. Hence, lightweight alternative materials with a higher melting point have been considered. The only serious possibility appears to be titanium. However, it is known that this material disintegrates if heated in hydrogen, and hence would not be compatible with the GaAs film growth process. There appears to exist the possibility that the hydrogen furnace ambient could be replaced with an inert gas such as helium or argon, but this has not been investigated experimentally.

D. LARGE-AREA CELLS

In most of the work done under this and previous contracts, the areas of fabricated cells have been between 0.5 and 1.0 cm^2. Such a cell is clearly of no interest for production purposes, and consequently an effort has been made to form large-area cells.

The principal difficulty anticipated was the growth of GaAs layers of satisfactory quality, using the vapor transport process. Experience confirmed this expectation. The equipment used is described in detail in reference 1, and is a development of the furnaces used for small-area cells.

The films obtained showed nonuniformities which were believed to arise from temperature gradients and gas flow patterns in the growth region. Portions of the films grown were suitable for cell fabrication, but at no time was a layer of 10 cm^2 (the furnace capacity) obtained with uniformity adequate for the fabrication of a cell with this area.

It appears that the difficulties encountered with this furnace are not insuperable. However, the halide transport process described above (Section VIII. B. 3) appears to be fundamentally better suited to large-area GaAs layer growth, especially when the economic factors of production are considered.

SECTION IX

CONCLUSIONS AND RECOMMENDATIONS

At the present time, modest cell efficiencies and small cell areas are the major problems to be overcome before the cells can be considered seriously for practical application. Unless cell efficiencies can be improved, however, effort spent on increasing cell areas has little point. The following conclusions have been drawn concerning cell efficiencies:

(i) No single factor causes the present cell efficiencies, and approximately equal increases in cell performance could be attained by improving the V_{oc} and I_{sc} values to the theoretical limit. However, work during the reporting period has shown that improvements in V_{oc} are very difficult to obtain, whereas I_{sc} improvements may be more easily achieved.

(ii) A small improvement in cell efficiency may be obtained by reducing the series resistance of the cells. This series resistance has been shown not to be due to the barrier layer, but to arise in the GaAs layer.

Other conclusions on cell performance which have been drawn from the work during the reporting period are:

(i) The cells operate by mechanisms which are understood and controllable.

(ii) The techniques which have been developed for stabilizing the cell operation are successful.

In view of these results, it is recommended that future work should be concentrated in the following areas:

(i) Improvement of cell efficiency by the use of an antireflection coat and optimization of the Cu_2Se film thickness to improve the I_{sc} values.

(ii) Investigation of methods for reducing the I_o values of the cells, by examining the effects of different GaAs film growth conditions and surface preparation techniques.

If efficiencies of 5% or higher can be achieved, techniques for forming large-area cells should be investigated. It appears that the halide transport process is fundamentally better suited to the formation of large-area GaAs layers than the vapor transport process employed at present.

REFERENCES

1. Midpoint Report, Contract NAS3-8510 (Nov. 1966).

2. R. Paff (private communication).

3. R. D. Heyding, Can. J. Chem. 44, 1233 (1966)

4. S. Tolansky, Multiple Beam Interferometry (Oxford University Press, 1948).

5. Final Report, Contract NAS3-6466, NASA CR-54959 (Jan. 1966).

6. R. Williams, J. Appl. Phys. 37, 3411 (1966).

7. O. S. Heavens, Optical Properties of Thin Solid Films (Dover Publications, New York, 1965).

8. L. Holland, The Vacuum Deposition of Thin Films (John Wiley and Sons, Inc., New York, 1961).

9. J. J. Wysocki, RCA Rev. 22, 57 (1961).

10. J. J. Loferski, J. Appl. Phys. 27, 777 (1956).

11. W. Shockley, Bell Syst. Tech. J. 28, 435 (1949).

12. H. K. Henisch, Rectifying Semiconductor Contacts (Oxford, 1957).

13. M. D. Sturge, Phys. Rev. 127, 768 (1962).

14. M. Wolf and E. L. Ralph, IEEE Trans. Electron Devices ED-12, 470 (1965).

15. M. B. Prince, Proc. 14th Ann. Power Sources Conf. p. 26 (1960).

16. J. E. Davey and T. Pankey, J. Appl. Phys. 35, 2203 (1964).

17. J. J. Tietjen and J. A. Amick, J. Electrochem. Soc. 113, 724 (1966).

DISTRIBUTION LIST
CONTRACT NAS 3-8510

National Aeronautics and Space Administration
Washington, D. C. 20546
Attn: Arvin H. Smith/RNW (2)
H. B. Finger/RP
Millie Ruda/AFSS-LD

National Aeronautics and Space Administration
Scientific and Technical Information Facility
P. O. Box 33
College Park, Maryland 20740
Attn: Acquisitions Branch (SQT-34054) (2+1 repro.)

National Aeronautics and Space Administration
Goddars Space Flight Center
Greenbelt, Maryland 20771
Attn: W. R. Cherry
M. Schach
B. Mermelstein, Code 672
J. W. Callaghan, Code 621
Librarian
P. H. Fang, Code 633

National Aeronautics and Space Administration
Lewis Research Center
21000 Brookpark Road
Cleveland, Ohio 44135
Attn: John E. Dilley, MS 500-309
B. Lubarsky, MS 500-201
A. F. Forestieri, MS 500-201
R. L. Cummings, MS 500-201
C. K. Swartz, MS 500-201 (3+1 Repro)
N. D. Sanders, MS 302-1
A. E. Potter, MS 302-1 (3)
George Mandel, MS 5-1 (2)
Report Control Office, MS 5-5
Technology Utilization Office, MS 3-19
V. L. Hlavin, MS 3-14

National Aeronautics and Space Administration
Langley Research Center
Langley Station
Hampton, Virginia 23365
Attn: W. C. Hulton
E. Rind

National Aeronautics and Space Administration
Electronic Research Center
Power Conditioning & Distribution Lab.
575 Technology Square
Cambridge, Massachusetts 02139

Jet Propulsion Laboratory
4800 Oak Grove Drive
Pasadena, California 91103
Attn: John V. Goldsmith
Don W. Ritchie

Institute for Defense Analysis
400 Army-Navy Drive
Arlington, Virginia 22202
Attn: R. Hamilton

Advanced Research Projects Agency
Department of Defense
Pentagon
Washington, D. C. 20546
Attn: Dr. C. Yost

Naval Research Laboratory
Department of the Navy
Washington, D. C. 20546
Attn: E. Broncato, Code 6464
M. Wotaw, Code 5170
Dr. V. Linnenbom, Code 7450
Dr. C. Klick, Code 6440

Commanding Officer
U. S. Army Electronics R&D Labs
Fort Monmouth, New Jersey 07703
Attn: Power Sources Division SELRA/PS

Air Force Cambridge Research Center
Air Research and Development Command
United States Air Force
Laurence G. Hanscom Field
Bedford, Massachusetts 01731
Attn: Col. G. de Giacomo

Air Force Ballistic Missile Division
Air Force Unit Post Office
Los Angeles, California 90045
Attn: Col. L. Norman, SSEM
Lt. Col. G. Austin, SSZAS
Lt. Col. A. Bush, SSZME
Capt. A. Johnson, SSZDT
Capt. W. Hoover, SSTRE

Office of the Chief of Engineers
Technical Development Branch
Washington, D. C. 20546
Attn: James E. Melcoln/ENGMC-ED

Aeronautical Research Laboratories
Office of Aerospace Research, USAF
Wright-Patterson Air Force Base
Dayton, Ohio 45433
Attn: D. C. Reynolds, ARX

Aeronautical Systems Division
Air Force Systems Command, USAF
Wright-Patterson Air Force Base, Ohio 45433
Attn: P. R. Bertheaud
Mrs. E. Tarrants/WWRNEM-1

Flight Vehicle Power Branch
Air Force Aero Propulsion Laboratory
Wright-Patterson Air Force Base, Ohio 45433
Attn: J. F. Wise/Code APIP-2

Flight Accessories Aeronautics Systems Division
Wright-Patterson Air Force Base
Dayton, Ohio 45433
Attn: Mr. James L. Matice, ASRCM-22

Aerospace Corporation
P. O. Box 95085
Los Angeles, California 90045
Attn: Dr. G. Hove
Dr. F. Mozer
V. J. Porfune
Dr. I. Spiro
Technical Library Documents Group

Battelle Memorial Institute
505 King Avenue
Columbus, Ohio 43201
Attn: L. W. Aukerman
R. E. Bowman
T. Shielladay

Bell and Howell Research Center
360 Sierre Madre Villa
Pasadena, California 91109
Attn: Alan G. Richards

Bell Telephone Laboratories
Murray Hill, New Jersey 07971
Attn: W. L. Brown
U. B. Thomas

Clevite Corporation
Electronic Research Division
540 West 105th Street
Cleveland, Ohio 44108
Attn: Fred A. Shirland
Dr. Hans Jaffe

The Eagle-Picher Company
Chemical and Material Division
Miami Research Laboratories
200 Ninth Avenue, N.E.
Miami, Oklahoma 74354
Attn: John R. Musgrave

Energy Conversion, Incorporated
336 Main Street
Cambridge, Massachusetts 02142
Attn: G. J. McCaul

General Electric Company
Electric Components Division
316 East Ninth Street
Owensboro, Kentucky 42301
Attn: F. D. Dyer, Jr.

Harshaw Chemical Company
Crystal-Solid State Division
2240 Prospect Avenue
Cleveland, Ohio 44115
Attn: James Schaefer

Heliotek Corporation
12500 Gladstone Avenue
Sylmar, California 91342
Attn: Eugene Ralph

Hughes Aircraft Company
Aerospace Group, R&D Division
Culver City, California
Attn: C. A. Escoffery

International Rectifier Corporation
239 Kansas Street
El Segundo, California 90245
Attn: Irwin Rubin

Leesona Moos Laboratories
90-28 VanWyck Expressway
Jamaica, New York 11021
Attn: Stanley Wallack

Lockheed Missile and Space Division
3251 Hanover Street
Palo Alto, California 94304
Attn: D. Marks, Dept. 5230

Material Research Corporation
Orangeburg, New York 10962
Attn: Vernon E. Adler

National Cash Register Company
Physical Research Department
Dayton, Ohio 45409
Attn: R. R. Chamberlin

North American Aviation, Inc.
Autonetics Division
Anaheim, California 92803
Attn: R. R. August

Perkin-Elmer Company
Optical Coating Section
Norwalk, Connecticut 06845
Attn: Jim Peardsley

Philco Corporation
Blue Bell, Pennsylvania 19422
Attn: A. E. Mace

Physics Technology Laboratories, Inc.
7841 El Cajon Boulevard
La Masa, California 92041
Attn: W. E. Richards

RCA Laboratories
Radio Corporation of America
Princeton, New Jersey 08540
Attn: P. Rappaport
M. Wolf
M. L. Topfer

Ryan Aeronautical Company
Lindbergh Field
San Diego, California 92112
Attn: K. D. Hawkins

Sandia Corporation
Albuquerque, New Mexico 87116
Attn: F. Smits

Sylvania Electronic Products, Incorporated
Electron Tube Division
Emporium, Pennsylvania 15834
Attn: Georgiana Larrabee, Librarian

Tyco Laboratories, Incorporated
Bear Hill
Waltham, Massachusetts 02154
Attn: A. I. Mlavsky

Union Carbide Corporation
Parma Research Center
Technical Information Services
P. O. Box 6116
Cleveland, Ohio 44101

Solid-State Electronics Laboratory
Stanford Electronics Laboratories
Stanford University
Stanford, California 94305
Attn: Professor G. L. Pearson

Westinghouse Electric Corporation
Research and Development Laboratories
Churchill Borough, Pennsylvania 15235
Attn: H. G. Chang

Westinghouse Electric Corporation
Semiconductor Division
Youngwood, Pennsylvania 15697
Attn: Don Gunther

Massachusetts Institute of Technology
Security Records Office
Room 14-0641
Cambridge, Massachusetts 02139

G. T. Schjeldahl Company
Northfield, Minnesota 55057
Attn: Don Roiseland

The Boeing Company
P. O. Box 3707
Seattle, Washington 98124